Fault detection, identification and economic impact assessment for a pressure leaching process
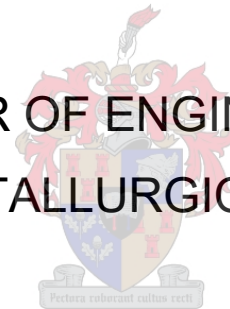
by

Johannes Jacobus Strydom

Thesis presented in partial fulfilment

of the requirements for the Degree

of

MASTER OF ENGINEERING

(EXTRACTIVE METALLURGICAL ENGINEERING)

in the Faculty of Engineering

at Stellenbosch University

Supervisor

Dr. L Auret

Co-Supervisor

Prof. C Dorfling

December 2017

Declaration

By submitting this thesis electronically, I declare that the entirety of the work contained therein is my own, original work, that I am the sole author thereof (save to the extent explicitly otherwise stated), that reproduction and publication thereof by Stellenbosch University will not infringe any third party rights and that I have not previously in its entirety or in part submitted it for obtaining any qualification.

Date: December 2017

Abstract

Modern chemical and metallurgical processes consist of numerous process units with several complex interactions existing between them. The increased process complexity has in turn amplified the effect of faulty process conditions on the overall process performance. Fault diagnosis forms a critical part of a process monitoring strategy and is crucial for improved process performance.

The increased amount of process measurements readily available in modern process plants allows for more complex data-driven fault diagnosis methods. Linear and nonlinear feature extraction methods are popular multivariate fault diagnosis procedures employed in literature. However, these methods are yet to find wide spread industrial application. The multivariate fault diagnosis methods are not often evaluated on real-world modern chemical processes. The lack of real world application has in turn led to the absence of economic performance assessments evaluating the potential profitability of these fault diagnosis methods.

The aim of this study is to design and investigate the performance of a fault diagnosis strategy with both traditional fault diagnosis performance metrics and an economic impact assessment (EIA). A complex dynamic process model of the pressure leach at a base metal refinery (BMR) was developed by Dorfling (2012). The model was recently updated by Miskin (2015), who included the actual process control layers present at the BMR. A fault library was developed, through consultation of expert knowledge from the BMR, and incorporated into the dynamic model by Miskin (2015). The pressure leach dynamic model will form the basis for the investigation.

Principal component analysis (PCA) and kernel PCA (KPCA) were employed as feature extraction methods. Traditional and reconstruction based contributions were employed as fault identification methods. Economic Performance Functions (EPFs) were developed from expert knowledge from the plant. The fault diagnosis performance was evaluated through the traditional performance metrics and the EPFs.

Both PCA and KPCA provided improved fault detection results when compared to a simple univariate method. PCA provided significantly improved detection results for five of the eight faults evaluated, when compared to univariate detection. Fault identification results suffered from significant fault smearing.

The significant fault detection results did not translate into a significant economic benefit. The EIA proved the process to be robust against faults, when implementing a basic univariate fault detection approach. Recommendations were made for possible industrial application and future work focusing on EIAs, training data selection and fault smearing.

Opsomming

Moderne chemiese- en metallurgiese-prosesse bestaan uit 'n verskeidenheid proseseenhede met talle komplekse interaksies wat tussen die proseseenhede bestaan. Die toename in die komplekse interaksies versterk die effek van foutiewe prosesomstandighede op die algehele prosesverrigting.

Die toename in die beskikbaarheid van prosesmetings in moderne prosesse, laat meer komplekse datagedrewe fout-diagnostiese metodes toe. Lineêre en nie-lineêre kenmerk-ekstraksie metodes is gewilde meerveranderlike fout-diagnostiese prosedures wat in literatuur gebruik word. Dié metodes het egter nog nie 'n algemene toepassing in die industrie gevind nie. Die meerveranderlike fout-diagnostiese metodes word egter nie gereeld op die werklik moderne chemiese-prosesse toegepas nie; die gebrek aan dié toepassings veroorsaak die afwesigheid van ekonomiese impakstudies wat die winsgewendheid van hierdie fout-diagnostiese metodes evalueer.

Die doel van hierdie studie is om 'n fout-diagnostiese strategie te ontwerp en om die werkverrigting te ondersoek met beide tradisionele fout-diagnostiese werkverrigtingstatistieke en ekonomiese impak assessering (EIA). 'n Komplekse dinamiese prosesmodel van die drukloogproses by 'n basismetaalraffinadery (BMR) is ontwikkel deur Dorfling (2012). Die model is onlangs deur Miskin (2015) opdateer wat die werklike BMR prosesbeheerstrategie geïmplementeer het. 'n Biblioteek van foute is ontwikkel d.m.v. die konsultering met kundiges by die BMR en is suksesvol opgeneem in die dinamiese model deur Miskin (2015). Die dinamiese drukloogmodel vorm die basis van hierdie projek.

Hoofkomponentanalise (HKA) en Kern-HKA (KHKA) is gebruik as metodes vir kenmerk-ekstraksie. Tradisionele- en rekonstruksie-gebaseerde bydraberekeninge is gebruik as fout-identifikasie metodes. Ekonomiese-verrigtingfunksies (EVF's) is ontwikkel met die hulp van kundiges by die BMR. Die fout-diagnose werkverrigting is geëvalueer met beide tradisionele fout-diagnostiese werkverrigtingstatistieke en die EVF's.

Beide HKA en KHKA het verbeterde foutopsporings resultate gelewer in vergelyking met 'n eenvoudige eenveranderlike metode. HKA het beduidende verbeterde foutopsporingsresultate vir vyf van die agt foute gelewer, in vergelyking met eenveranderlike foutopsporing. Fout-identifikasie resultate het aan beduidende fout smeer-effekte gely.

Dié beduidende foutopsporings resultate het nie tot 'n beduidende ekonomiese voordeel gelei nie. Die EIA het bewys dat die proses wel robuus is teen foute, wanneer 'n basiese eenveranderlike foutopspring strategie gevolg word. Aanbevelings is gemaak vir moontlike industriële aanwending en toekomstige werk wat fokus op EIA's, opleidingsdata-seleksie en foutsmeer-effek.

Acknowledgements

I wish to express my appreciation to everyone who made this project possible and specifically:

- Dr. Lidia Auret, for her continuous patience, support and guidance.

- Dr. John McCoy, for all your patience and guidance.

- My co-supervisor, Prof. Christie Dorfling, for the valuable technical contributions.

- Mr. Brian Lindner, who were always available to help with Matlab® and Simulink®.

- The entire process monitoring and systems research group and Dr. JP Barnard.

- My parents, for your continuous support and encouragement.

- SAMMRI for their financial support of this project.

Table of Contents

Nomenclature

Acronym	Description
ANOVA	Analysis of variance
APC	Advanced process control
AUC	Area under curve
BMR	Base metal refinery
CUSUM	Cumulative sum
DD	Detection delay
EWMA	Exponentially weighted moving average
EIA	Economic impact assessment
EPF	Economic performance function
FAR	False alarm rate
KPCA	Kernel principal component analysis
KPI	Key performance indicator
LSD	Least significance difference
MAR	Missing alarm rate
MIP	Metals in process
NOC	Normal operating conditions
PCA	Principal component analysis
PGE	Platinum group element
PGM	Platinum group mineral
PF	Performance function
JPF	Joint performance function
PI	Proportional integral
PID	Proportional integral derivative
PMR	Precious metal refinery
RBC	Reconstruction based contribution
ROC	Receiver operating curve
SPE	Squared prediction error
TAR	True alarm rate
TEP	Tennessee Eastman process
Tsq	T_A^2-statistic
T1	First principal component scores
T2	Second principal component scores

Symbol	Description
A	Number of retained principal components
C	Covariance matrix
C_j	Traditional contribution
c	Kernel width
μ	Sample mean
E	Residual matrix
F	General score matrix
F_i	PGE$_i$ flowrate
F_{is}	PGE$_i$ steady state flowrate
f_i	PGE$_i$ fraction lost
n	Number of observations
m	Number of variables
P	Principal component matrix
P$_A$	Retained principal component matrix
p^m	Eigenvector m
λ_m	Eigenvalue corresponding to mth eigenvector
P_i	PGE$_i$ price
λ	Eigenvalues
T	Principal component score matrix
T^{TEST}	Test data score matrix
T^2	T^2-statistic
α	Eigenvector
K	Kernel matrix
K^{TEST}	Test data kernel matrix
$\breve{\mathbf{K}}$	Centred kernel matrix
$\breve{\mathbf{K}}^{TEST}$	Centred test data kernel matrix
$\widetilde{\lambda_m}$	Scaled eigenvalue
X	Input data
$\widetilde{\mathbf{X}}$	Scaled input data
x_i	Input data vector at time i
X^{TEST}	Input Test data
$\widetilde{\mathbf{X}}^{TEST}$	Scaled input test data
{H}	Implicit dot product space

Symbol	Description
{X}	Reconstructed data
σ	Sample standard deviation
$\Phi(\ )$	Mapping function

List of Figures

List of Tables

Chapter 1: Introduction

Chapter 1 provides a brief background and introduction on process monitoring and the application of dynamic process models. The chapter aims to provide the reader with some background on process monitoring and the use of dynamic process models, before providing the specific project aim and objectives. The thesis layout is summarized in section 1.5.

1.1 A background to process monitoring

Modern industrial chemical processes consist of several process units with complex interactions existing between these units. These complex interactions have made the monitoring of these processes more challenging. The strong growth in process automation technology has also increased process efficiency and further decreased the demand for process supervision.

Fault diagnosis is the main focus of process monitoring and consists of fault detection followed by fault identification. Abnormal (faulty) process conditions need to be detected and identified as soon as possible using some fault detection and identification method. Once the abnormal conditions and its locations have been identified, corrective action can be taken. The longer a process is operated at abnormal conditions, the risk of possible unsafe operation or environmental damage is increased.

Process monitoring, and especially fault detection and identification, has received significant research focus in the last decade. This is in part due to the vast increase in measurement instrumentation available on modern industrial chemical plants. The result is an increased amount of process data being readily available. The increase in computational resources has also contributed to the increased investigation of multivariate fault detection and identification methods. These multivariate statistical methods allow for the inclusion of the complex interactions present in modern industrial chemical processes. The multivariate results are then used to identify when a process is moving away from the desired operating conditions.

1.1.1 Process control layers

It is important to recognize that a fault detection and identification strategy, forms part of the overall plant wide control strategy. In order to understand where a fault detection and identification strategy fits in, the different control layers needs to be discussed. The different control layers are shown in Figure 1.1.
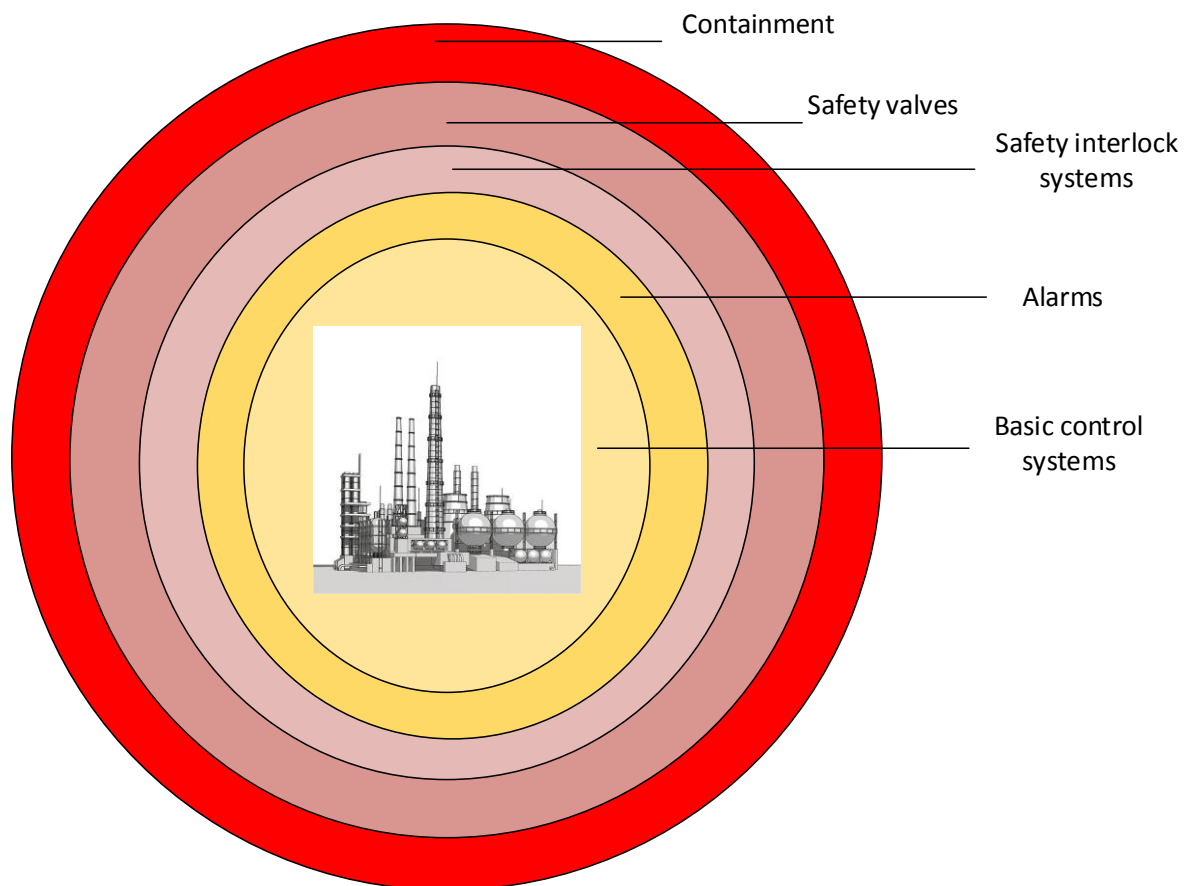
Figure 1.1: Typical process control layers.

The first control layer consists of the basic process control systems. These systems are designed to control several process variables through a simple feedback and/or feedforward system. The controller aims to operate at the desired conditions with as little possible variance. If a certain process measurement moves outside an allowable range, an alarm is triggered. The alarm in turn notifies the plant operator who can then take corrective action. The alarms form the second control layer.

The third control layer is safety interlock systems. If a process moves into dangerous or unstable operating zones, valves automatically default to avoid any harm to personnel or the environment. This usually results in immediate plant shut down and unplanned maintenance.

Safety valves, rupture disks and other relief devices are designed to relieve a process from dangerous operating conditions through some self-actuating reaction. These valves act as the fourth control layer. The fifth control layer is containment. The containment objective is to limit the damage once a process has become out of control. For example: the required response to contain a chemical spillage.

1.1.2 Fault detection and identification as part of overall control strategy

Fault detection and identification will form part of the second control layer (alarms) of the overall control strategy shown in Figure 1.1. Multivariate statistical methods are applied to process data. If the multivariate statistical results indicate a deviation from the desired conditions, alarms are triggered. The operator can then decide to take further action after the alarm is triggered. However, the amount of alarms triggered per operator is regulated by international standards. The ISA regulations state a maximum of twelve alarms triggered an hour per operator (Izadi *et al*. 2011). These regulations further emphasises the need for accurate process monitoring methods.

Once the fault has been detected, the location of the abnormal conditions needs to be identified. The results from the multivariate statistical methods are used to identify the possible location of the fault. The fault location can then aid the operator in taking swift corrective actions.

1.1.3 A multivariate statistical approach to fault detection and identification

As mentioned in section 1.1, multivariate statistical methods have received significant research attention. These methods are employed to extract features from the available process data. A feature can be thought of as an inferential variable, a calculated variable that is more informative or useful in further processing than the measured variables it is calculated from.

There are several multivariate feature extraction methods available. The most common multivariate feature extraction method is principal component analysis (PCA). PCA is a linear feature extraction method. Non-linear feature extraction methods have also received significant attention in literature. A common nonlinear feature extraction method employed in process monitoring literature is kernel principal component analysis (KPCA).

Although significant research has focused on the use of multivariate statistical methods, these methods are yet to find wide spread industrial application. The lack of industrial application is in part due to a shortage of cost/benefit analysis and case studies, since the process monitoring and fault diagnosis benefits are difficult to quantify. A cost/benefit analysis will also require either accurate historical plant data or a complex dynamic model, based on a real-life process.

1.1.4 Profitable operation

The current economic environment has also increased the demand for profitable operation. Increased competition and varying customer demands need to be met with strict quality control measures. The possible economic benefit of fault detection and identification methods in modern metallurgical/chemical processes is yet to be evaluated. Early fault detection and identification may result in an increased time spent at the optimal operating conditions. Early fault detection may prevent unplanned maintenance, emergency shut-downs and decrease unsafe process conditions.

1.2 Mining in South Africa and process monitoring

The South African mining industry continuous to face economic challenges. The difficult economic environment is mainly due to hushed commodity prices, regulatory uncertainty and short term volatility. Mining safety has also continued to receive significant attention, with the overall fatality rate declining substantially over the past 20 years (PWC 2016).

The economic challenges and safety requirements have increased the need for resource efficiency, specifically to minimize process downtime and maximize process safety through advanced process control methods. Process monitoring is an advanced process control method where potential disastrous and unsafe events are detected early to ultimately avoid the unwanted consequences.

In order to investigate the application and potential implementation of process monitoring, it should be applied and evaluated on an actual industrial process. With testing on the actual plant usually not being an option, another methodology is usually required. A possible method is to test the application of process monitoring on a dynamic process model. Considering the complexity of most modern chemical processes, the dynamic model should include these complexities to accurately evaluate the possibility of process monitoring. However, the requirement of a complex dynamic process model is the major drawback for cost/benefit analysis, due to the effort required for the development of such a dynamic model.

1.3 Application of dynamic process models

Dynamic process models are mathematical models developed to mimic the operation of a given process. These models can be developed from first principles, historical process data or a combination of both first principles and historical process data. Once the dynamic model has been developed, it can be used to optimize processes or assess possible process changes. These changes could be the possible implementation of advanced control or process monitoring systems. Dynamic process models can also be further used to train operators. Operators first evaluate process changes using the dynamic model, before transitioning to the actual process.

With the ongoing increase in computational resources, more complex models are being developed in the metallurgical industry. Extensive research has been done on metal concentrators. This includes SAG mills, ball mills, crushers, screens, cyclones and flotation cells (Karelovic *et al*. 2016; dos Santos *et al*. 2014; Quist and Evertsson 2016; Salazar *et al*. 2009; Salazar *et al*. 2010).

Not much work has been conducted towards the development of hydrometallurgical complex dynamic models. Faris *et al.* (1992) developed a nickel and copper acid leach model. The work confirmed the possible use of dynamic models for operator training.

A dynamic model of the pressure leach at a base metal refinery (BMR) was developed by Dorfling (2012). The BMR removes copper and nickel from a precious metal containing residue. The dynamic process model accurately simulates the extent of both precious and base metals present in the process. The dynamic process model was more recently updated by Miskin (2015). A combination of expert knowledge and historical plant data were used to increase the accuracy of the dynamic model. The dynamic model includes the actual process control layers, a fault library and varying input conditions. Therefore the dynamic model poses the potential for accurately assessing possible process additions or changes.

1.4 Project aim and objectives

The main aim of this project is to determine whether abnormal process conditions can be detected and identified using multivariate detection methods at the BMR pressure leach and whether the multivariate fault detection will result in an economic gain. In order to achieve the main outcome, four objectives are identified:

1. Design and application of a process monitoring approach for fault detection and identification to simulated fault data.
2. Evaluation of a fault detection and identification approach based on process monitoring performance metrics.
3. Definition of economic key performance indicators for the pressure leaching process.
4. Evaluation of a fault detection and identification approach based on economic key performance indicators for the pressure leaching process.

The dynamic process model, developed by Dorfling (2012), can be used to simulate abnormal conditions and input process disturbances. The model was more recently updated by Miskin (2015), who increased the model complexity, to more accurately mimic actual plant operating conditions. The dynamic model will be the base from which the project aim is investigated.

1.5 Thesis layout

Chapter 2 provides a brief description of the BMR. A short process description and a summary of the process chemistry are included. The dynamic model developed by Dorfling (2012) is briefly described. A summary of the model validation and control implementation results by Miskin (2015) are provided.

Chapter 3 provides the relevant literature for each project objective. Multivariate fault diagnosis is described followed by a summary of significant results from previous studies. The development of economic performance functions are described with a focus on previous economic impact assessments.

The relevant tasks relating to each objective are outlined in Chapter 4. The first objective is addressed in Chapter 5. A fault detection and identification approach is designed. A methodology is provided for the application of the fault detection and identification approach to the simulated data.

The second objective is addressed in Chapter 6. The performance of the developed fault detection and identification approach is evaluated utilizing the traditional fault detection performance metrics. Chapter 7 addresses the third objective. Economic indicators are identified for the pressure leaching process. The economic indicators are used to develop specific economic performance functions for the process.

The final objective is addressed in Chapter 8. The performance of the fault detection and identification approach is evaluated with the economic performance functions developed in Chapter 7. Chapter 9 summarizes the work conducted in Chapters 5 – 8. Conclusions and recommendations are provided in Chapter 9.

Chapter 2: Process description

As discussed in Chapter 1, the base metal refinery (BMR) pressure leach model, developed by Dorfling (2012), will be used to assess the benefits of adding multivariate process monitoring methods. Chapter 2 aims to familiarize the reader with the dynamic model and the changes made by Miskin (2015).

A brief process description of the BMR is provided in section 2.1, followed by a summary of the process chemistry in section 2.2. The dynamic model developed by Dorfling (2012) is briefly described in section 2.3, while the model validation and control implementation results from Miskin (2015) is also summarized. The Chapter is summarized in section 2.4.

2.1 Base metal refinery

The Bushveld complex, located in South Africa, is home to the world's largest deposit of Platinum Group Elements (PGEs). Today the world's three largest PGE producers, Anglo American Platinum, Lonmin Platinum and Impala Platinum are operating on the Bushveld complex (van Schalkwyk, 2011).

After ore has been extracted from the Bushveld complex, it is sent to comminution circuits followed by flotation circuits. Thereafter the ore is sent to a smelter where a Ni-Cu-Fe-S converter matte is produced which contains the Platinum Group Minerals (PGMs) (van Schalkwyk, 2011).

The converter matte is then sent to the Base Metal Refinery (BMR), situated northwest of Johannesburg, South Africa. An overall schematic of the process is provided in Figure 2.1. The converter matte is sent through a milling circuit in preparation for the BMR. The milled converter matte is next sent to the first stage atmospheric leach. The first stage leach consists of five continuously stirred reactors (CSTRs) and oxygen is continuously sparged into the first three reactors (Lamya, 2007). Spent electrolyte is recycled from the copper electrowinning circuit and added to the first stage atmospheric leach. Approximately 70% of the nickel present in the feed is dissolved as well as most of the sulphuric acid is depleted from the recycled spent electrolyte (Dorfling *et al*. 2013). Refer to van Schalkwyk (2011) and Coetzee (2016) for an in-depth review of the first stage leach and nickel crystallizer.

The first stage leach residue is then sent to the second and third stage pressure leach. The autoclave consists of four compartments. The second stage consists of the first three compartments, while the third stage is defined as the fourth compartment of the autoclave. The compartments allow for improved control of the temperature and residence time. The pressure in the autoclave is controlled by manipulating the oxygen flow to the autoclave. The pressure control ensures the oxygen partial

pressure is adequate for the reactions presented in section 2.2. The second stage product is sent to a solid/liquid separator and the residue sent to the fourth compartment (Dorfling 2012).

The solid residue from the pressure leaching system is then sent to a caustic leach and a formic acid leach. The remaining copper, selenium and tellurium is removed, resulting in a concentrated PGE stream. The PGE concentrate is sent to the precious metal refinery (PMR) where pure PGEs are produced (Dorfling 2012).

The liquid residue of the pressure leach consists mainly of copper, nickel, diluted sulphuric acid and traces of iron. The liquid residue is first sent to a selenium and tellurium removal unit. Once the selenium and tellurium have been removed, the product is sent to a copper electrowinning circuit. The selenium and tellurium needs to be removed in order to prevent poisoning of the copper cathodes in the electrowinning circuit (Lamya 2007).

This project will focus on the second and third stage pressure leaching process. The typical operating conditions are given in Table 2.1 (Miskin 2015).

Table 2.1: Pressure leach process typical operating conditions (Miskin 2015).

Operating condition	Compartment			
	1	**2**	**3**	**4**
Temperature (^{o}C)	130	130	125	140
Level (%)	-	-	70	80
Redox potential (mV)	350 - 380	-	450 - 480	520 - 550
Acid concentration (g/L)	18 - 25	15 – 20	-	35 - 45

The autoclave is typically operated at a pressure of 5.5 bar and temperatures of 125˚C - 140˚C (Dorfling 2012). Temperatures above 150˚C will damage the linings in the autoclave. There are two autoclaves available at the BMR. The autoclaves can be operated in parallel if an increased production rate is required. A complete process flow diagram of the pressure leach section is provided in Appendix A.
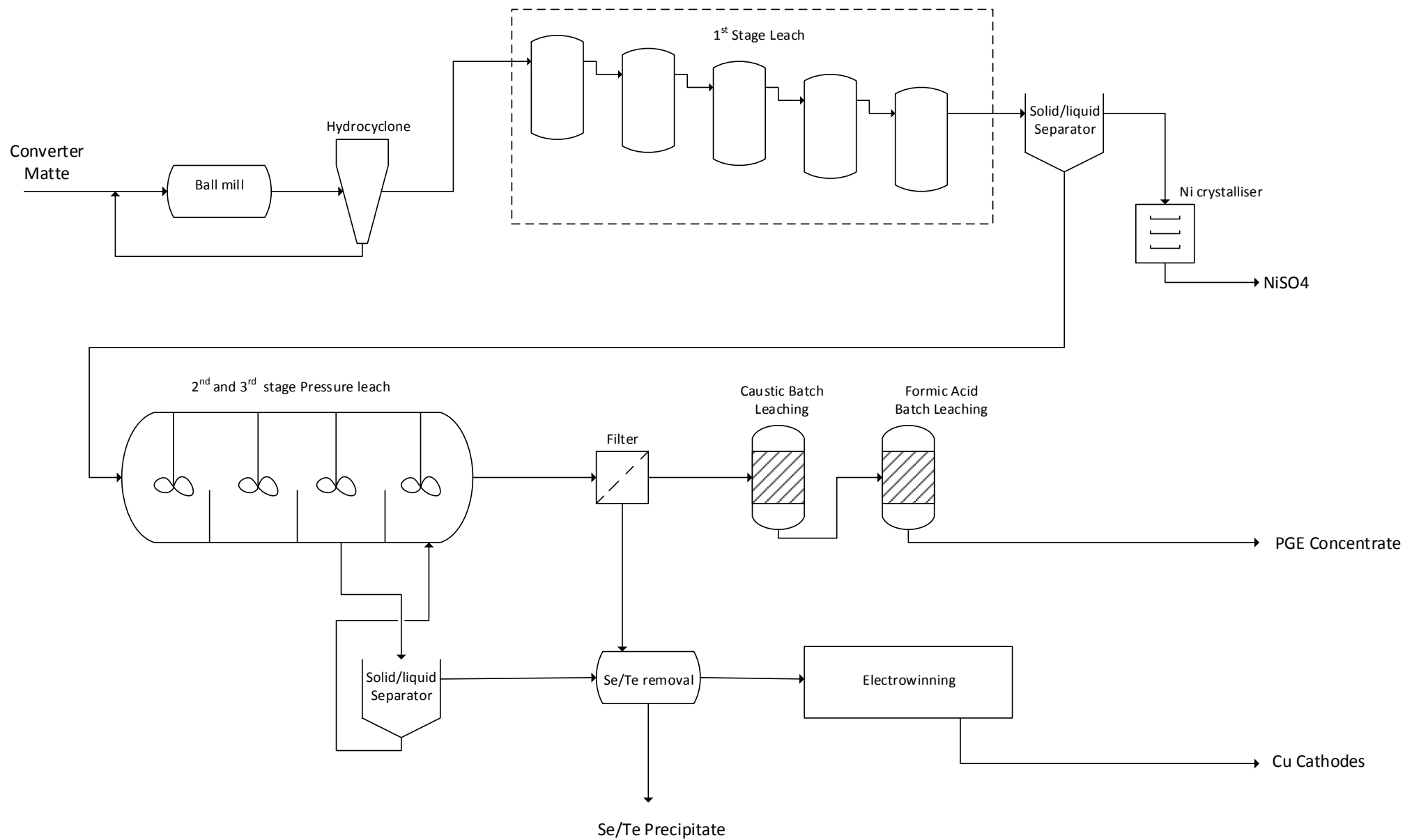
Figure 2.1: Simplified flowsheet of the BMR..

2.2 Process Chemistry

The process chemistry of the pressure leaching process can be categorized as either base metal leaching chemistry or PGM leaching chemistry. The base metal leaching chemistry is provided in section 2.2.1 and the PGM leaching chemistry is provided in section 2.2.2.

2.2.1 Base Metals

Rademan *et al*. (1999), Lamya (2007) and van Schalkwyk (2011) all investigated the first stage Ni-Cu-Fe-S matte leaching with sulphuric acid. Both oxygen and sulphuric acid are required to rapidly remove the Ni from the matte, while Cu present in the recycled spent electrolyte is precipitated back through cementation and metathesis reactions.

Rademan *et al*. (1999) investigated the pressure leaching of the first stage leach residue. It was concluded that the base metal leaching chemistry is observed in three steps.In the first step, nickel is leached from the residue, while copper ions are precipitated back. Reactions 1 – 4 shows both the nickel dissolution and cupper precipitation (Rademan *et al*. 1999)

$Ni + 2H^+ + 0.5O_2 \rightarrow Ni^{2+} + H_2O$ **Reaction 1**

$Ni_3S_2 + 2H^+ + 0.5O_2 \rightarrow Ni^{2+} + 2NiS + H_2O$ **Reaction 2**

$Ni_3S_2 + 2Cu^{2+} \rightarrow Cu_2S + NiS + 2Ni^{2+}$ **Reaction 3**

$Ni_3S_2 + Ni + 4Cu^{2+} \rightarrow 2Cu_2S + 4Ni^{2+}$ **Reaction 4**

The copper can then be removed through reaction 5 (Dorfling 2012).

$5Cu_2S + 2H^+ + 0.5O_2 \rightarrow Cu^{2+} + 5Cu_{1.8}S + H_2O$ **Reaction 5**

Copper is both leached and precipitated in the second step. The dissolution of copper is given in reaction mechanisms 6 – 8 (Rademan *et al*. 1999)

$25Cu_{1.96}S + 8H^+ + 2O_2 \rightarrow 4Cu^{2+} 25Cu_{1.8}S + 4H_2O$ **Reaction 6**

$16Cu_2S + 2H^+ + 0.5O_2 \rightarrow Cu^{2+} + Cu_{31}S_{16} + H_2O$ **Reaction 7**

$10Cu_{31}S_{16} + 44H^+ + 11O_2 \rightarrow 22Cu^{2+} + 16Cu_{1.8}S + 22H_2O$ **Reaction 8**
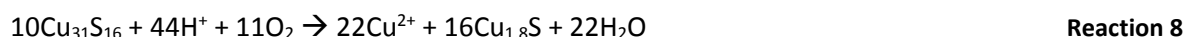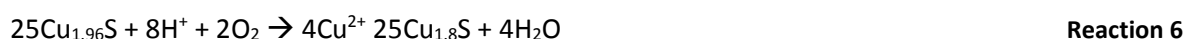
The final step, step three, involves the simultaneous leaching of both copper and nickel as given in reaction mechanisms 9 – 12 (Rademan *et al*. 1999)

$5Cu_{1.8}S + 8H^+ + 2O_2 \rightarrow 4Cu^{2+} + 5CuS + 4H_2O$ **Reaction 9**

$5Cu_{1.8}S + 8Fe^{3+} \rightarrow 4Cu^{2+} + 5CuS + 8Fe^{2+}$ **Reaction 10**

$$2Ni_3S_4 + 2H_2O + 15O_2 \rightarrow 6Ni^{2+} + 4H^+ + 8SO_4^{2-}$$ **Reaction 11**

$$2Ni_3S_4 + 6Cu^{2+} + 2H_2O + 3O_2 \rightarrow 6Ni^{2+} + 6CuS + 4H^+ + 2SO_4^{2-}$$ **Reaction 12**
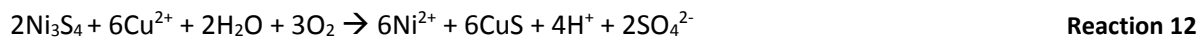
Two groups of the most important reactions occurring in the fourth and final leaching compartment were defined by Steenkamp and Dunn (1999). The first group involves the leaching of the first stage leach hydrolysis products as given by reactions 13 -14.

$$Cu(OH)_2CuSO_4 + H_2SO_4 \rightarrow 2CuSO_4 + 4H_2O$$ **Reaction 13**

$$2Fe(OH)SO_4 + H_2SO_4 \rightarrow Fe_2(SO_4)_3 + 2H_2O$$ **Reaction 14**

The second group is defined by the oxidation of the sulphide minerals, as given by reactions 15 – 17 (Steenkamp and Dunn 1999).

$$NiS + 2O_2 \rightarrow NiSO_4$$ **Reaction 15**

$$2Cu_2S + 2H_2SO_4 + 5O_2 \rightarrow 4CuSO_4 + 2H_2O$$ **Reaction 16**

$$CuS + 2O_2 \rightarrow CuSO_4$$ **Reaction 17**

2.2.2 Platinum Group Metals

The PGMs consists out of platinum (Pt), rhodium (Rh), ruthenium (Ru) and iridium (Ir), other precious metals (OPMs) is defined as the latter three. Dorfling (2012) investigated the leaching mechanisms of the OPMs.

Cementation reactions occurs with all OPMs, resulting in the formation of oxides as shown in reaction 18 and 19, with {X} representing the OPM. The cementation can either occur with copper or nickel (Dorfling 2012).

$$8\{X\}^{3+} + 3Cu_9S_5 + 38O_2 \rightarrow 8\{X\}O_2 + 27Cu^{2+} + 15SO_4^{2-}$$ **Reaction 18**

$$2\{X\}^{3+} + Ni_3S_4 + 4H_2O + 8O_2 \rightarrow 2\{X\}O_2 + 3Ni^{2+} + 8H^+ + 4SO_4^{2-}$$ **Reaction 19**
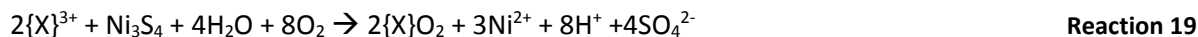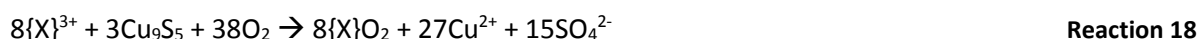
The OPM's present in the alloy phase or as an oxide, can be leached according to reactions 20 and 21 (Dorfling 2012).

$$4\{X\} + 3O_2 + 12H^+ \rightarrow 4\{X\}^{3+} + 6H_2O$$ **Reaction 20**

$$2\{X\}O_2 + 6H^+ \rightarrow 2\{X\}^{3+} + 3H_2O + 0.5O_2$$ **Reaction 21**

The remaining OPM-sulphide minerals can be leached through reactions 22 – 24 respectively (Dorfling 2012).

$Ir_2S_3 + 6O_2 \rightarrow 2Ir^{3+} + 3SO_4^{2-}$ **Reaction 22**

$Rh_2S_3 + 6O_2 \rightarrow 2Rh^{3+} + 3SO_4^{2-}$ **Reaction 23**

$4RuS_2 + 2H_2O + 15O_2 \rightarrow 4Ru^{3+} + 8SO_4^{2-} + 4H^+$ **Reaction 24**
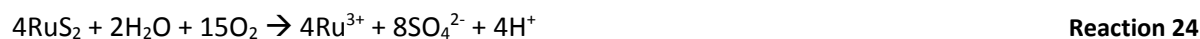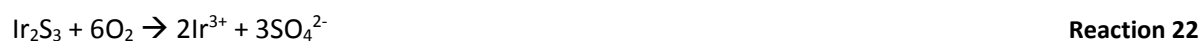
2.3 Pressure leaching system dynamic model

2.3.1 Model development

A dynamic model of the pressure leaching process was developed by Dorfling (2012). Batch experiments were conducted by Dorfling (2012) in order to determine the rate constants for 21 of the chemical reactions in the pressure leaching process. Mass and energy balances along with constitutive equations were used to complete the open-loop dynamic model. The final model consists of 217 ordinary differential equations. The model predicts the extent of leaching of Cu, Fe, Ni, Rh, Ir and Rh. Pt and Pd leaching are not included in the dynamic model.

The MATLAB® model was transferred to a Simulink® model by Haasbroek and Lindner (2015). A flow-sheet of the dynamic model is provided in Figure 2.2. Refer to Appendix A for a complete process flow diagram of the Simulink® model.

Several assumptions were made by Dorfling (2012) with the development of the dynamic model. These assumptions were investigated by Miskin (2015) through model validation. A summary of the model validation is provided in section 2.3.2.
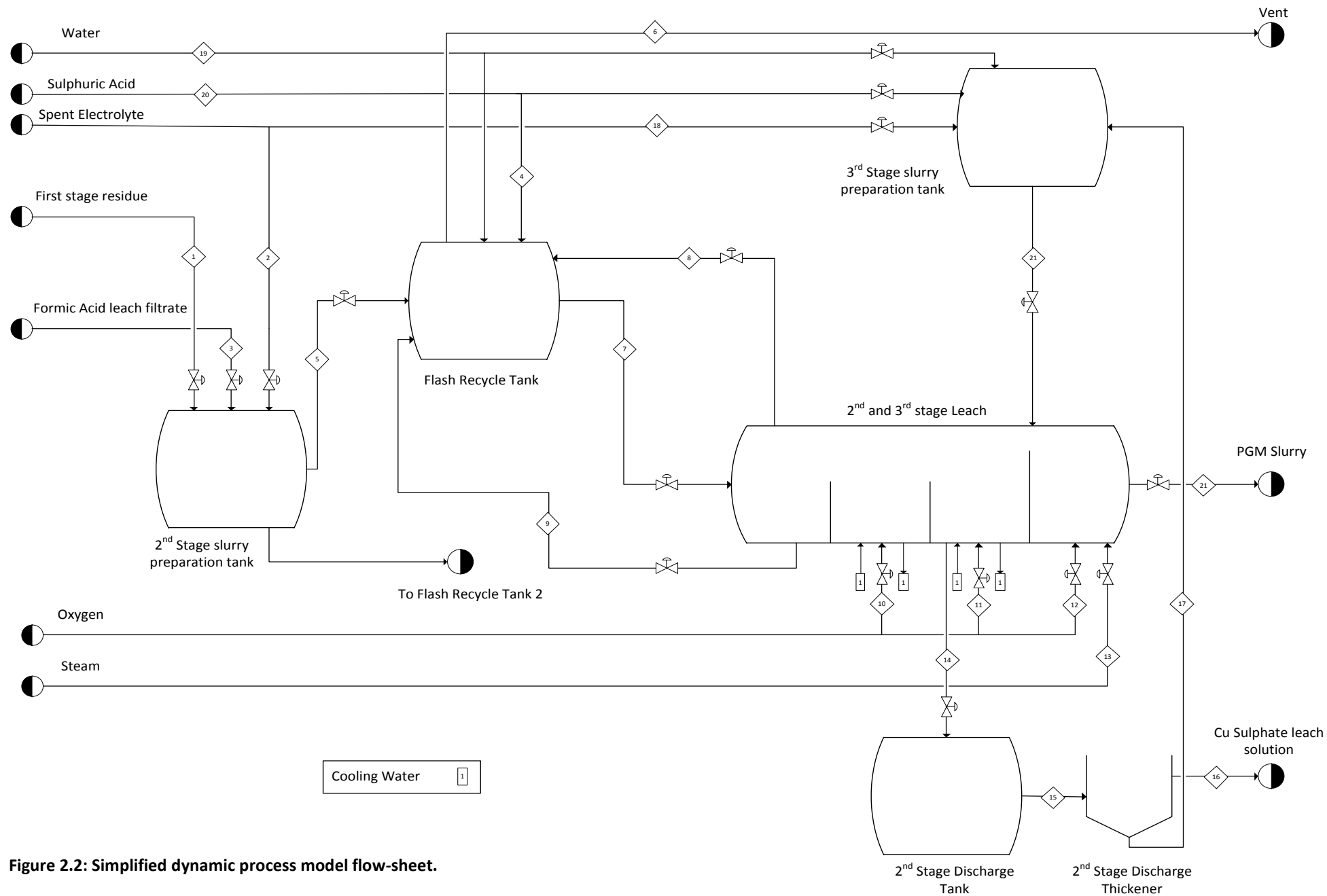
Figure 2.2: Simplified dynamic process model flow-sheet.

Labels in figure: Water, Sulphuric Acid, Spent Electrolyte, First stage residue, Formic Acid leach filtrate, Oxygen, Steam, Cooling Water, Vent, PGM Slurry, Cu Sulphate leach solution, 3rd Stage slurry preparation tank, 2nd Stage slurry preparation tank, Flash Recycle Tank, To Flash Recycle Tank 2, 2nd and 3rd stage Leach, 2nd Stage Discharge Tank, 2nd Stage Discharge Thickener

2.3.2 Model validation

Miskin (2015) followed a validation approach set out by Sargent (2005). The Sargent (2005) validation approach consists of four categories: data validity, conceptual model validation, computerized model validation and operational validation. The assumptions made by Dorfling (2012) were all included in the four validation categories.

Several model updates were incorporated by Miskin (2015) during the model validation process. The updates resulted in a more robust model with the final goal of being able to accurately simulate abnormal process conditions.

Dorfling *et al*. (2013) noted that the extent of leaching predicted by the model was inaccurate. Miskin (2015) was unable to improve the extent of leaching predicted by the dynamic model. This is due to the experimental constants determined through the experimental leaching tests. Higher acid concentrations were used by Dorfling (2012) during the experimental tests than is typically observed in the BMR. However, the dynamic model can adequately predict the dynamic changes from process changes and disturbances.

2.3.3 Control implementation

Miskin (2015) further aimed to improve the dynamic process model with the implementation of the actual control layers present at the BMR. Miskin (2015) first implemented the regulatory control present at the BMR. All regulatory controllers currently present at the pressure leaching process were successfully incorporated and validated. A summary of the regulatory controllers present at the pressure leaching process are provided in Table 2.2. Table 2.2 provides the controller tag, controlled variable (CV), manipulated variable (MV) and controller algorithm. Controller algorithms include proportional integral (PI) and proportional integral derivative (PID) controllers. Refer to appendix A for a complete process flow diagram with process controller tags.

Four supervisory controllers present at the pressure leaching process were also included in the dynamic process model. 33 alarm systems and 37 interlocks were included by Miskin (2015). It was also noted by Miskin (2015) that most alarm systems were set to default values and not in use. However, the alarm systems set points are not suitable when using the dynamic model, due to the offset in predictions between the plant and the dynamic model.

Table 2.2: Dynamic process model regulatory process controllers.

Controller Tag	Controlled Variable (CV)	Manipulated Variable (MV)	Control algorithm
Flow control			
FIC-0106	Flow (Stream 1)	Valve (Stream 1)	PI
FIC-0101	Valve (Stream 2)	Valve (Stream 2)	PI
FIC-1102	Valve (Stream 3)	Valve (Stream 3)	PI
FIC-0202	Valve (Stream 4)	Valve (Stream 4)	PI
FIC-0201	Valve (Stream 5)	Valve (Stream 5)	PI
FIC-0203	Valve (Stream 7)	Valve (Stream 7)	PI
FIC-0205	Valve (Stream 9)	Valve (Stream 9)	PI
FIC-3001A	Valve (Stream 10)	Valve (Stream 10)	PI
FIC-3001B	Valve (Stream 11)	Valve (Stream 11)	PI
FIC-3001C	Valve (Stream 12)	Valve (Stream 12)	PID
FIC-3002	Valve (Stream 14)	Valve (Stream 14)	PI
FIC-0401	Valve (Stream 15)	Valve (Stream 15)	PI
FIC-0150-3	Valve (Stream 21)	Valve (Stream 21)	PI
FIC-0150-4	Valve (Stream 20)	Valve (Stream 20)	PI
FIC-0150-5	Valve (Stream 18)	Valve (Stream 18)	PI
FIC-0150-9	Valve (Stream 19)	Valve (Stream 19)	PI
FIC-3003	Valve (Stream 22)	Valve (Stream 22)	PI
Level control			
LIC-0101	Level (TK-10)	Flow (FIC-0106)	Cascade PI
LIC-0201	Level (TK-20)	Flow (FIC-0203)	Cascade PI
LIC-0401	Level (TK-40)	Flow (FIC-0401)	Cascade PID
LIC-151	Level (TK-150)	Flow (FIC-0150-9)	Cascade PID
LIC-3002	Level (compartment 3)	Flow (FIC-3002)	Cascade PI
LIC-3003	Level (compartment 4)	Flow (FIC-3003)	Cascade PI
Density control			
-	Density (Stream 5)	Flow (FIC-0101)	Feedforward
Temperature control			
TIC-3001	Temperature (compartment 1)	Flow (FIC-0205)	Cascade PI
TIC-3003	Temperature (compartment 2)	Valve (CW in AC2)	PID
TIC-3004	Temperature (compartment 3)	Valve (CW in AC3)	PI
TIC-0401	Temperature (TK-40)	Valve (CW in TK-40)	PI
TIC-3005	Temperature (compartment 4)	Valve (Stream 13)	PI
Pressure control			
PIC-3001	Pressure (Autoclave)	Flow (Stream 10+11+12)	Cascade PI

2.3.4 Stochastic disturbance modelling (random walks)

In order to further mimic true plant operation, Miskin (2015) introduced stochastic input disturbance changes in the form of input random walks. These random walks simulate varying compositional input conditions. Upper and lower bounds were determined from historical plant data. A random seed is used to initialize the random walk from a random position.

Figure 2.3 show Ru, Rh, Fe, Ir, Ni, Cu input concentration variations. The scaled concentrations variations are similar to that observed from historical plant data.
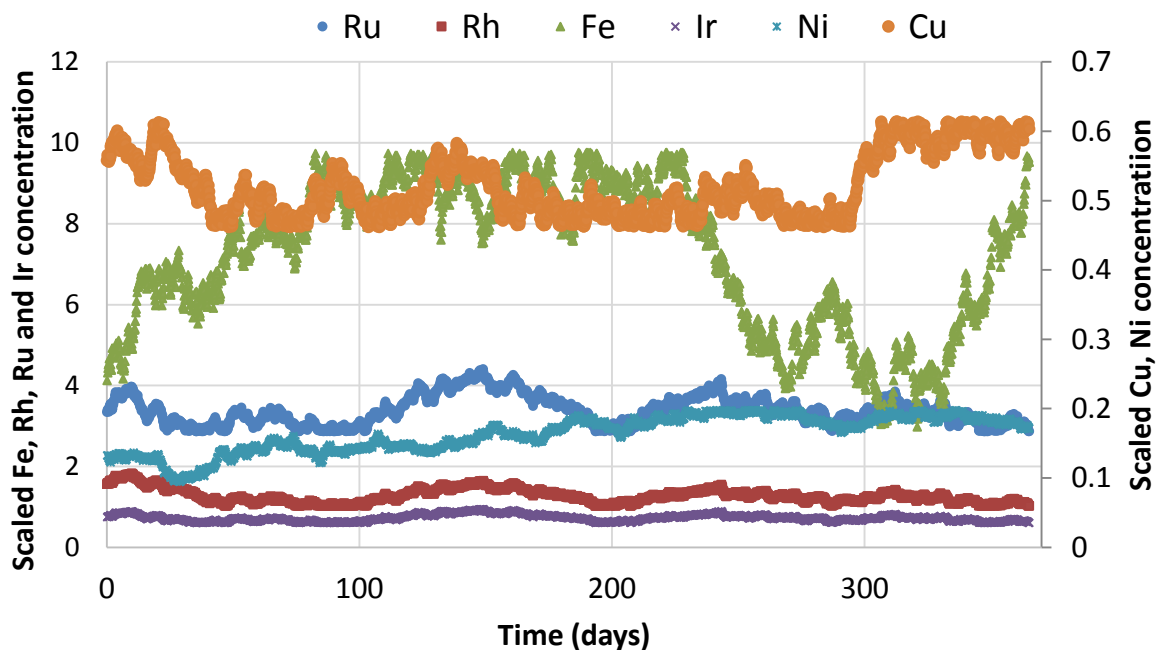
Figure 2.3: Stochastic input disturbance modelling example. **Concentrations are scaled, and show the variation over a 365 day period (Miskin 2015).**

2.4 Summary

It is clear that the pressure leach at the BMR has received significant attention through, most recently, the research conducted by Miskin (2015) and Dorfling (2012). The dynamic model now poses the potential to be used for the accurate evaluation of potential process changes as mentioned in Chapter 1, section 1.3. Furthermore, the dynamic model provides the potential to not only investigate the efficacy of potential process changes, but also to investigate the profitability of these potential process changes.

Chapter 3: Literature review

Chapter 3 provides an in-depth literature review on multivariate fault diagnosis and economic impact assessment. The literature will form the basis from which to evaluate the potential benefit and implementation of the multivariate fault diagnosis methods.

A fault library developed by Miskin (2015) is described in section 3.1, followed by a brief summary on the impact of each individual fault on the process. Linear and nonlinear multivariate statistical fault detection and identification methods are described in sections 3.2 – 3.4. Hyper-parameter selection for both PCA and KPCA is described. Significant results from previous fault detection and identification results are investigated and summarized.

An economic performance evaluation technique is discussed in section 3.5. Significant results from previous economic impact assessments are investigated and summarized.

3.1 Faults in the process engineering industry

3.1.1 Process faults and failures

A fault is defined by Isermann (2005) as "an unpermitted deviation of at least one characteristic property of the system from the acceptable, usual, standard condition." (Isermann, 2005, p.20). A failure is defined by Isermann (2005) as "a permanent interruption of a system's ability to perform a required function under specific operating conditions" (Isermann, 2005, p.20).

Faults in the chemical/metallurgical engineering industry can be further categorized according to the sources of the specific faults. These faults can be abrupt, intermittent or can develop over several months depending on the nature of the fault. Each type of fault appearance is described in Figure 3.1. The abrupt fault is immediate, while the incipient fault effect develops over a certain period of time. The intermittent appears and disappears inconsistently with time (Isermann, 2005).
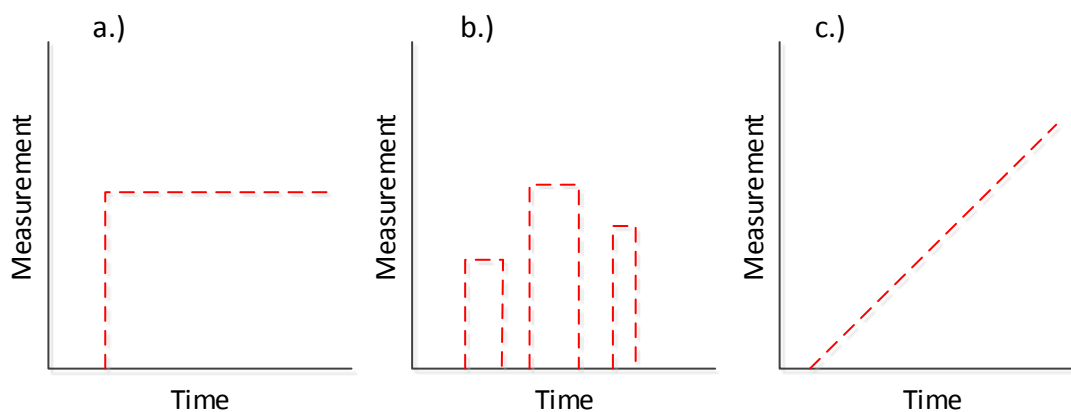
Figure 3.1: Fault types: a) abrupt, b) intermittent and c) incipient.

3.1.2 Impact of faults in the process engineering industry

Any abnormal process behaviour can lead to a number of problems, including deviations in product purity, production/throughput limitations, increased maintenance etc. (Russel *et al*. 2000). According to Venkatasubramanian *et al.* (2003) the petrochemical industry loses $20 billion a year due to abnormal (faulty) process conditions.

3.1.3 BMR fault database

Miskin (2015) developed a fault database for the pressure leaching process present at the BMR. The faults were obtained from expert knowledge, following a site visit by Miskin (2015). A total of seventeen faults were identified and categorized as actuator failure, structural failure, incorrect operator intervention, sensor failure or controller malfunctions.

A total of eight faults were successfully modelled and incorporated into the dynamic pressure leaching model. It is possible to simulate some faults; however, it is impossible to incorporate some faults into the current dynamic model resolution or the current dynamic model scope e.g. the simulation of the crystallization of metals cannot be incorporated into the resolution of the current reaction kinetics.

All the simulated faults are provided in Table 3.1. All the faults either have a medium or high priority for mitigation according to expert knowledge collected by Miskin (2015).

Table 3.1: Simulated fault database. All faults have either a medium or high priority for mitigation (Miskin 2015).

#	Fault	Classification	Priority for fault mitigation
1	Valve blockage (density disturbance)	Actuator failure	High
2	Valve wear	Actuator failure	High
3	Valve stiction	Actuator failure	Medium
4	Pump impeller wear	Structural failure	High
5	Solid build-up in cooling coils	Structural failure	High
6	Peristaltic pump tube failure	Structural failure	High
7	Sulphuric acid controller misuse	Operator intervention	Medium
8	Bubbler level sensor blockage	Sensor failure	Medium

The above faults simulated by Miskin (2015) will be the faults considered in this project. Single fault simulations were carried out by Miskin (2015) and the individual fault impacts were noted through key performance indicators (KPIs). Results obtained by Miskin (2015) for each fault are summarized in sections 3.1.3.1 – 3.1.3.8. The location of each fault is indicated in Figure 3.2.
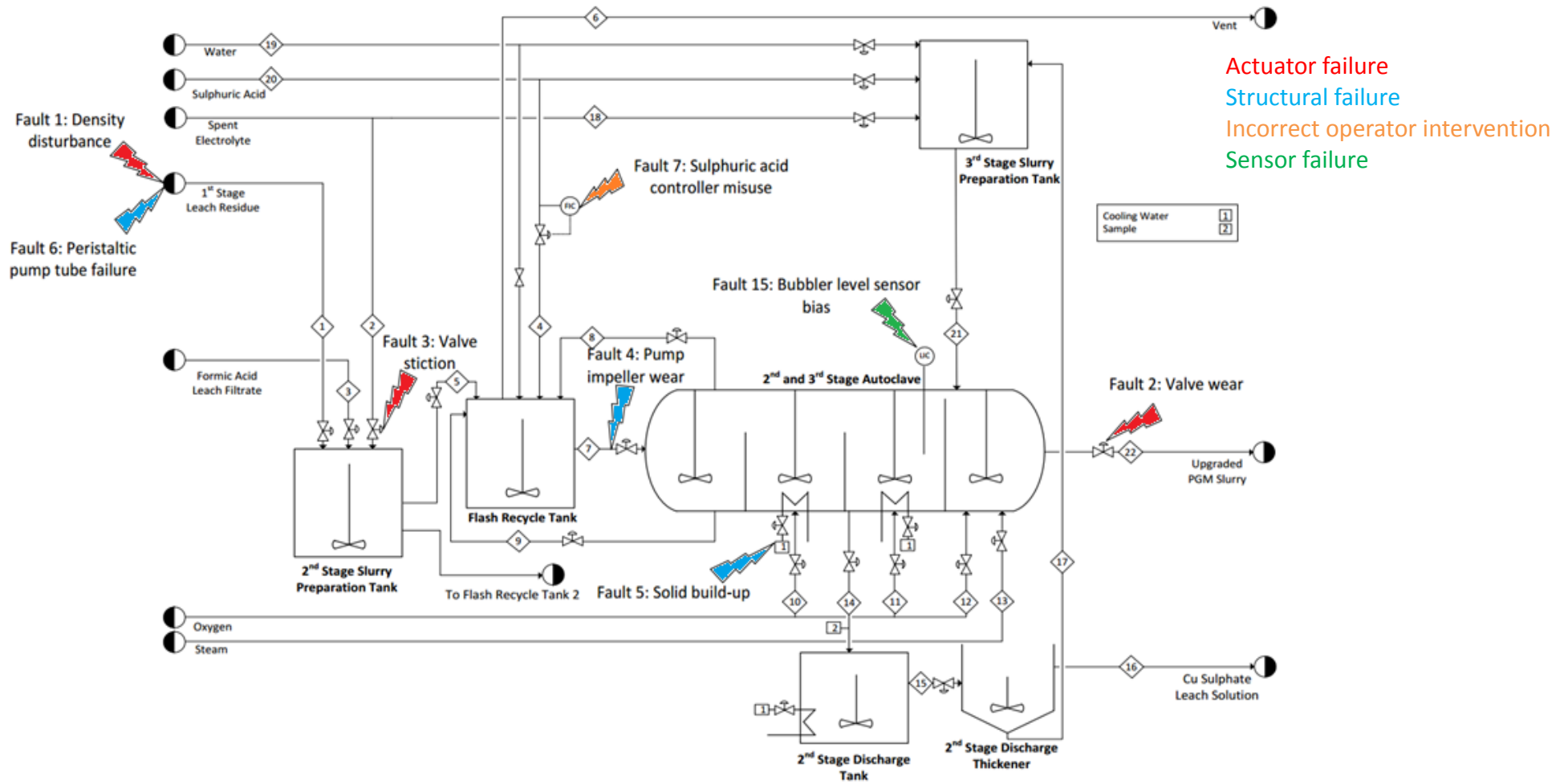
Figure 3.2: BMR simulated fault locations and fault types.

3.1.3.1 Valve Blockage (density disturbance)

A valve in the first stage leach residue stream often blocks, resulting in a density disturbance. Five density spikes were incorporated into the first stage residue feed stream, in order to simulate the fault occurrence. The density spikes are based on historical plant data of the fault (Miskin 2015).

The largest deviation was observed in the level of second stage slurry preparation stage. However, the disturbance had a lesser effect on downstream processing. Increased base metal filtrate content in all the pressure leach compartments was observed. This was attributed to an increase in first stage solid residue flow. The resulting increase in solids resulted in a decreased PGM concentration in the pressure leach liquid residue, due to an increased reaction surface area (Miskin 2015).

Miskin (2015) noted that although the effects of the disturbance were quite small and the changes in base metal and PGM concentration is not unwanted, the fault occurs almost every 24 hours. The cumulative impact of the fault can have a detrimental impact on the process.

3.1.3.2 Valve Wear

The outlet valve of the fourth pressure leaching compartment suffers from significant valve wear. The valve wear was modelled by simulating the change of the valve towards a quick opening valve. Historical plant data of the valve wear was used to determine the degree of wear (Miskin 2015).

The largest variation occurred at the origin of the fault i.e. the fourth compartment outlet stream. The fault had an overall insignificant impact, since the valve travel distance was decreased, resulting in better process performance. However, the controllers will struggle to mitigate further disturbances, since they were tuned for a linear response valve and not a quick opening valve (Miskin 2015).

3.1.3.3 Valve Stiction

The valve on the second stage slurry preparation tank spent electrolyte feed was identified as being subject to the occurrence of valve stiction (Miskin 2015).

The fault caused oscillatory behaviour in the flow controller input. The resulting valve stiction heavily influences both the performance of the spent electrolyte controller and the second stage slurry preparation tank density controller. The final result is a decrease in the outlet density of the second stage preparation tank (Miskin 2015).

The resulting decrease in density has a significant effect on the temperature and pressure of the pressure leaching system. Since the entry stream to the pressure leaching system has a constant volumetric flow rate, the decrease in density causes a decrease in solids concentration and an increase in both sulphuric acid and formic acid concentrations. The decrease in solids presence

resulted in a decreased amount of heat released per unit of volume. The lack of heat released caused significant deviations in both temperature and pressure throughout each compartment (Miskin 2015).

Furthermore, the amount of PGMs in the liquid phase increased on average by 78% throughout each compartment. Miskin (2015) concluded that this is due to an increase in the rates at which the PGMs are leached.

3.1.3.4 Pump Impeller Wear

The pump at the outlet of the flash recycle tank often suffers from impeller wear, due to the highly abrasive slurries. Miskin (2015) incorporated the fault by assuming a constant rate of impeller wear.

Initially the flash recycle tank outlet valve is able to deal with the disturbance, however, once it became saturated, the flow in the flash recycle tank outlet stream decreased dramatically. The fault caused large deviations throughout the process. The largest deviations occurred in the third compartment (Miskin 2015).

The first compartment temperature and outlet flow-rate oscillated significantly. In order to rectify the temperature variation, the controller tries to increase the inlet flow-rate; however, the worn pump impeller is unable to increase the flow-rate. The result is significant increases in the flash recycle tank level (Miskin 2015).

The first compartment level immediately decreases. The temperature controllers are unable to reach their set-points in all compartments. The largest deviations are noted in the third leaching compartment (Miskin 2015).

In order to keep the flash recycle tank from overflowing, the feed stream from the second stage preparation tank is decreased. This causes the level in the second stage slurry preparation tank to start rising significantly. The first stage leach residue feed stream flow is then reduced, to combat the rapid rise in tank volume. The spent electrolyte and formic acid flow-rates are controlled via a feed-forward controller, with the first stage leach residue stream as input. However, due to large noise in the first stage leach residue measurement, the second stage slurry preparation tank increases for several hours, before the level starts to drop again. This resulted in an unacceptable decrease in the second stage slurry preparation tank outlet density (Miskin 2015).

3.1.3.5 Solid Build-up in cooling coils

Cooling coils present in the pressure leaching system compartments can get blocked due to solid build-up from hard water being used. The second compartment cooling coil was considered as the location of the fault (Miskin 2015).

Initially the valve present on the cooling coil tries to increase the flow-rate, however it quickly reaches saturation. The second compartment temperature can then no longer be controlled. The fault then caused large deviations in several sections of the process (Miskin 2015).

Large temperature deviations were noted in both compartments one and two. The second compartment temperature increases significantly, reducing the partial pressure of oxygen, which in turn reduces the rate at which base metals are leached in the first compartment. The lack of base metal leaching results in a temperature decrease in the first compartment (Miskin 2015).

Again, significant increases in PGM concentrations were noted in all the compartments. An increase in base metal concentration was observed in the solid phase for all compartments. The reason for the deviations is mainly due to the temperature variations, which directly influence the reaction rates (Miskin 2015).

3.1.3.6 Peristaltic Pump tube failure

A peristaltic pump tube upstream from the pressure leaching system often fails and causes the pipe to block. The fault was simulated as an abrupt stoppage of the first stage residue stream (Miskin 2015).

The largest deviation was observed to be the PGM concentration in the exit stream of the pressure leaching system. Again, the density in the second stage slurry preparation tank is decreased, resulting in a decreased availability of base metal reaction surface. The PGM leaching rate is then increased which results in an increased concentration of PGMs in all compartments (Miskin 2015).

3.1.3.7 Sulphuric Acid controller misuse

The sulphuric acid concentration in the flash recycle tank is manually kept above 20 g/L. Operators often open the flow of sulphuric acid into the flash recycle tank and then forget to close it again. Miskin (2015) determined that the sulphuric acid stream will be left unattended for 2 hours, before it is realized that the sulphuric acid concentration is too high. The result is simulated as a sulphuric acid concentration spike approximately every two hours (Miskin 2015).

The largest deviation was observed in the pressure of each compartment. Furthermore, a decrease in base metal concentrations in all compartments was observed. This is primarily due to the increased acid availability, resulting in an increased leaching of base metals. Furthermore, the same is true for the PGM concentration in the liquid phase (Miskin 2015).

3.1.3.8 Bubbler level sensor blockage

Most level sensors currently present in the BMR are bubbler level sensors. Occasionally solids are lodged into the bubbler level sense tubes, resulting in an increased pressure drop and ultimately in a positive biased level reading (Miskin 2015).

A level sensor situated in the third compartment was identified as the possible location of the fault. A bias is added to level reading in order to simulate the fault. The result is an immediate decrease in the actual level of compartment three (Miskin 2015).

The largest deviation was observed in the third compartment level controller performance. Furthermore a significant increase in the PGM concentration in the third compartment liquid phase was observed. Since the volume is decreased, the residence time is also decreased, resulting in insufficient time for PGM precipitation. The insufficient PGM precipitation resulted in an increased amount of base metals present in the third compartment solid phase (Miskin 2015).

3.2 Fault detection

3.2.1 Univariate fault detection

Univariate statistical monitoring involves the monitoring of individual process variables and is the traditional and most basic process monitoring method. The upper and lower control limit of the variable are pre-defined and an alarm is triggered when the variable is detected outside its set control limits (Russell *et al*. 2000). A univariate monitored process variable example is provided in Figure 3.3. Once an observation moves outside either the lower or upper control limit, it indicates a potential abnormal process condition.
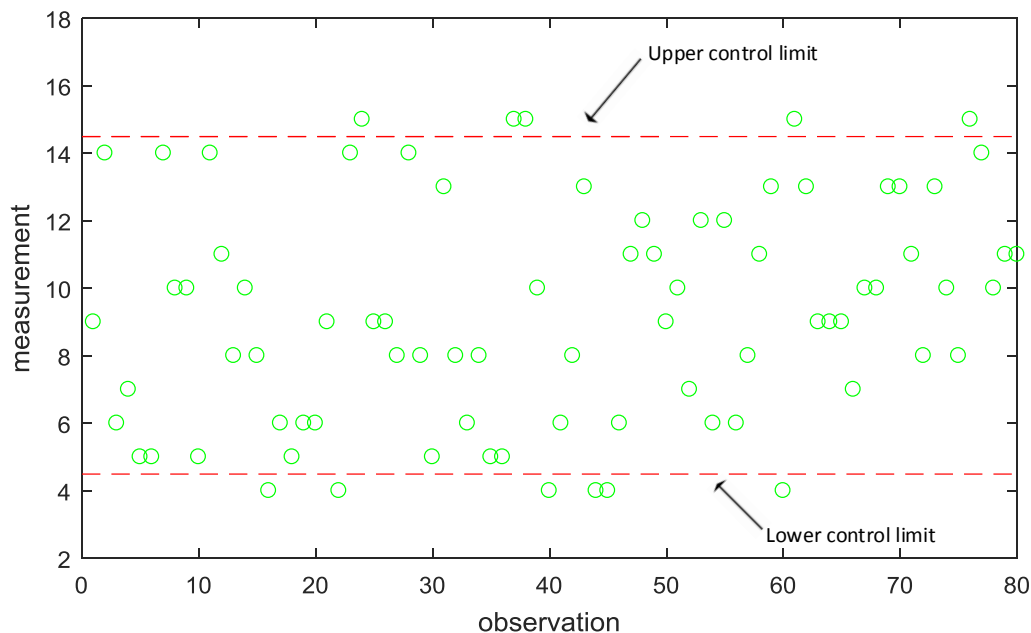
Figure 3.3: Univariate monitoring chart example. Both upper and lower limits are indicated in red. Process measurements are indicated in green.

The main drawback of univariate statistical monitoring is the lack of considering the other process variables when determining the upper and lower control thresholds for an individual process variable. Most modern chemical processes require that the information contained within the correlation between variables is taken into account for accurate process monitoring (Russell *et al*. 2000).

Another potential problem with univariate process monitoring is the high dimensionality of the process data. Most modern chemical and metallurgical processes have multiple process measurements which results in a highly dimensional process measurement data set. Monitoring each of these process measurements individually will be challenging and can easily result in alarms triggered exceeding the allowed amount per process operator.

Figure 3.4 provides an example where univariate monitoring will be ineffective. The individual upper and lower control limits of each process variables do not indicate any abnormal process condition. However, observing the trend in Figure 3.4, it is clear that there is an abnormal (faulty) measurement.
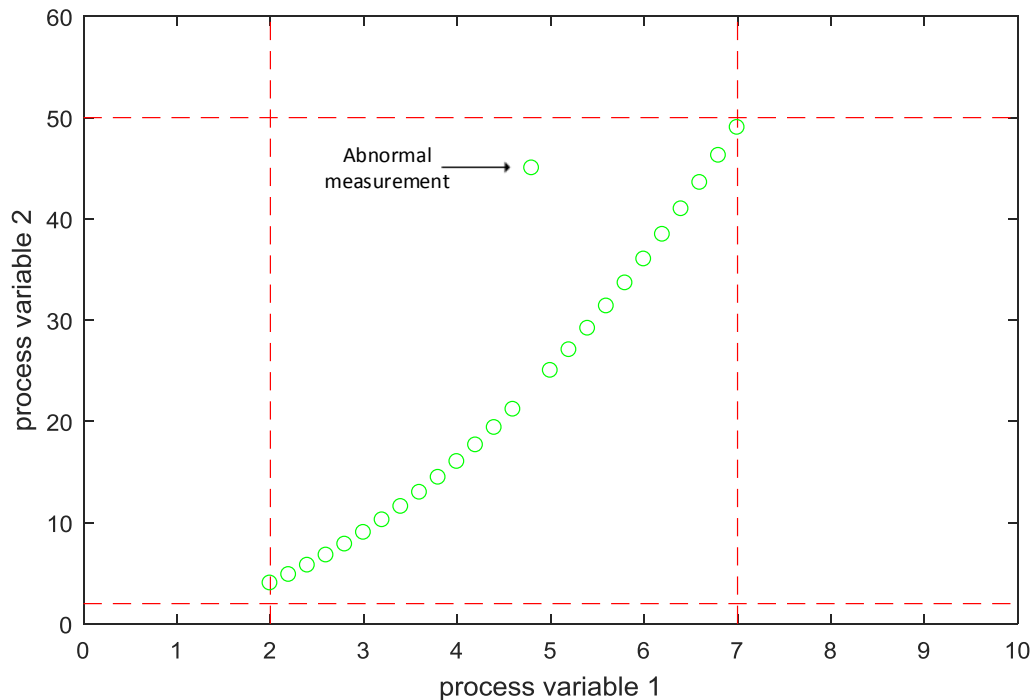
Figure 3.4: Univariate detection unable to capture correlation between process variables. Univariate control limits are indicated in red. Process measurements are indicated in green.

Correlations between process variables need to be taken into account for accurate fault detection results. Multivariate statistical methods are utilized to capture these inter correlations.

3.2.2 Multivariate fault detection

As discussed in section 3.2.1, univariate statistical monitoring is an insufficient fault detection method. The correlations between process variables need to be taken into account for accurate fault detection results. Multivariate statistical monitoring techniques have been developed to capture the 'hidden' information in variables and thus offer a more accurate and safe fault detection technique.

A generalized framework for data-driven fault detection methods is given by Aldrich and Auret (2013) in Figure 3.5. Process operation data, **X**, is collected from the specific process. The process operation data consist of all measured variables at specific time intervals. Features are extracted from the process operation data matrix and captured in a score matrix **F**. The score matrix **F**, is then projected back to the original input space, resulting in a new reconstructed data matrix **{X}**. Finally a residual matrix **E** can be calculated from the original and reconstructed input space. Changes in the projection, and therefore the process, can be monitored with the **E** and **F** matrices (Aldrich and Auret 2013).
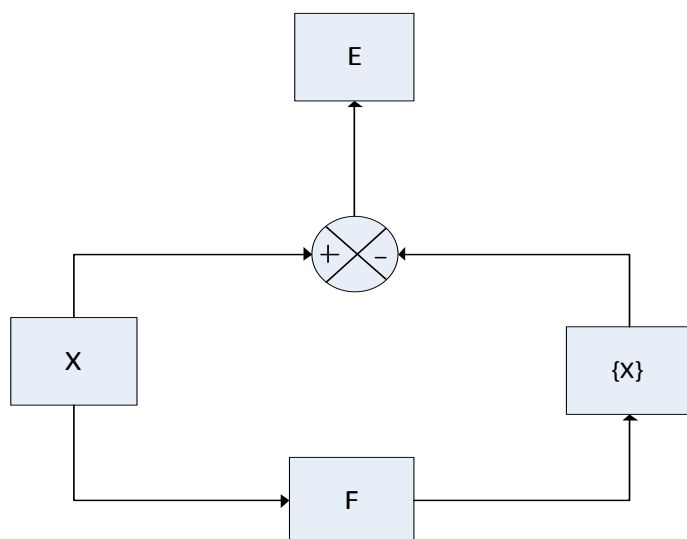
Figure 3.5: Generalized Framework for data-driven fault detection. X is the scaled process operation data. Changes in the projections can be monitored using the E (residual) and F (score) matrix (Redrawn from Aldrich and Auret 2013).

Data driven fault detection methods can further be classified between steady-state and non-steady-state processes. The non-steady-state processes consist of either batch or continuous processes (Aldrich and Auret 2013).

Although the dynamic model is continuous non-steady-state, the study will focus on the steady-state, data-driven, multivariate fault detection methods. This is due to the robustness of the steady-state methods and the general simplicity when compared to dynamic methods. The steady-state process data can be classified as either classical Gaussian/linear data, or non-Gaussian/nonlinear data (Aldrich and Auret 2013).

3.2.3 Linear feature extraction

Principal Component Analysis (PCA) is a linear feature extraction method involving the orthogonal transformation of data from the original coordinate system. The new coordinate system is defined by the principal components of the original system. The main goal is then to define a certain number of principal components which captures most of the variability in the data and thus reduce the original dimensions of the input data (Scholkopf *et al.* 1998).

Figure 3.6 provides a two-dimensional example of orthogonal transformation. The data are projected onto the principal components which are transformed to a new coordinate system. The new coordinate system is referred to as the feature space (Scholkopf *et al.* 1998).
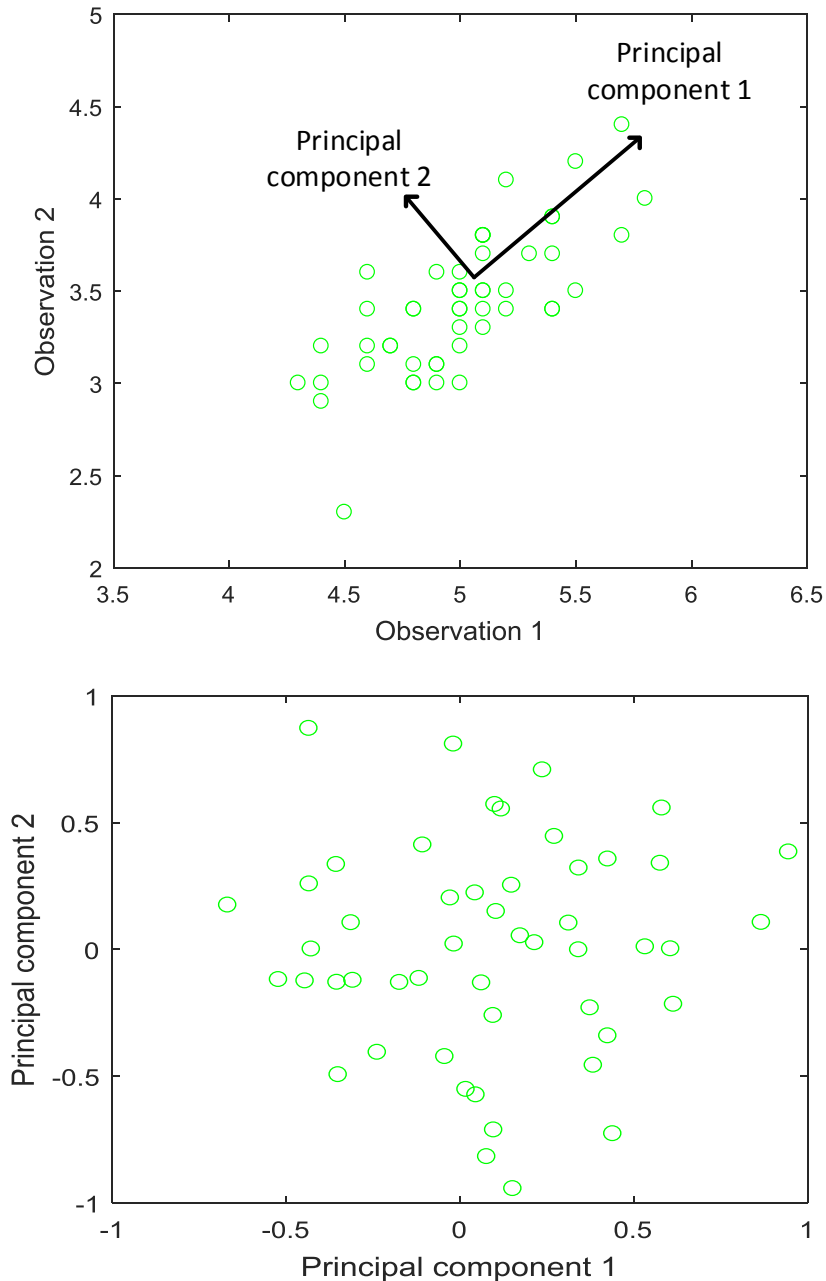
Figure 3.6: Two-dimensional orthogonal transformation. Process measurements are indicated in green. First plot represent the input space and second plot represent the principal component feature space.

When considering a multi-dimensional input space, a significant amount of the input space variance can be explained with the first few principal components, assuming a significant amount of correlation exists in the input space. These principal components can be used to reduce the size of and denoise the original input space (Scholkopf *et al.* 1998).

PCA, when used as a fault detection method, consists of a training stage followed by a verification stage and finally the application stage. The training stage involves the application of PCA on pre-defined normal operating condition (NOC) data. The NOC-data should contain no faults and only

process disturbances. However, this can be problematic in industry, since data is not readily available with no unwanted process deviations (Aldrich and Auret 2013).

After the validation stage, the results obtained from the training stage can be used on new, unseen, data. Faults can then be detected with the new projected data moving outside the training feature space (Aldrich and Auret 2013).

The quality of the fault detection results is not only dependent on the quality of the NOC data, but also the amount of NOC data. Russel *et al*. (2000) calculated the minimum required amount of data for the given amount of process variables at a 95% significance level. The data requirements are provided in Table 3.2 for a specific amount of observation variables.

Table 3.2: Minimum data requirements for specific amounts of observation variables (Russel *et al*. 2000).

Observation variables	Data sample size requirement
1	19
2	30
5	63
10	118
25	284
50	559
100	1110

3.2.3.1 Principal component analysis calculation

Consider a NOC data matrix **X** with n samples and m process variables. The data first needs to be standardized. The mean, μ, and standard deviation, σ, of each variable vector x_i [1 x m] is calculated as shown in equations 3.1 and 3.2, followed by the calculation of the centred NOC-data vector $\widetilde{x_i}$, as shown in equation 3.3 (Aldrich and Auret 2013).

$$\mu = \frac{1}{n} \sum_{i=1}^{n} x_i \tag{3.1}$$

$$\sigma = \sqrt{\sum_{i=1}^{n}(x_i - \mu)^2/n} \tag{3.2}$$

$$\widetilde{x_i} = \left(\frac{x - \mu}{\sigma}\right) \tag{3.3}$$

The centred data matrix $\widetilde{X}$ is used to calculate the covariance matrix **C**.

$$C = \frac{1}{n} \sum_{i=1}^{n} \widetilde{x_i} \widetilde{x_i}^{T} \tag{3.4}$$

Next, Eigen decomposition of the covariance matrix results in the eigenvectors **P** and eigenvalues **λ**.

$$\mathbf{CP} = \lambda\mathbf{P} \tag{3.5}$$

The variance in the data is accounted for in the eigenvalues λ. Each principal component, $\mathbf{p_i}$, corresponds to the specific eigenvalue λ_i. Typically the first few principal components will account for most of the variance in the original data set **X**. The scaled data can now be projected onto the principal components, resulting in the score matrix, **T**, as shown in equation 3.6 (Russel *et al*. 2000).

$$\mathbf{T} = \mathbf{XP} \tag{3.6}$$

The number of retained principal components A is determined by calculating the cumulative fraction of variance contribution for each principal component up to a certain pre-specified variance threshold (Aldrich and Auret 2013).

Once the number of retained principal component has been calculated, the original data can be reconstructed. The reconstructed data matrix **{X}** is calculated as shown in equation 3.7. The retained principle components is given in the matrix $\mathbf{P_A}$ and the corresponding scores are given in the score matrix $\mathbf{T_A}$ (Russel *et al*. 2000).

$$\{\mathbf{X}\} = \mathbf{T_A P_A^T} \tag{3.7}$$

Now that most of the variance in the data is reserved in the retained principle components, $\mathbf{P_A}$, new/unseen scaled process data can be mapped onto these principle components as shown in equation 3.8. The resulting feature matrix $\mathbf{T_A^{Test}}$ can then be used to reconstruct the new process data, as shown in equation 3.9 (Aldrich and Auret 2013).

$$\mathbf{T_A^{Test}} = \mathbf{X^{Test} P_A} \tag{3.8}$$

$$\{\mathbf{X}\}_{\mathbf{Test}} = \mathbf{T_A^{Test} P_A^T} \tag{3.9}$$

If the number of retained variables is less than four, a simple automated visualization of the score matrices, of both the NOC-data and unseen data, will be sufficient for process monitoring, since abnormal behaviour will be easily recognized from the automated visualization. However, when the number of retained variables exceeds three, it is no longer possible to visualize the score matrices (Aldrich and Auret 2013).

It is therefore required that results are summarized and monitored against some threshold. Abnormal behaviour can then be automatically detected once results moves outside the threshold. In order to summarize the PCA results, fault detection diagnostics are used. The fault detection diagnostics are described in section 3.2.3.1.

3.2.3.1 PCA fault detection diagnostics

Two fault detection diagnostics are utilized. As described in Figure 3.5, deviations can be noted from either the score matrix or the reconstructed matrix. The principal component feature space are monitored with the Modified Hotelling's T^2 statistic. The reconstructed matrix is monitored using the Q-statistic or Squared Prediction Error (SPE).

The Modified Hotelling's T^2 statistic (T_A^2) represents the deviation (distance) of a projection from the centre of the space defined by the retained principal components (Aldrich and Auret 2013). The calculation of $T_{A\,i}^2$ for a given sample i is given in equation 3.10 (Kourti 2002).

$$T_{A\,i}^2 = \sum_{i=1}^{A}\left(t_i^2 \Big/ \lambda_i \right) \tag{3.10}$$

The T_A^2 statistic is therefore used to monitor whether a new projected score has moved further away from the centre of the retained principal components, as first predicted under the NOC. An upper threshold can be set for the T_A^2 statistic from the NOC results, which can be used to detect abnormal conditions when new calculated T_A^2 statistics exceed the calculated threshold.

The SPE represents the distance between a real observation and its reconstructed sample (Aldrich and Auret 2013). The SPE calculation for a sample i is provided in equation 3.11 (Kourti 2002).

$$SPE_i = \sum_{i=1}^{m}(\tilde{\mathbf{x}}_i - \{\mathbf{x}\}_i)^2 \tag{3.11}$$

A large deviation in the SPE statistic indicates that the original retained principal components are no longer adequate in explaining the input space variance. As with the T_A^2 statistic, a threshold is calculated from the NOC PCA results. The determination of the threshold will be discussed in section 3.3.

3.2.4 Non-linear feature extraction

PCA exploits the linear correlations in the data to detect abnormal behaviour. However, when non-linear correlations are present in the data, PCA might no longer be an adequate fault detection technique (Jemwa 2006). Kernel methods are used to capture non-linear correlations in data. Kernel Principal Component Analysis (KPCA) is a popular non-linear fault detection method (Aldrich and Auret 2013).

In order to account for the non-linearity, instead of determining orthogonal vectors in the input space, {X}, the KPCA finds orthogonal vectors in an implicit dot-product space: {H} (Scholkopf *et al.* 1998). In this input space, {H}, the data is expected to be more linear and thus PCA is again applicable. The data is transferred from the input space, {X} to the feature space, {H} is done with a nonlinear mapping function (Aldrich and Auret 2013).

The KPCA mapping is described in Figure 3.7. The measurement vector **x**, is first projected to the dot-product space with a nonlinear mapping function Φ. The mapped vector Φ(**x**) is then projected to the linear feature space with PCA (Aldrich and Auret 2013).
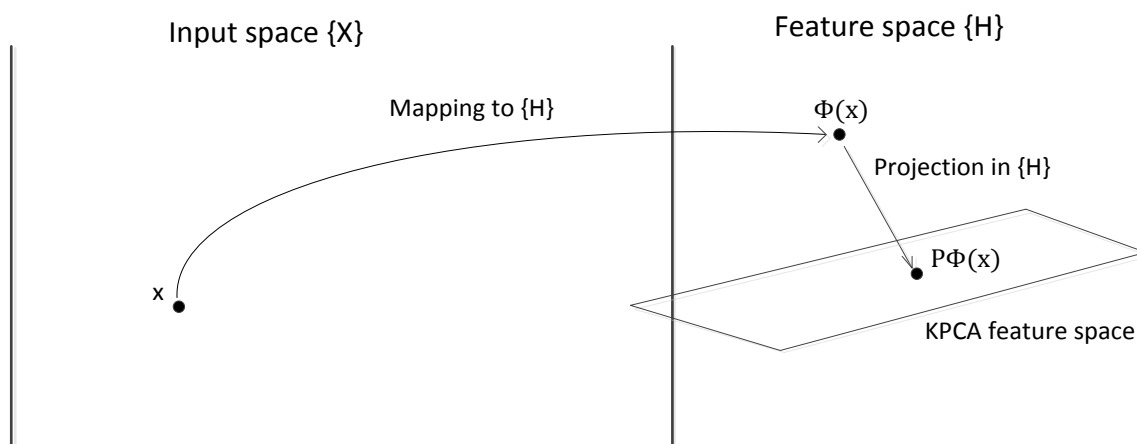
Figure 3.7: KPCA projection redrawn from Auret and Aldrich (2013). A single observation from the input space is first mapped to an infinite dimensional plane ϕ(x). PCA is then applied, and ϕ(x) is mapped to the linear KPCA feature space.

3.2.4.1 Kernel-PCA calculation

In the feature space, {H}, the covariance matrix, **C** can be calculated with equation 3.12. The mapping function is represented by Φ(x) (Scholkopf *et al.* 1998)

$$\mathbf{C} = \frac{1}{n} \sum_{i=1}^{n} \Phi(x_i)\Phi(x_i)^T, \quad with \quad \sum_{i=1}^{n} \Phi(x_i) = 0 \tag{3.12}$$

The dot product can be replaced by a kernel trick. The kernel trick avoids the non-linear explicit mapping shown in equation 3.12, with the use of a kernel function (Scholkopf *et al.* 1998). Eigen decomposition is used to diagonalize the covariance matrix C, as shown in equation 3.13, where m refers to the single eigenvector and eigenvalue pair (Aldrich & Auret 2013).

$$\mathbf{C}p^m = \lambda_m p^m \tag{3.13}$$

The eigenvector, **p^m**, can be calculated with equation 3.14 with the coefficients α_i (Lee *et al*. 2004).

$$\mathbf{p^m} = \sum_{i=1}^{n} \alpha_i \Phi(\mathbf{x_i}) \tag{3.14}$$

Substituting equations 3.12 and 3.14 into 3.13 will result in equation 3.15.

$$\boldsymbol{\lambda_m} \sum_{i=1}^{n} \alpha_i \, \Phi(x_i)\Phi(x_j)^T = \frac{1}{n} \sum_{i=1}^{n} \alpha_i \Phi(\mathbf{x_i}) \cdot \sum_{i=1}^{n}(\Phi(x_i)\Phi(x_i) \cdot \Phi(x_j)) \tag{3.15}$$

The kernel matrix, **K**, can then be defined as:

$$\mathbf{K_{ij}} = \Phi(x_i) \cdot \Phi(x_j) \tag{3.16}$$

Equation 3.16 can now be substituted into equation 3.15 and be reduced to equation 3.17.

$$\mathbf{K}^2 \boldsymbol{\alpha}_m = n\lambda_m \boldsymbol{\alpha}_m \mathbf{K} \tag{3.17}$$

Equation 3.17 can be reduced to the eigenvalue problem shown in equation 3.18. (Scholkopf 1998). The eigenvalue in equation 3.17 is scaled: $\widetilde{\lambda_m} = \lambda_m/n$.

$$\mathbf{K}\boldsymbol{\alpha}_m = \widetilde{\lambda_m}\boldsymbol{\alpha}_m \tag{3.18}$$

The Kernel matrix given in equation 3.16 can be defined by a kernel function. There are several types of kernel functions. The Gaussian kernel is the most common and is given in equation 3.19. (Lindner 2014).

$$\mathbf{K_{ij}} = k(x_i, x_j) = \exp(-\frac{\|x_i - x_j\|}{2c^2}) \tag{3.19}$$

The norm between two sample vectors i and j is calculated in the nominator, while c is the kernel width. The kernel width can be selected *a priori* and will be discussed in section 3.2.4.2.

The calculated kernel matrix needs to be centred as shown in equation 3.20. 1_{nxn} is a matrix of ones of size [n x n]. (Aldrich and Auret 2013).

$$\breve{\mathbf{K}} = \mathbf{K} - \mathbf{K}\frac{1_{n\times n}}{n} - \frac{1_{n\times n}}{n}\mathbf{K} + \frac{1_{n\times n}}{n}\mathbf{K}\frac{1_{n\times n}}{n} \tag{3.20}$$

The scores can now be calculated by projecting the mapping Φ(x) onto the eigenvectors.

$$\mathbf{t^m} = \frac{1}{\sqrt{\widetilde{\lambda_m}}} \sum_{i=1}^{n} \alpha_{i,m} \mathbf{K_{ij}} \tag{3.21}$$

New unseen data, consisting of q observations, can now be projected onto the eigenvectors obtained from the training data. The kernel matrix for the test data is first calculated as shown in equation 3.22 (Gutteriez-Osuna, R, 2013).

$$\mathbf{K_{ji}^{Test}} = k(x_j^{Test}, x_i) \tag{3.22}$$

The test kernel should then be centred as shown in equation 3.23 (Gutteriez-Osuna, R, 2013).

$$\breve{K}^{Test} = \mathbf{K^{Test}} - \mathbf{K^{Test}}\frac{1_{n\times n}}{n} - \frac{1_{q\times n}}{n}\mathbf{K} + \frac{1_{q\times n}}{n}\mathbf{K}\frac{1_{n\times n}}{n} \tag{3.23}$$

Finally the scores can be calculated for the test data as given in equation 3.24 (Gutteriez-Osuna, R, 2013).

$$\mathbf{t^m} = \frac{1}{\sqrt{\widetilde{\lambda_m}}} \sum_{i=1}^{n} \alpha_{i,m} \; \mathbf{K}_{ji}^{Test} \tag{3.24}$$

3.2.4.2 KPCA detection diagnostics

The T_A^2 and SPE statistics are again used as monitoring statistics for KPCA. The T_A^2 is calculated again as given in equation 3.9.

Since data are not reconstructed as with PCA, the SPE statistic needs to be modified. Lee *et al*. (2004) proposed a method to calculate the SPE statistic, by defining the SPE as the difference in the sum of scores, when all principle components are retained and the actual number of retained principal components. The SPE can be calculated as shown in equation 3.25 (Lee *et al*. 2004).

$$SPE = \sum_{j=1}^{m}(t_n^j)^2 - \sum_{j=1}^{A}(t_n^j)^2 \tag{3.25}$$

3.2.4.3 Kernel width selection

The kernel width c used in the equation 3.19 is an important hyper parameter. Selecting an acceptable kernel width is crucial for optimal KPCA performance. However, there is a lack of robust fault detection kernel width selection methods in literature. Popular methods used in literature require prior knowledge of both the NOC and fault data.

The Gaussian kernel function uses a multivariate normal distribution to determine the similarity (kernel matrix entry) between samples i and j. The kernel width determines the standard deviation of the multivariate normal distribution.

A smaller kernel width will result in less similarity between a samples i and j. This will in turn result in more sparsely mapped data. A larger kernel width will in turn increase the similarity between samples and result in more concentrated mapped data.

Aldrich and Auret (2013) suggest that the kernel width is calculated using cross-validation with the use of the pair wise distances of the calculated norms in the input space. The method aims to minimize the reconstruction error (SPE). However, Aldrich and Auret (2013) used a different SPE than the one provided in equation 3.25.

Therefore, a new kernel width selection method is proposed and is provided in Appendix B. The proposed kernel width selection method aims to select a kernel width only based on the normal operating conditions (NOC) data. Furthermore, the method is based on the assumption that the optimal kernel width will result in a Gaussian projected feature space. The effect of kernel width is also further discussed in Appendix B.

The proposed method is compared to published KPCA fault identification studies. The studies investigated the Tennessee Eastman process (TEP). The TEP is a popular benchmark process used in fault detection studies. The process data consist of 54 process variables and 21 fault data. Refer to Russel *et al*. (2000) for an in depth description of the process.

3.2.5 Significant results from previous fault detection studies

The following section will focus on significant results from previous fault detection studies. The studies are categorized according to their respective applications.

3.2.5.1 Metallurgical application

Groenewald *et al*. (2006) investigated the application of PCA on an industrial grinding circuit. PCA in conjunction with expert knowledge from the grinding circuit successfully detected shifts in the process. It was noted that the availability of good quality process data has a significant effect on the PCA performance. It was recommended that non-linear feature extraction methods should be further investigated.

Wang *et al*. (2015) applied Dynamic PCA (DPCA) to a simulated industrial Se/Te removal and copper electrowinning circuit. DPCA is an extension of PCA which allows for time-lagged information which was used to allow for the large residence times present at the copper electrowinning circuit. It was found that the DPCA was effective in detecting process faults.

Wu *et al*. (2002) investigated the design of an expert controller for a zinc leaching process. The expert controller was based on several steady-state models. An inference engine was used to detect and diagnose faults. Knowledge base and plant data was used to identify and locate faults from the inference engine. The system was implemented on a real-world process. Results showed that faults can be detected early and be successfully diagnosed.

Jemwa and Aldrich (2006) investigated the use of KPCA as fault detection method in mineral processing operations. A framework was developed for the use of kernel methods for fault detection. Support vector multi-classifiers were used to determine the optimal kernel width. The framework was applied to a PGM froth flotation case study and a calcium carbide furnace case study. The study highlighted the importance of proper confidence interval selection for detection diagnostics.

3.2.5.1 Non - Metallurgical application

Lee *et al*. (2004) developed a new KPCA online monitoring strategy. The strategy was applied to a simple simulation case study and a biological waste water treatment case study. The results were compared to PCA results. The results showed that KPCA effectively captured the correlations between process variables. The problem of selecting the kernel width parameter was discussed and

suggested as future work. The problem of mapping KPCA scores back to the original input space was also discussed.

Phillpotts (2016) investigated the use of non-linear fault detection and diagnosis methods on a pilot scale distillation column. PCA, KPCA, linear discriminant analysis and kernel discriminant analysis were all investigated as fault detection methods. The importance of optimal kernel width selection was noted. Both PCA and KPCA successfully detected abnormal operating conditions.

3.2.5.3 Summary

The significant results from previous studies, discussed in sections 3.2.5.1 and 3.2.5.2 emphasized the importance of accurate NOC data selection. The potential for fault diagnosis strategies on metallurgical processes was further emphasized. Furthermore, the literature show that KPCA has the potential to provide improved fault detection results, when compared to PCA.

3.3 Fault detection performance metrics

3.3.1 Monitoring charts

The detection diagnostics, T_A^2 and SPE, can be evaluated over time in order to monitor the process performance. The simplest monitoring chart is the Shewhart chart. The Shewhart chart is a plot of both T_A^2 and SPE over time, which only considers the current process conditions. If there is significant movement in either of the T_A^2 or SPE statistics, an alarm will be triggered, indicating abnormal conditions (Russell *et al.* 2000). The drawback of the Shewhart chart is the lack of consideration of small NOC changes. These small NOC changes can result in false alarms being triggered. The PCA and KPCA models will then have to be retrained. Figure 3.8 provides a Shewhart chart example.
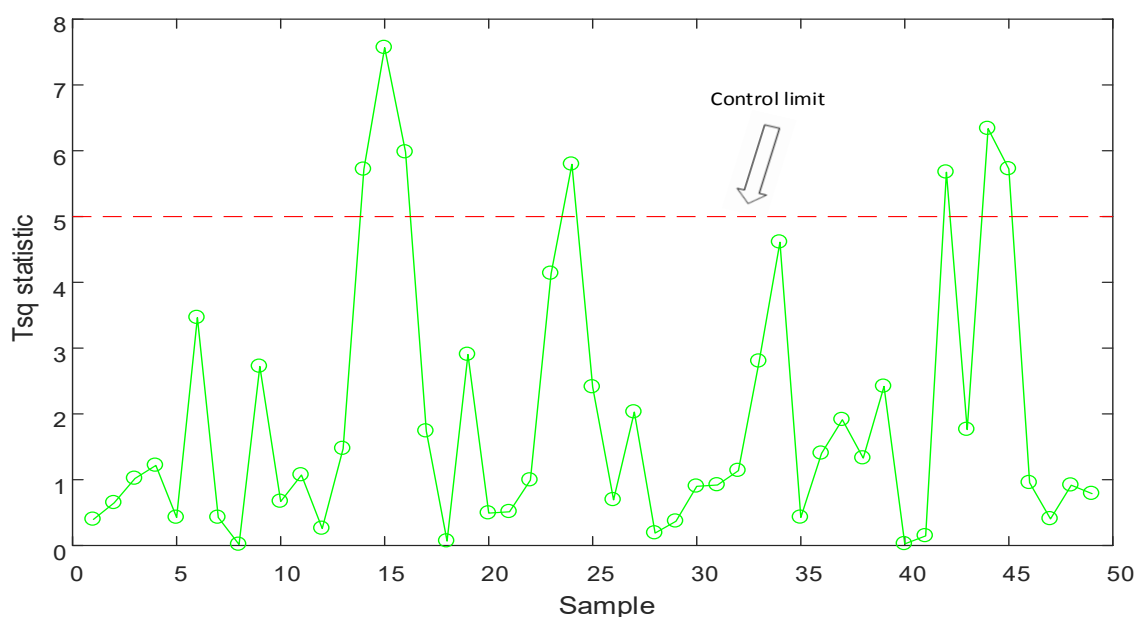
Figure 3.8: Shewhart chart example. Green samples indicate T_A^2 statistic and control limit is indicated in red.

3.3.2 Missing and false alarms

When a T_A^2 or SPE observation exceeds the calculated control limit, an alarm is triggered. The false alarm rate (FAR) is the percentage of total samples observed outside the control limit when no fault is occurring (Aldrich and Auret 2013).

A missing alarm is defined as an observation where no alarm is raised under known fault conditions. The missing alarm rate (MAR) is defined as the percentage of total samples observed as missed alarms (Aldrich and Auret 2013).

The true alarm rate (TAR) is defined as the amount of successful alarms triggered under fault conditions and can be calculated using equation 3.26, when the MAR is defined as a percentage (Lindner 2014).

$$\text{TAR}\,(\%) = 100 - \text{MAR}(\%) \tag{3.26}$$

3.3.3 Receiver operator curve

The receiver operator curve (ROC) is a plot of the TAR and FAR at different detection diagnostic control limits. Therefore it is a method for evaluating the chosen control threshold. A FAR of 0% and TAR of 100% is desired (Aldrich and Auret 2013).

An example of a receiver operating curve is provided in Figure 3.9. From the receiver operating curve the upper limit selection can be evaluated. The TAR at a desired FAR can indicate the optimal performance achievable when moving the detection diagnostic control limit.
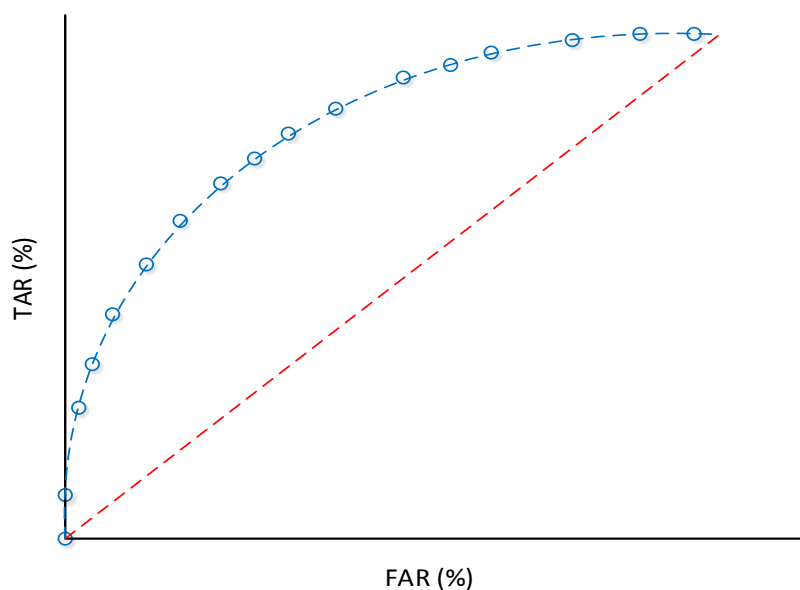
Figure 3.9: Example Receiver Operating curve.

From the ROC, the area under the curve (AUC) can be calculated with numerical integration as shown in Figure 3.10.
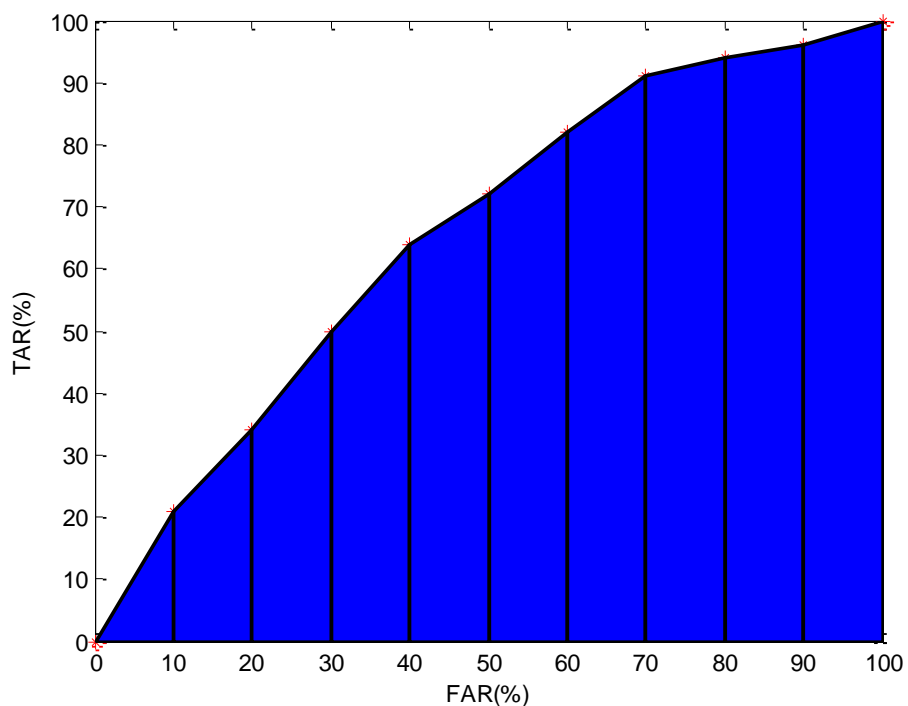
Figure 3.10: AUC calculation example. AUC is calculated with numerical integration as shown in blue.

The AUC can be calculated to assess how close the ROC is to the ideal conditions. If the AUC is one, it indicates optimum fault detection performance; however, an AUC below 0.5 indicates that the performance is worse than a random selection of whether a fault is occurring (Lindner 2014).

3.3.4 Detection delay

The detection delay is used to evaluate how fast a fault is detected. It is defined as the time taken, before a certain number of consecutive alarms are triggered. A small detection delay is desired. A detection delay of three samples were used by both Aldrich and Auret (2013) and Lindner (2014).

3.4 Fault identification

Once a fault detection diagnostic exceeds its threshold, the location of the fault needs to be identified. The fault location refers to the variables indicating the cause of the fault and not the fault symptoms. The following section will describe methods to be used to identify the fault location.

3.4.1 Traditional contribution plots

SPE and score distance (T_A^2) contribution plots are traditionally used to identify faults (Russel *et al*. 2000). The fault location is identified as the process variables who contribute most to an out of control detection diagnostic. The SPE contribution of variable j for each sample i is calculated as follows (Alcala and Qin 2009).

$$C_{i,j}\,(SPE) = \left(\mathbf{X_{i,j}} - \{\mathbf{X}\}_{i,j}\right)^2 \tag{3.27}$$

The score distance contributions can be calculated as follows (Auret 2010).

$$C_{i,j}\,(T_A^2) = \mathbf{T_{i,j}}\lambda^{-1}{}_i\mathbf{P_j^T X_{i,j}} \tag{3.28}$$

The traditional contribution plots can suffer from fault smearing. Fault smearing occurs when several process variables are flagged as abnormal from the contribution plots. However, these flagged process variables only point to the symptoms of the fault and not the cause of the fault. This is problematic, since a delayed fault identification negates the gain from the early fault detection (Alcala and Qin 2009).

3.4.2 Reconstruction based contribution plot

Alcala and Qin (2009) proposed reconstruction based contributions (RBC) to address the problem of fault smearing for PCA. The reconstruction based contribution is defined as the amount of reconstruction required along each variable direction that minimizes the detection diagnostic. The SPE RBC is given in the following equation (Alcala and Qin 2009).

$$RBC_j^{SPE} = \frac{C_j}{\widetilde{C_{JJ}}} \tag{3.29}$$

C_j is the traditional contribution and C_{jj} is the jth diagonal element of the residual subspace matrix. The residual subspace is the principal components not retained and can be calculated as:

$$\widetilde{\mathbf{C}} = \widetilde{\mathbf{P}}\widetilde{\mathbf{P}}^T \;, \;\; \widetilde{\mathbf{P}} = \mathbf{P}^{i\times(j-A)} \tag{3.30}$$

The T^2-statistic RBC is given in the following equation. (Alcala and Qin 2009).

$$RBC_j^{T^2} = \frac{\left(\delta_i^T \mathbf{Dx}\right)^2}{d_{ii}} \tag{3.31}$$

D can be calculated as follows, with d$_{ii}$ the ith diagonal element of **D**.

$$\mathbf{D} = \mathbf{P_A \lambda_A P_A^T}$$
(3.32)

A threshold is calculated from the 99th percentile of the NOC contributions for each monitored process variable. Relative contributions can then be calculated and the largest contributing variables can be identified once a fault has been detected (Auret 2010).

3.5 Economic impact assessment

The section aims to provide the required background information for an economic impact assessment. Economic impact assessments are used to evaluate the profitability of process changes. Economic performance functions (EPFs) provide the basis for an economic impact assessment. Advanced process controllers utilize EPFs to optimize process operating by decreasing variations through control. Fault diagnosis utilize EPFs to minimize the time spent away from a predetermined optimal economic process operating conditions.

The possible economic benefits from a process addition can further be subdivided into the tangible and nontangible benefits. The tangible benefits are usually easy to measure and is the focus of most economic impact studies. The intangible benefits are more difficult to measure, e.g. increased process safety. These benefits are often not considered in economic impact assessments.

3.5.1 Economic performance function development methodology

Wei (2010) developed an economic performance function (EPFs) and joint performance functions (JEPFs) methodology. The methodology was developed to help in economic performance assessment of process controllers. A schematic outline of the methodology is provided in Figure 3.11 followed by a brief description.
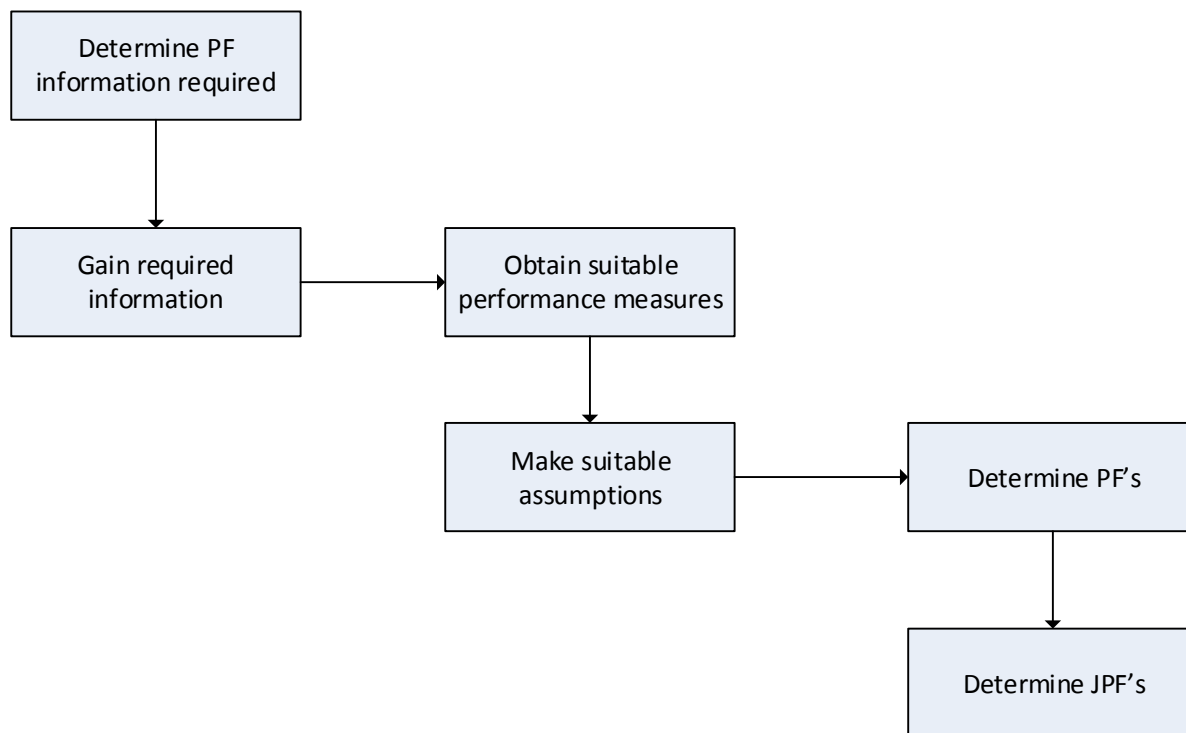
Figure 3.11: Performance function development methodology by Wei (2010).

The first stage in the methodology is to determine the required information to successfully develop the EPFs. A clear understanding of the process operations and process economics is required in this stage (Wei 2010).

The second stage involves the gathering of the required information determined in the first stage. There are three sources of information for the development of the EPFs. These sources are: surveys, literature and plant tests. Surveys focus on expert information gathered from the process in question, while literature refers to the different types of EPFs and previously developed EPFs (Wei 2010).

The third stage is especially important when only considering a section of a processing plant. The specific control objectives might not always be to optimize profit, but rather to optimize throughput, process safety etc. The control objectives specific to the section of the process should aim to represent the corporate and manufacturing strategies and therefore the EPF should be constrained to operate in line with these strategies (Wei 2010).

The assumptions made when developing EPFs are crucial for the overall accuracy of the EPF. The clear understanding of the process objectives developed in the previous stages is required to make suitable assumptions. Small or negligible economic impacts should be neglected when it will simplify the development of the EPF (Wei 2010).

All the information gathered in the first four stages are then used to develop the performance functions. Plant data can be used, however, such data is usually confidential (Wei 2010). This can be avoided with the use of percentage values. Oosthuizen *et al*. (2004) conducted an economic evaluation of an electric arc furnace controller, described the additional costs as a percentage of the normal operating cost of the electric arc furnace.

Finally, JEPFs can be developed, if required. The aim of JEPFs is to not report overlapping economic information. Due to the highly correlated systems present in most modern chemical processes, process variables often overlap, which could result in EPFs reporting a single economic gains/losses repeatedly (Wei 2010).

3.5.2 Economic performance evaluation of advanced process controllers

Bauer and Craig (2007) introduced an advanced process controller (APC) economic performance evaluation framework. The framework aims to provide an APC life-cycle economic assessment. Although the focus is on APCs, there are many similarities when considering a fault diagnosis method. The life-cycle assessment framework is provided in Figure 3.12.

The life-cycle assessment highlights the importance of re-assessing the APC performance once it has been implemented. If the APC performance is unsatisfactory, the base case APC design should be re-evaluated. The survey conducted by Bauer and Craig (2007) confirmed that many APCs are abandoned following shifts in the process normal operating conditions (NOC).

The observations made by Bauer and Craig (2007) can be translated to a fault diagnosis system. When considering a fault diagnosis system, the base case refers to the NOC training data. If the system performance is unsatisfactory, the NOC data should be re-evaluated. Furthermore, poor model training will result in either poor fault detection or high false alarm rates. Both will result in the fault diagnosis system being abandoned by plant operators.

These observations are important when considering the durability and ultimately the profitability of a fault diagnosis system. The system should be robust to process disturbances and shifts in the NOC, while still detecting faulty process conditions prior to any significant deviations in the process NOC.
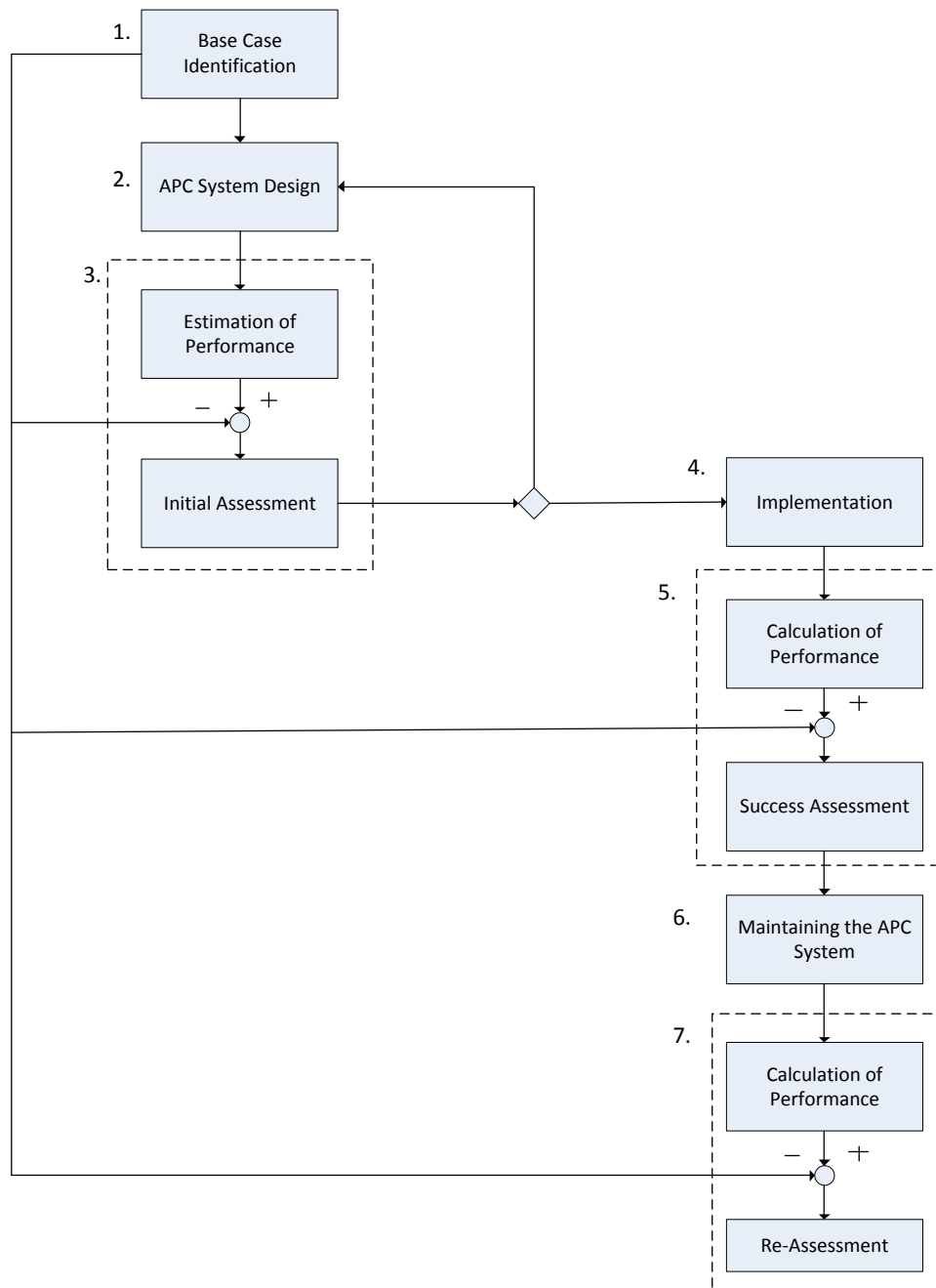
**Figure 3.12: APC economic performance evaluation Figure redrawn from Bauer and Craig (2007). + And −
refer to the decision whether controller performance is acceptable.**

3.5.3 Significant results from previous economic performance studies

Bauer *et al*. (2007) developed a profit index to evaluate the potential economic benefit from
improved process control. The linear, quadratic and Clifftent performance functions were individually
investigated. The profit index quantifies the possible economic gain from shifting the operation point
closer to a specified operating limit. The main drawback with this method is the implementation of
exponential functions for the profit index.

Bauer and Craig (2007) conducted an industry survey on APC economic performance estimation. Following the survey, an APC economic performance framework was developed. The survey concluded that economic benefit estimation methods have not kept up with the fast growth in APC.

The survey identified the main profit contributors as: increased throughput, increased process stability, reduced energy consumption and increased yield without quality giveaway. Another survey in Japan also noted that APC stopped operating following changes in the process NOC. This is due to the lack of APC benefit re-assessment after a shift in the NOC.

Bin Shams (2010) developed a methodology to quantify the economic loss when faults are not detected under standard fault detection (univariate) conditions. Cumulative sum (CUMSUM) charts and PCA were investigated as fault detection methods. A methodology was developed for tuning the process controllers in conjunction with a monitoring system. A minimization function was used to determine controller tuning parameters. The minimization function aimed to optimization of the related cost without any fault detection and the cost variability in the manipulated and controller variables. Three TEP faults which were not detected in previous fault detection studies were investigated. Controllers were re-tuned, resulting in early detection of these faults and therefore a potential economic benefit. The importance of optimal controller tuning in conjunction with a monitoring system was highlighted by the study.

Wei and Craig (2009) completed an economic performance assessment of two run-of-mine (ROM) process controllers. Economic performance functions were specifically created for the ROM circuits with the methodology developed by Wei (2010). The economic performance functions were used to compare a proportional-integral-derivative (PID) controller with a nonlinear model predictive controller (NMPC). The NMPC outperformed the PID controller, since it allowed for operating conditions closer to the optimal economic performance set point as determined by the economic performance function.

Olivier and Craig (2017) investigated the economic operability in the presence of abnormal conditions. Monte Carlo-based analysis is first used to determine whether process controllers can still operate within a desired state in the presence of abnormal conditions. EPFs are then used to determine whether the process will be more profitable if the process is shut down in order to repair the fault. The proposed method was applied to a simulation of a run-of-mine ore milling circuit. The results were promising, highlighting the importance of an economic analysis when deciding to shut down a process.

Chapter 4: Project Objectives and tasks

Chapter 3 provided the relevant literature on fault diagnosis and economic impact assessment. The literature is used to address the objectives set out in Chapter 1, section 1.4. Chapter 4 provides the subsequent tasks relating to each objective.

The four formal project objectives are:

1. Design and application of process monitoring approach for fault detection and identification to simulated fault data.
2. Evaluation of fault detection and identification approach based on process monitoring performance metrics.
3. Definition of economic key performance indicators for the pressure leaching process.
4. Evaluation of fault detection and identification approach based on economic key performance indicators for the pressure leaching process.

The first objective is the design of a fault detection and identification approach. Both PCA and KPCA will be used as fault detection methods. Traditional contributions and reconstruction-based contributions will be used as fault identification methods.

Following the completion of the first objective, the developed fault detection and identification models will be applied to simulated fault data. The simulated fault data is gathered from the fault library implemented by Miskin (2015). The performance of each method will be evaluated using the traditional performance measures discussed in section 3.3.

Economic key performance indicators will be identified and incorporated as economic performance functions using the methodology developed by Wei (2010). The performance of the fault detection and identification methods will then finally be evaluated using the economic key indicators identified in the third objective.

The tasks relating to each objective are provided and summarized in Figure 4.1.

1. Design fault detection and identification approach

- Develop PCA and KPCA Matlab® models
- Validate model results
- Develop traditional contribution plot models
- Develop RBC plot models

2. Apply fault detection and fault identification models

- Simulate fault conditions
- Apply fault detection and identification models to simulated fault data
- Evaluate fault detection performance using traditional performance metrics

3. Define economic key performance indicators

- Consult expert knowledge on economic key performance indicators
- Develop economic performance functions based on Wei (2010) methodology

4. Evaluate fault detection and identification performance based on economic performance

- Apply economic performance function to simulated fault data
- Evaluate potential economic gain from early fault detection

Figure 4.1: Project objectives and tasks summary.

Chapter 5: Methodology: Fault detection and identification

Chapter 5 addresses the first project objective. The fault detection and identification model development methodology is provided. The methodology is divided into three sections.

The first section describes the data pre-processing step. The main objective is to extract only the data which will be available at the actual BMR from the simulated data. The data is then sub-sampled to individual fault detection methods requirements.

Both PCA and KPCA model development methodologies are described in the second step. A general methodology is provided for each method. Hyper-parameter selection, specifically for the process, for each method is then discussed.

The fault identification methodology is provided in the third step. Traditional and reconstruction based contributions methodologies are provided for PCA and only traditional contributions for KPCA.

5.1 Data pre-processing

The objective of the data pre-processing step is to extract only the data which would be available on the actual process from the simulated process data. The data should then be sub-sampled at a pre-determined sampling interval. The simulation data should be the same as that available at the actual plant in order to be more representative of reality and more accurately evaluate the fault detection and identification results.

5.1.1 Fault detection sampling interval

The amount of data available is unlimited, but the amount of data used is limited by the available computational power. This consideration is especially important when applying the hyperplane projection required for KPCA.

Once the fault detection sampling interval has been determined, the measurements which would be available on the plant need to be extracted from the simulated data. These measurements can be classified as either online or offline measurements.

5.1.2 Online Sampling

Online measurements include all sensor measurements with instantaneous measurement results available. A total of 35 sensor measurements are included in the scope of the dynamic model. The overall online measurement pre-processing approach is provided in Figure 5.1.
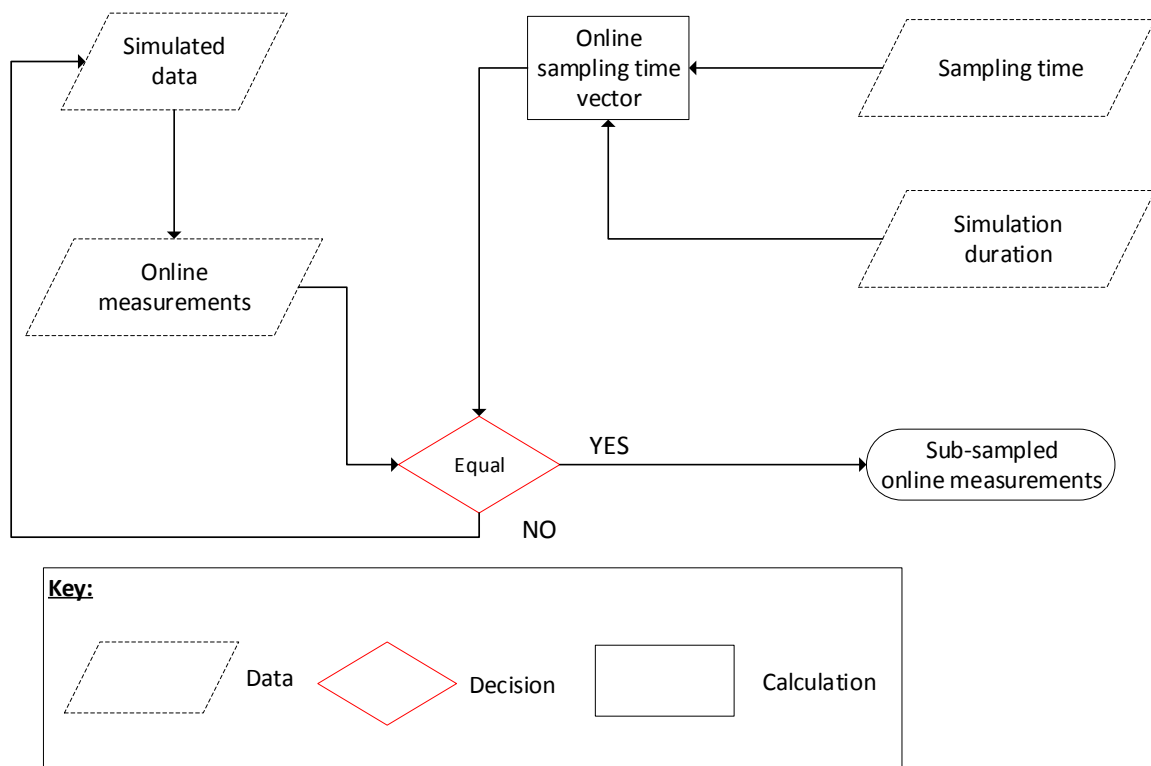
Figure 5.1: Online sub-sampling approach.

The data from the online measurements is first extracted from the simulated data set. At the same time, the desired online sampling time vector is calculated from the fault detection sampling time and the simulation duration, as shown in Figure 5.1.

The desired sampling vector is compared to the time vector of the extracted simulated data. If the time vectors are equal, the measurement data at that point is saved. This process is repeated until the data available at fault detection sampling interval has been saved. Online data is readily available (every few seconds) at the plant.

5.1.3 Offline Sampling

Filtrate and residue samples are collected within the process and analysed offline. The composition of each sample is determined during offline analysis. Offline samples can be collected as either a grab or a composite sample. Grab samples are samples taken at some discrete time intervals. Composite samples are numerous smaller samples collected over a given time period. Offline samples collected within the pressure leaching system are provided in Table 5.1.

Table 5.1: Offline sample types and required analysis times.

Sample	Sample type	Time before results are available (hours)
first stage residue	Grab	8
third stage residue	Grab	8
fourth stage residue	Composite	24
third stage filtrate	Grab	8
fourth stage filtrate	Grab	8
Preparation tank density	Grab	1

The analysis time in table 5.1 indicates the time required before results become available. The fourth compartment residue is the only composite sample and is collected in a filter press over a 24-hour period. The offline sub-sampling approach is given in Figure 5.2.

Similar to the online sub-sampling method, the offline measurements are first extracted from the simulated data and compared to the desired offline sampling vector. However, when the compared vectors are unequal the previous available measurement is displayed. Once all the measurements have been extracted, a specific sample time lag is introduced. The objective of the time lag is to allow for the required offline analysis time. Therefore, composition results will only be available once the simulated offline analysis has been completed.

Only the instantaneous data is saved for grab samples. The 24 hour average compositions are saved for the composite sample.
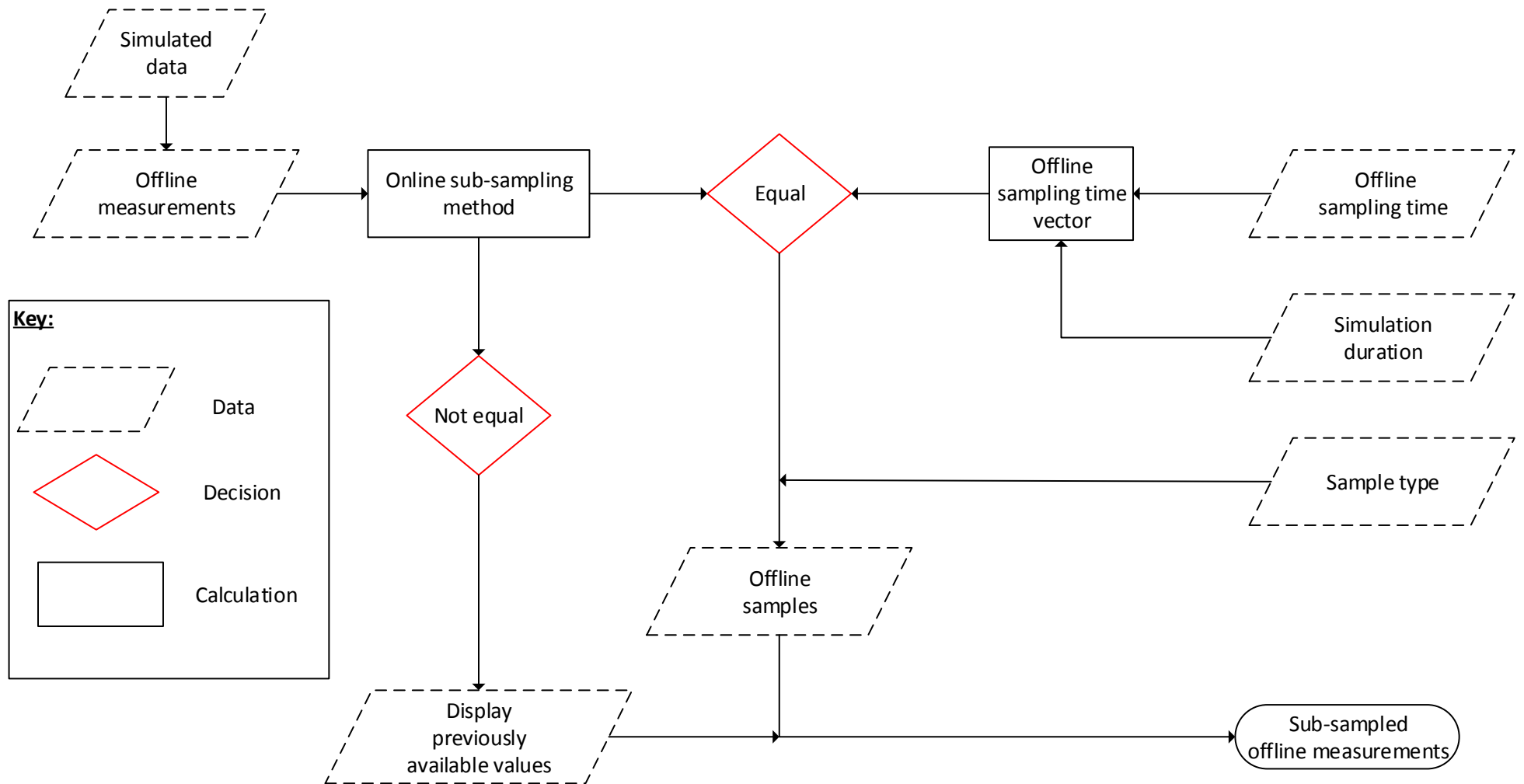
Figure 5.2: Offline sub-sampling approach.

5.2 Fault detection

A general fault detection methodology for both PCA and KPCA is provided followed by a discussion of the specific hyper-parameter selection methodology.

5.2.1 General PCA fault detection approach

A general PCA fault detection training approach is provided in Figure 5.3. The processed training dataset serves as input. The input data is standardized and the input mean and standard deviation are saved. PCA is then applied to the standardized data with the amount of retained variance serving as the only hyper-parameter. The selection of the amount of retained variance is discussed in section 5.2.3. The number of retained principal components and the principal components are then calculated and saved.

Next the fault detection diagnostics can be calculated. The scores from the reduced feature space are reconstructed to calculate the SPE statistic. The scores are used to calculate the T^2-statistic.

Verification NOC data serves as input in order to calculate the detection diagnostic control limit. The selection of the upper percentile is discussed in section 5.2.3. The control limits for both detection diagnostics are consequently saved.
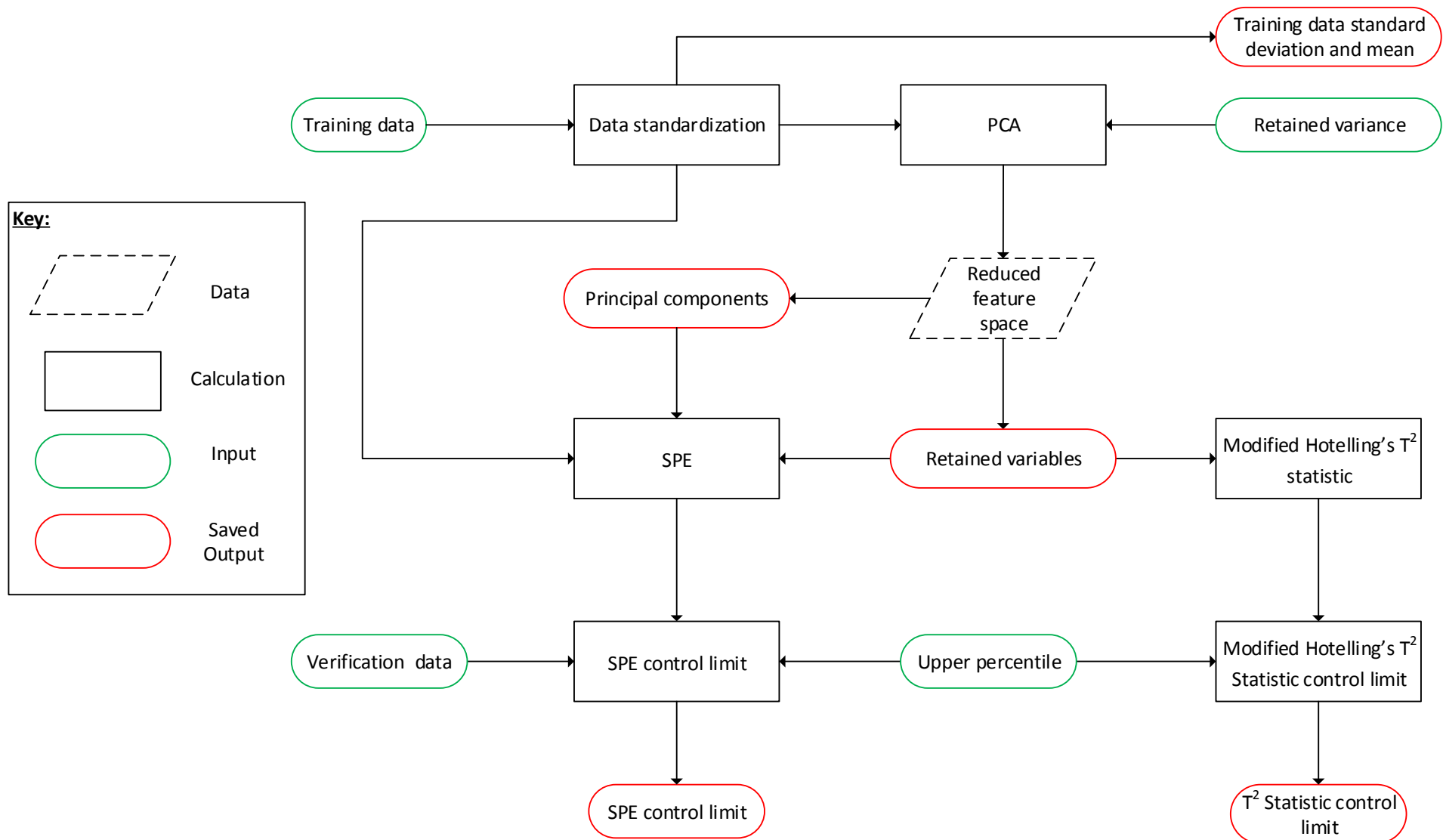
Figure 5.3: General PCA fault detection training approach.

Following the PCA application on the training and verification data, PCA is applied to new unseen data. A PCA application approach is provided in Figure 5.4.

The pre-processed unseen data includes NOC data and fault data. The unseen data is first standardized with the saved training set mean and standard deviation. The standardized unseen data is then projected onto the reduced feature space using the saved principal components and number of retained principal components.

The fault detection diagnostics can then be calculated as in the training case. The detection diagnostics are then compared to their respective control limits. The traditional fault detection performance metrics are then calculated. The FAR is calculated using the NOC data from the unseen data. The MAR and DD is calculated from the fault data. The ROC is determined by varying the upper control limit using the unseen NOC data. The AUC is then calculated from the ROC. The performance of PCA as fault detection method can then be evaluated with the use of the traditional fault detection performance metrics.
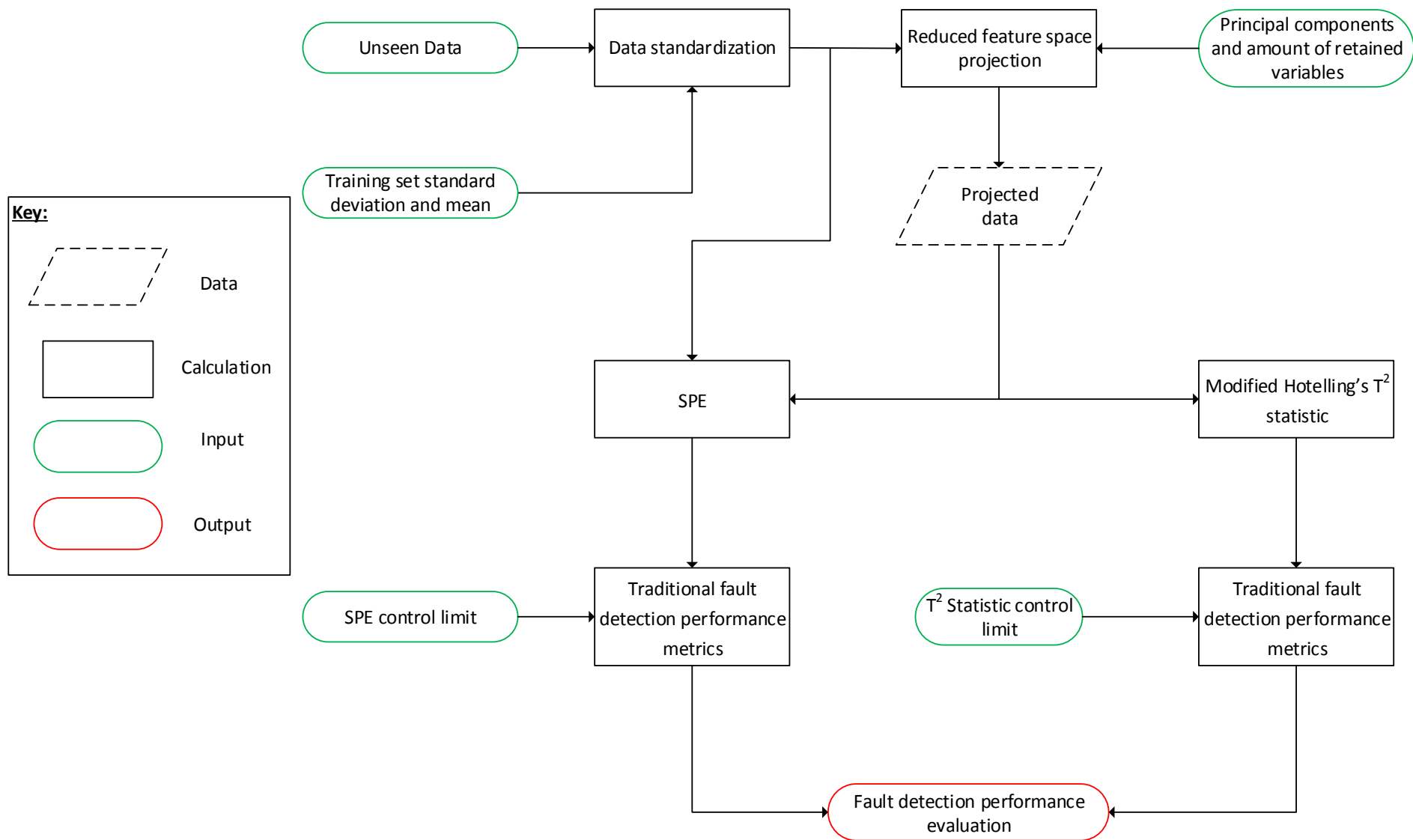
Figure 5.4: PCA fault detection application.

5.2.2 General KPCA fault detection approach

The KPCA training approach is provided in Figure 5.5. The NOC training set used is limited by the computational power available. Therefore, the NOC training set from PCA is sub-sampled in order to allow for the increased computational requirement.

The sub-sampled processed NOC training data is first standardized. The training set mean and standard deviation is saved. The standardized data is then projected to an infinitely large hyperplane with the kernel width and Gaussian kernel function. The kernel matrix is centred and the centred kernel matrix is saved.

PCA is then applied in the hyperplane which results in a reduced feature space. The principal components and number of retained principal components are saved. The T_A^2 statistic is calculated as with PCA. The SPE statistic is calculated from the scores and number of retained principal components. The control limits are calculated for both fault detection diagnostics with NOC verification data. Both control limits are then saved.
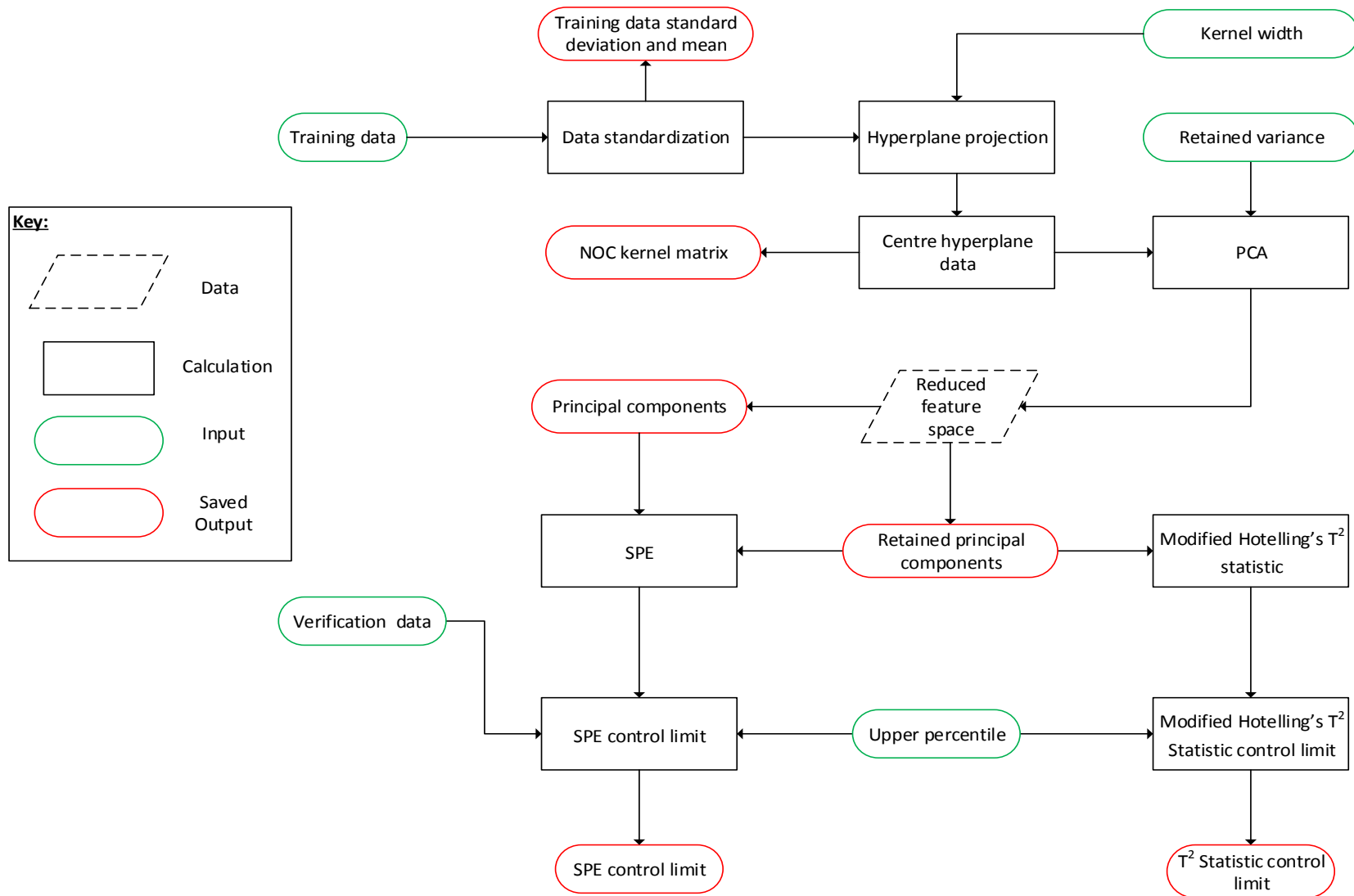
Figure 5.5: KPCA training approach

Following the KPCA application on the training and verification data, KPCA is applied to new unseen data. A KPCA application approach is provided in Figure 5.6.

The pre-processed unseen data includes NOC data and fault data. The unseen data is first standardized with the saved training set mean and standard deviation. The standardized unseen data is then projected onto the hyperplane with the Gaussian kernel function. The new data is then centred and projected onto the reduced feature space.

The fault detection diagnostics can then be calculated as in the training case. The detection diagnostics are then compared to their respective control limits. The traditional fault detection performance metrics are then calculated. The FAR is calculated using the NOC data available from the unseen data. The MAR and DD is calculated from the fault data. The ROC is determined by varying the upper control limit using the unseen NOC data. The AUC is then calculated from the ROC.

The performance of KPCA as fault detection method can then be evaluated with the use of the traditional fault detection performance metrics.
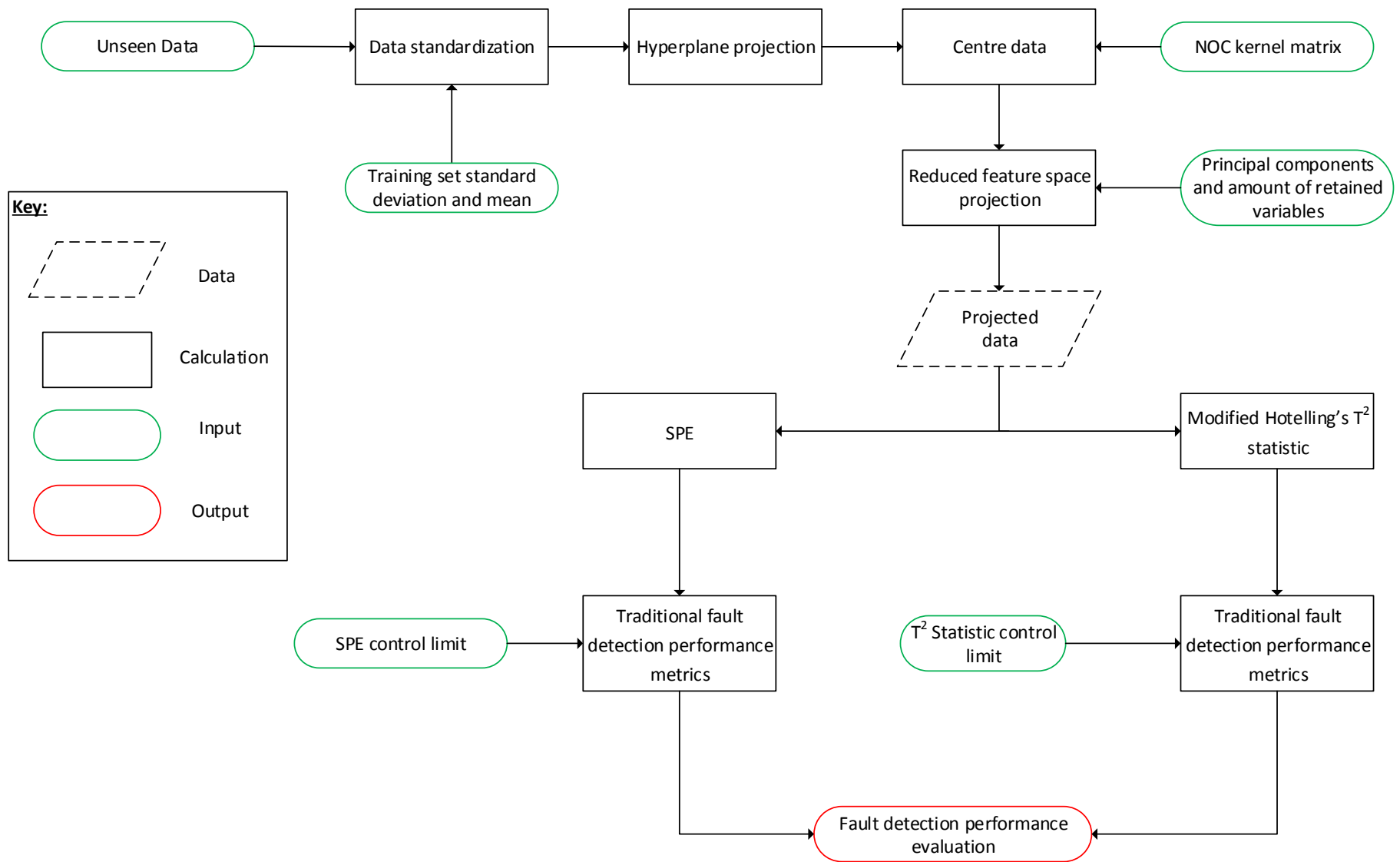
Figure 5.6: KPCA fault detection approach

5.2.3 Hyper-parameter selection

The hyper parameter selection for each fault detection method is discussed in the following section.

5.2.3.1 PCA

The amount of retained variance and detection diagnostics control limits serve as PCA model inputs. The amount of retained variance is set to 90% and upper control limits are calculated as the 99th percentile from the verification data detection diagnostics. The 90% variance retention is popular in fault detection studies. The 99th percentile control limit should result in a 1% FAR when applied to unseen NOC data.

5.2.3.2 KPCA

The amount of retained variance and detection diagnostics control limits is calculated similar to PCA when considering KPCA. This allows for a fair comparison between PCA and KPCA results.

The kernel width selection is important to ensure good KPCA fault detection performance. A proposed kernel width selection methodology was developed and is provided in Appendix B. In Appendix B the effect of kernel width is discussed and the method is also applied to the Tennessee Eastman case study to evaluate the proposed approach against other published kernel selection methods.

5.3 Fault identification

The following section provides the fault identification approach for each fault detection method. An overall contribution plot methodology is provided in Figure 5.7.
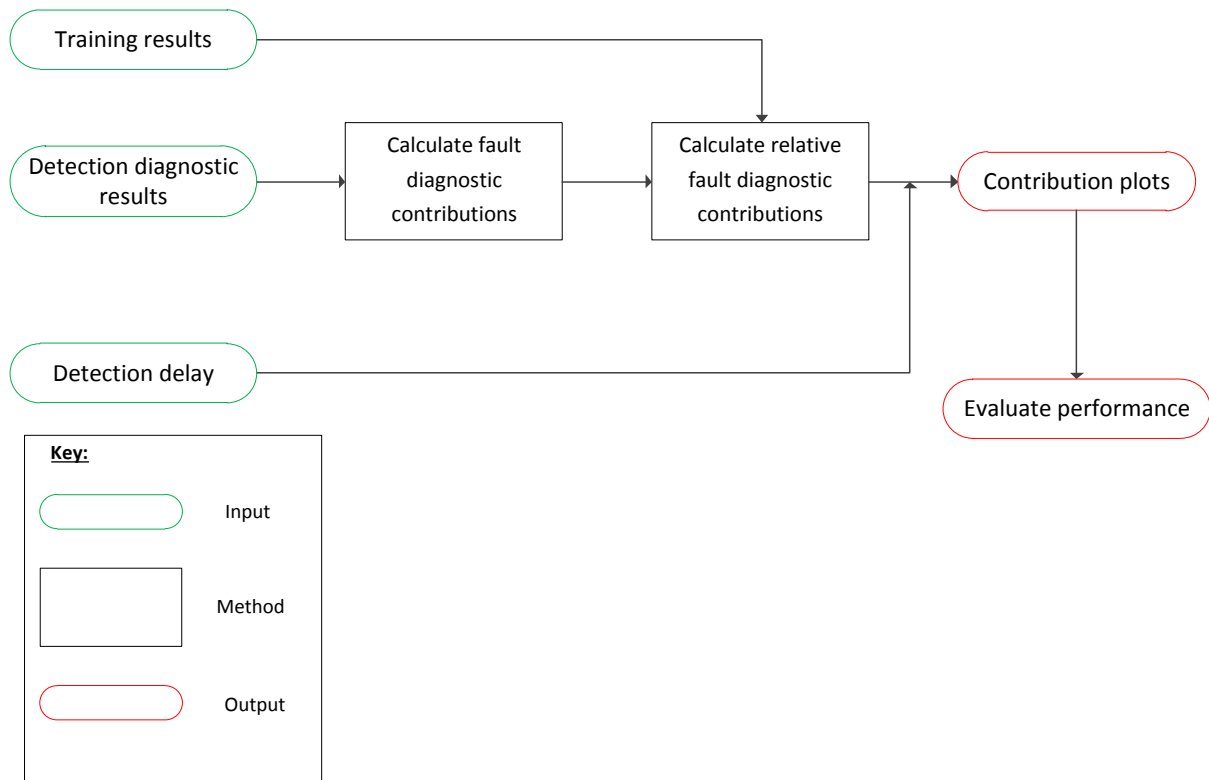
Figure 5.7: Contribution plot methodology.

The contribution plots are calculated for whichever fault diagnostic detects the fault first. The specific fault identification method is then applied to the fault data. The relative contributions are calculated from the training data contributions.

The contribution plots are then produced at the given detection delay. The average contributions from the detection delay and five consecutive samples are used to produce a real-time contribution plot. The fault identification performance can then be evaluated from the contribution plots.

Considering the large number of monitored variables, a single contribution plot will be difficult to evaluate. The contribution plots are therefore split into four sections as shown in Figure 5.8.
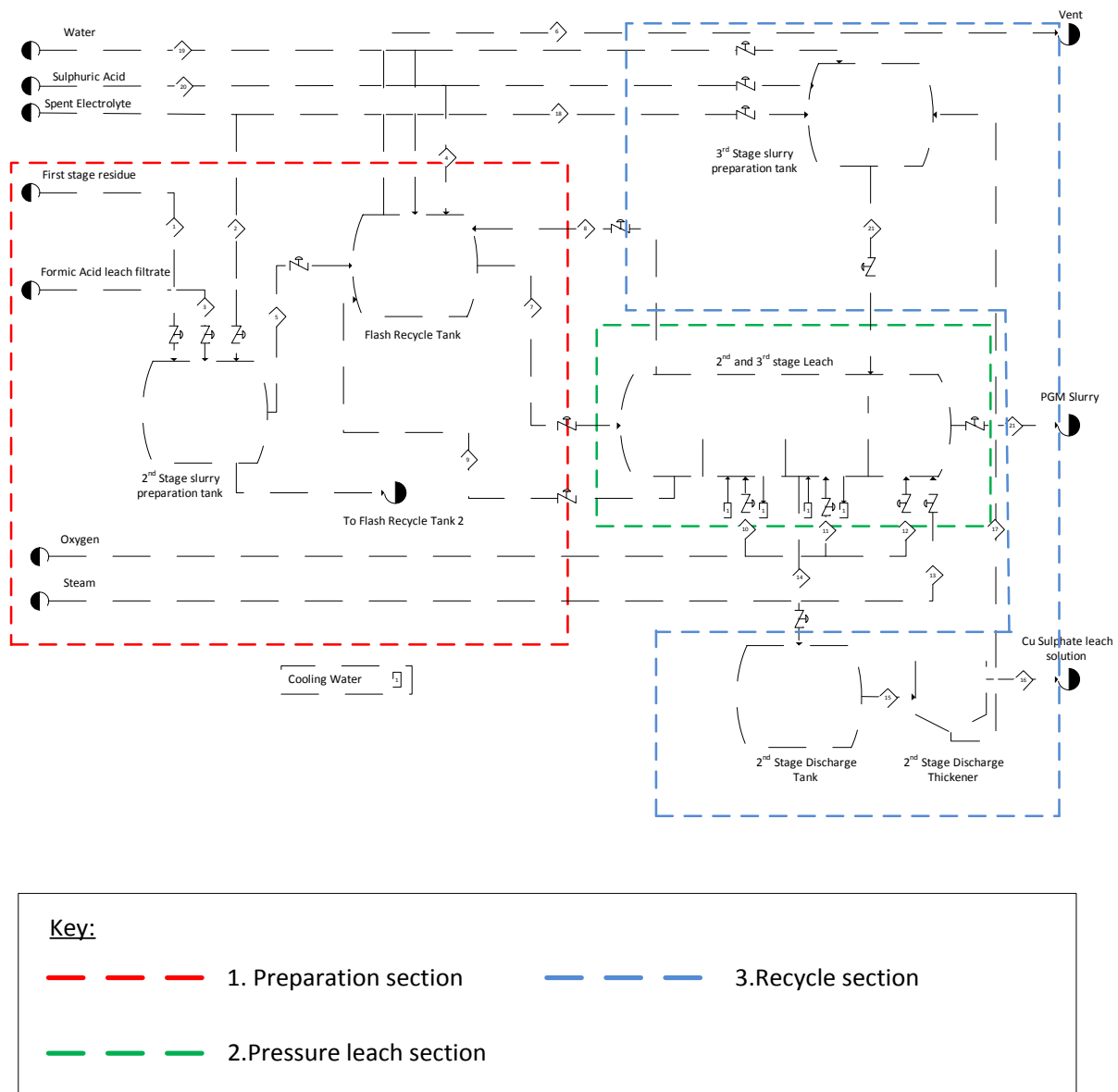
Figure 5.8: Process contribution plots representation. Preparation section indicated in red, pressure leach section indicated in green and recycle section indicated in blue.

The first section is the preparation section. This section includes the second stage preparation and flash recycle tank. The second section is the autoclave, including all four compartments. The third section is the recycle section. This section includes the second stage discharge tank, second stage discharge thickener and third stage preparation tank. Offline samples are considered as a separate section.

Process variable names are also abbreviated. The abbreviations are given in Table 5.2.

Table 5.2: Fault identification process variable abbreviations.

Abbreviation	Definition
PT	Pressure leach preparation tank.
FR	Flash recycle tank.
AT#	Autoclave. # indicates the compartment number.
RT	Third compartment recycle tank.
SL	Third compartment recycle solid/liquid separator.
RM	Third compartment recycle mixing tank
F	Flow measurement
L	Level measurement
T	Temperature measurement.
OX	Oxygen
SE	Spent electrolyte
SA	Sulphuric acid
W	Water
PROD	Product
REC	Recycle

The type of measurement is given first, followed by its location and the stream component. All flowrates are seen as feed rates e.g. 'FFRSA' is the sulphuric acid feed flow to the flash recycle tank.

5.4 Repeatability

As discussed in Chapter 2, section 2.3.4, random walks were incorporated by Miskin (2015) to simulate varying model inputs. This allows for each fault simulation to initiate from different initial conditions.

The different input compositions result in different model dynamic behaviour. This allows for each simulation run to be different. Each fault was simulated ten times to evaluate the robustness of each fault detection method. Initial random walk seeds were selected at random. The initial seeds are saved to allow for the replication of each simulation.

5.5 Post hoc analysis

Detection results needs to be statistically evaluated in order to determine whether a given method does provide increased detection performance. The fault detection results will be first evaluated using one-way analysis of variance (ANOVA). The ANOVA will compare the fault detection performance metrics results of the different fault detection methods. A significant ANOVA test result indicates at least one of the fault detection method results to differ from the other fault detection methods.

The main drawback of a one-way ANOVA test is that it will not indicate which fault detection methods provided significantly different results from the compared methods. In order to tell which method provided significantly different results, the least significant difference (LSD) test is applied.

The LSD test compares the individual means of each fault detection method by calculating the significant difference only for the two methods being compared (Fisher 1951).The one-way ANOVA test is first utilized in order to determine whether there is any significant difference in the fault detection performance metric results of the different fault detection methods. If ANOVA indicates a significant difference in fault detection method results, LSD test is applied to determine which detection method provides significant different results.

Chapter 6: Fault detection and identification results

Chapter 6 provides the model training, fault detection and fault identification results, following the methodologies described in Chapter 5.

Both PCA and KPCA model training results are discussed in section 6.1. Univariate fault detection results of each fault are compared to the PCA and KPCA detection results. The univariate fault detection methodology is provided in Appendix C.

The traditional fault detection performance metrics discussed in Chapter 3, section 3.3, are used to evaluate and compare the fault detection results in section 6.2. ANOVA is followed by LSD post hoc analysis to determine any significant differences in each detection performance metric. The complete fault detection and post hoc analysis results are provided in Appendix D.

Traditional and reconstruction based contribution plots are used to identify faults from both PCA and KPCA detection results (section 6.3). Complete contribution plots are provided in Appendix E. The fault detection and identification results are summarized in section 6.4.

6.1 Model training

As previously mentioned in Chapter 3, section 3.2.5, and Chapter 5, section 5.2; the selection of accurate normal operating conditions (NOC) data is challenging when considering the constant changes in the process operating conditions and feed compositions. It is important to include these input changes in the NOC training data set. This will allow for a more robust training model. The stochastic disturbance inputs (random walks) modelled by Miskin (2015) and discussed in Chapter 2, section 2.3, were used to develop a more robust training data set.

In order to allow the composition random walks to reach both upper and lower bounds, each random walk variable gradient was increased. The NOC training data simulation was therefore 'sped up' with a factor of twenty to offer a more robust training data set. Offline sampling times were reduced by a constant factor of eight. A shortened online sampling interval of 0.01 hours was used. This increased the representativeness (in terms of as much input condition states covered as possible) of the NOC training data set. The resulting training set consists of 19210 observations and 89 process variables.

The amount of retained variance was set at 90% for both PCA and KPCA. Detection diagnostic control limits were selected at the 99th percentile of NOC verification data. Therefore, detection results are comparable for both PCA and KPCA since the verification data set false alarm rate should

be similar for both detection methods. A detailed description of the univariate training and application is provided in Appendix C.

The PCA and KPCA application approaches were validated through a comparison to previously published fault detection studies. The validation results confirmed that both PCA and KPCA were comparable to previously published work. The validation results are provided in Appendix G.

6.1.1 PCA

The PCA model was successfully trained on the entire sped up training set. The number of retained components to explain 90% of the input variance is indicated in Figure 6.1.

Figure 6.1: PCA cumulative variance plot. The number of retained variables required to explain 90% of the input space variance is indicated in red.

Twenty eight principal components were retained in order to explain 90 of the input space variance. The first principal component explains approximately 22% of the input space variance. The cumulative variance plot clearly indicates that PCA can adequately reduce the input dimensions while still retaining significant input space variance.

The training and verification score plot for the first two retained components is shown in Figure 6.2. Training data is indicated in green and verification data is indicated in blue.

Figure 6.2: Two dimensional PCA training and verification score plot. Training data indicated in green and verification data indicated in blue.

Figure 6.2 shows a concentration of verification data. The verification data is not projected outside the two dimensional training data set projections and large variations are observed in the two dimensional projected space. These observations confirm the training data set is able to allow for significant variations in NOC data. The large training feature projection area is due to the large variations of the input random walks.

Figure 6.1 showed that approximately 33 % of the NOC training data set variance can be explained with the first two principal components. The specific variable contributions to the first two principal components are shown in Figure 6.3. A variable contribution furthest from the origin (0, 0) shows the most significant contribution to the first two principal components. Offline samples are variables numbered 37 and above.
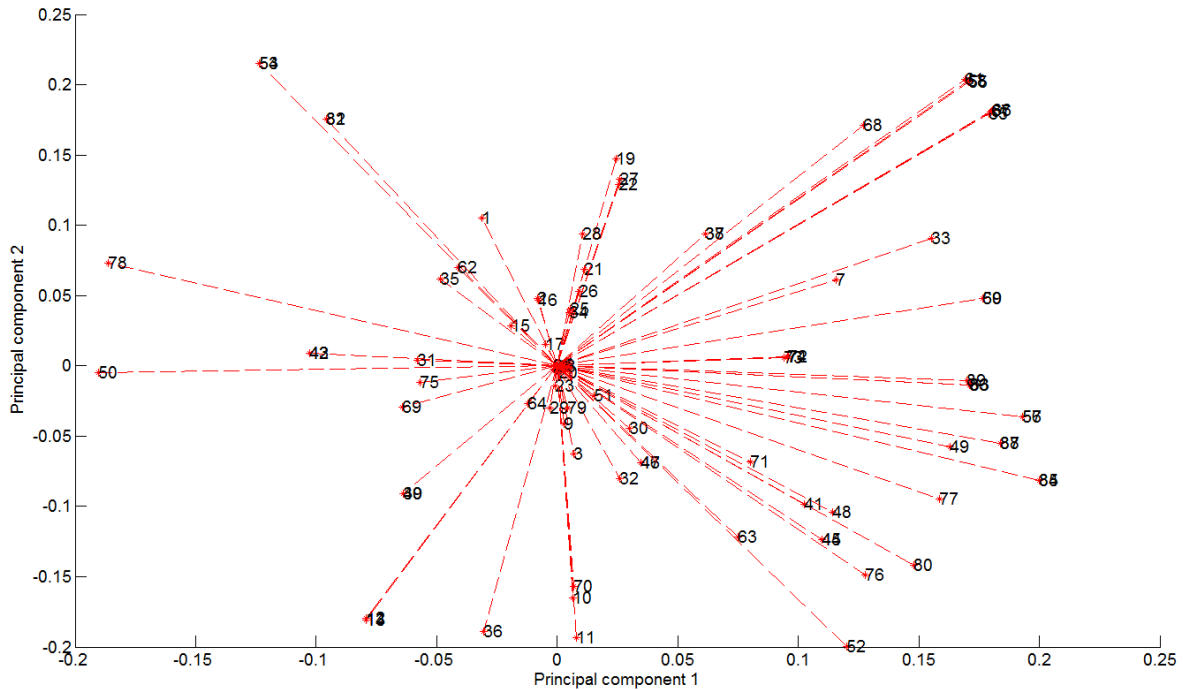
Figure 6.3: PCA first two principal components variable contributions. Process variables furthest from the origin (0, 0) provide the largest contributions to the first two principal components.

It is clear from Figure 6.3 that many process variables contribute significantly to the first two principal components. It is also noted from Figure 6.3 that offline sample variables contribute significantly more to the first two principal components, when compared to the online samples. This is again expected, when considering the large variations of the input random walks.

Some variables also offer very similar contributions to both principal components. This can be due to strong correlations existing between variables. This is especially noted with many offline sample variables. It is expected that strong correlations exist between these variables due to the chemical reactions present in the autoclave.

The training and verification data Shewhart charts are shown in Figure 6.4. The 99th verification percentile control limits are indicated in red.
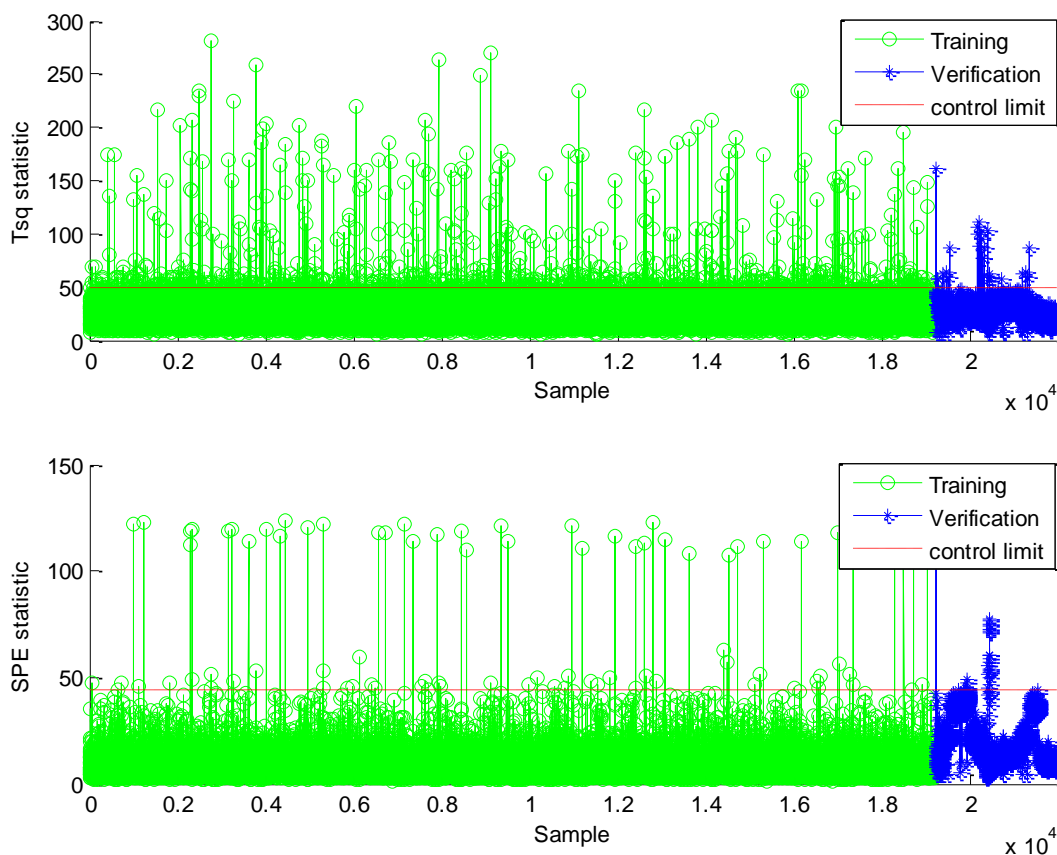
Figure 6.4: PCA training Shewhart charts. Training data are shown in green, verification data in blue and the 99th percentile control limit in red.

Figure 6.4 shows the detection diagnostic control limits selected. A T^2-statistic limit of 50.58 and SPE statistic limit of 49.14 were selected. Both detection diagnostics clearly do not deviate significantly from the training detection diagnostics. This confirms the observations made from Figure 6.2. The verification data is not projected outside the training data projection in all 28 dimensions.

6.1.2 KPCA

The sped-up training data set was sub-sampled due to computational power restrictions. The data is of type float and training required approximately 7-8 hours of CPU time. A 2nd generation Intel Core i7-980 processer was available with 16 GB RAM.

A constant sub-sampling interval of 7 was selected which resulted in a training set consisting of 2700 observations. The verification data was not sub-sampled in order to ensure fair detection diagnostic control limit selection. This will also potentially minimize the loss of NOC training data set information due to the sub-sampling.

The kernel width was selected based on the proposed kernel width selection method provided in Appendix B. The kernel width selection minimization function plot is provided in Figure 6.5. The minimization function (J) compares the Mahalonobis distances between training and verification data sets and chi-square distribution with A (retained variables) degrees of freedom.
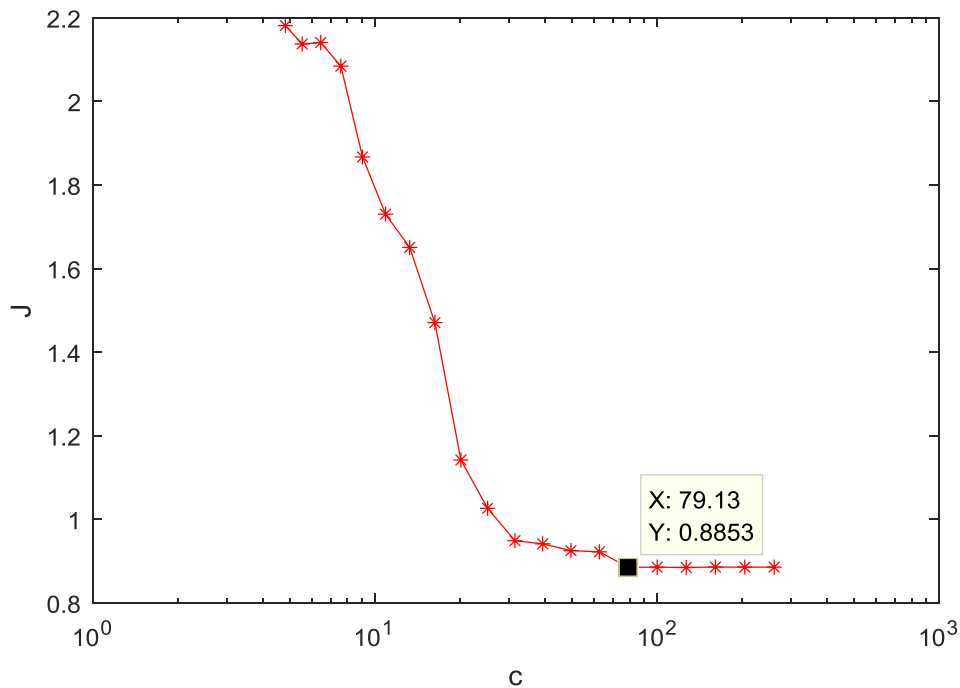
Figure 6.5: Kernel width minimization function. The minimization function (J) compares the Mahalonobis distances between training and verification data sets and chi-square distribution with A (retained variables) degrees of freedom.

As shown in Figure 6.5, a kernel width of c = 79.13 was selected based on the minimization function. Figure 6.6 show the effect of kernel width size on the NOC training and verification first two principal component scores.
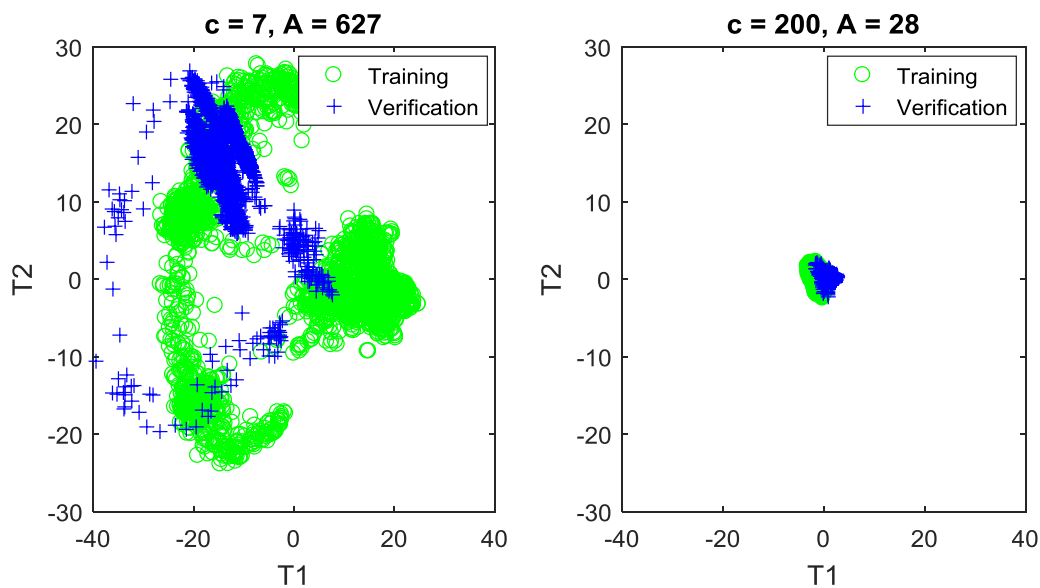
Figure 6.6: Effect of small and large kernel width on two dimensional feature space. The amount of retained variables (A) to explain 90% of the input space variance is indicated. Training data is indicated in green and verification data indicated in blue.

Figure 6.6 clearly shows the smaller kernel width results in a larger two-dimensional feature space, while the larger kernel width results in a smaller two-dimensional feature space. The smaller kernel width over fitted the training data set resulting in verification data being projected outside the training data projections. The large kernel width selected results in data overlapping in the nonlinear hyper plane. The overlapping reduces the non-linearity of the hyper plane. The effect of kernel width size is further investigated and discussed in Appendix B.

The KPCA cumulative variance plot for the first 89 principal components is provided in Figure 6.7. The number of principal components to be retained to explain 90 % of the NOC training set variance is shown in red.
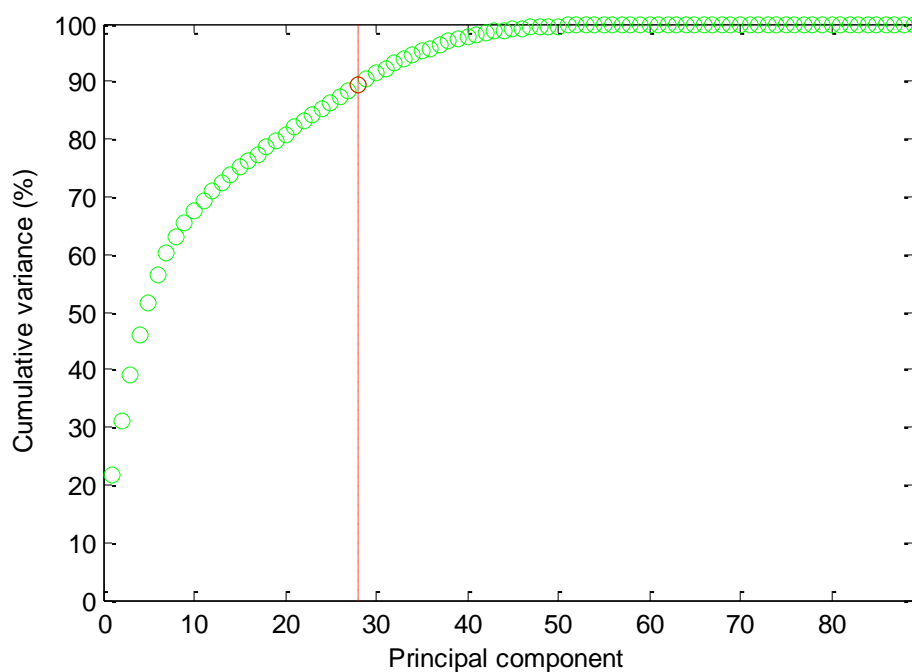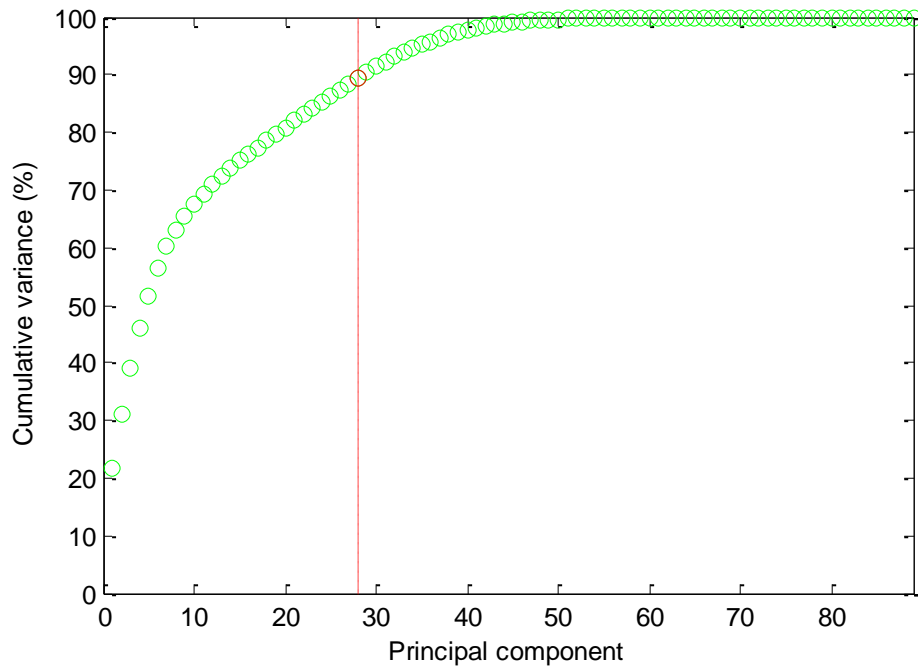
Figure 6.7: KPCA cumulative retained variance. The amount of retained variables required to explain 90% of the input space variance is indicated in red.

The cumulative variance plot in Figure 6.7 is exactly the same as the PCA cumulative variance plot in Figure 6.1. This is due to the large kernel width selected in Figure 6.5. The large kernel width results in the hyperplane projection, projecting data as if all data are from a multivariate normal distribution.

The two-dimensional feature space training and verification plot is shown in Figure 6.8. Training data is indicated in green and verification data is indicated in blue.
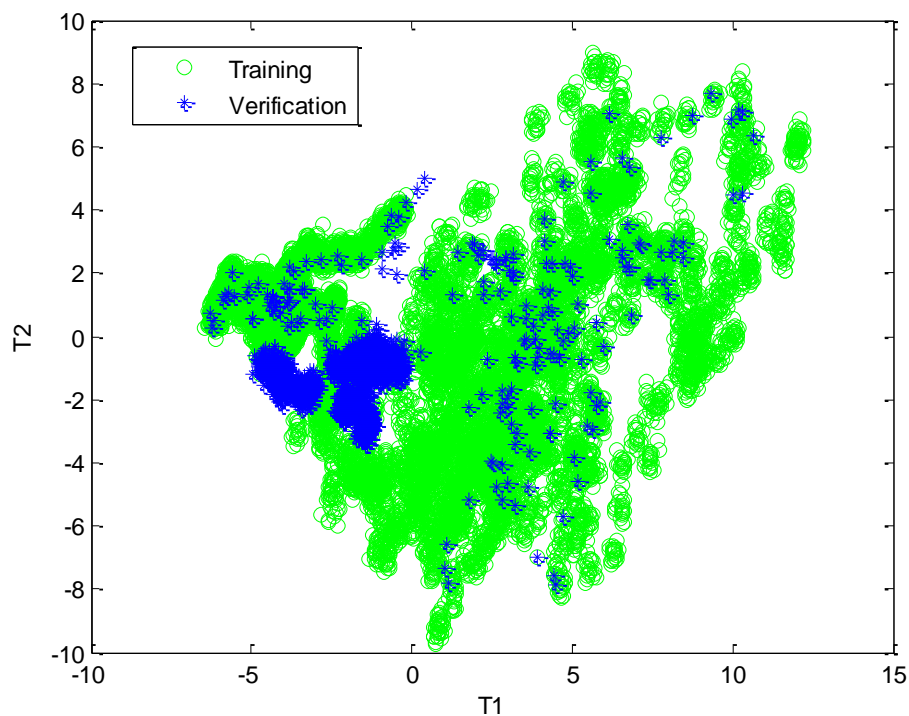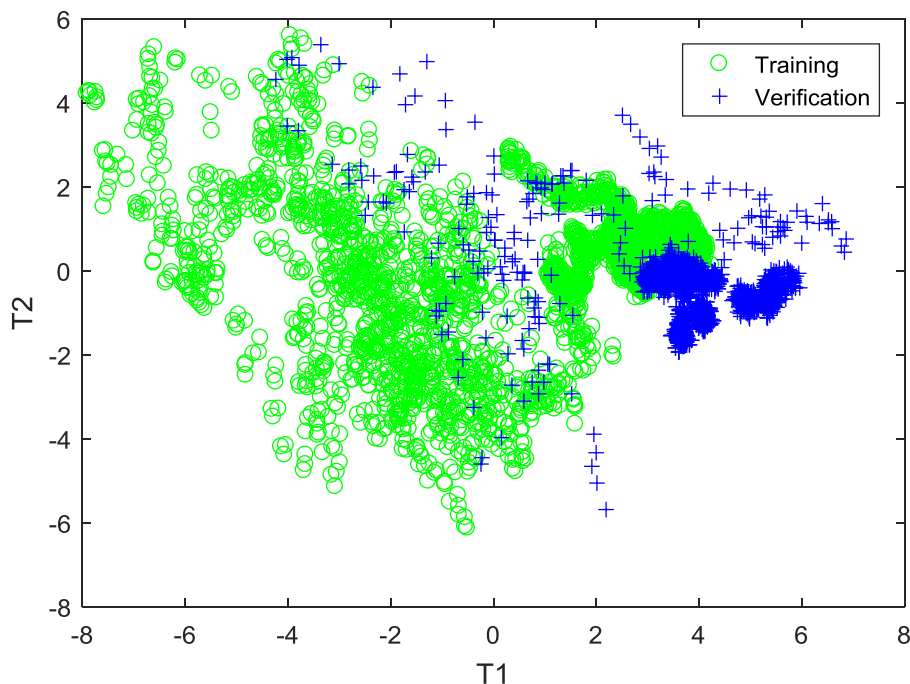
Figure 6.8: KPCA training and verification two dimensional score plot. Training data indicated in green and verification data indicated in blue.

The training and verification feature space projections is similar to that of PCA. Consider the shape of the verification data projection in both Figure 6.8 and Figure 6.2. The KPCA projection space seems to be a mirror image of the PCA projection space observed in Figure 6.2. However, the projected verification data clearly moves outside the two dimensional projected training data in Figure 6.8. This could be due to the significant sub-sampling for the KPCA training data set. The resulting projected training data is much sparser than the PCA projected training data. These observations again emphasises the importance of selecting the detection diagnostic control limits on the same verification data set.

The training and verification data KPCA Shewhart charts are provided in Figure 6.9. The 99th verification percentile control limits are indicated.
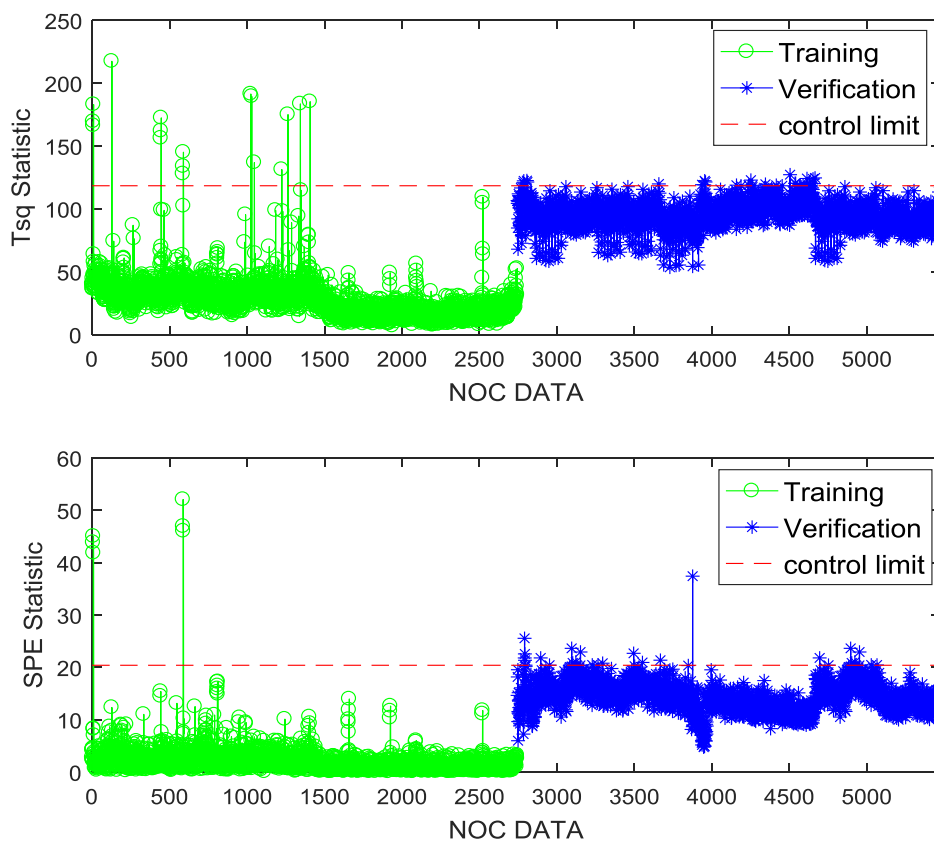
Figure 6.9: KPCA training and verification Shewhart charts. Training data are shown in green, verification data in blue and the 99th percentile control limit in red.

T^2-statistic and SPE control limits of 116.1 and 20.90 were selected from the verification data. The T^2-statistic clearly indicates that the projected verification data moves outside the training feature space.

Although the two-dimensional training feature spaces for both PCA and KPCA were similar in size, the KPCA T^2-statistic control limit is much larger than that of PCA. This is expected due to the projected verification data moving outside the training and feature space and the significant sub-sampling of the training data set. The larger control limits should in return provide realistic false alarm rates.

The fault detection results are discussed in section 6.2, using the detection performance metrics described in Chapter 3, section 3.3. Refer to section 3.1.3 for an impact summary for each fault.

6.2 Fault detection

Fault detection results are discussed in the following section. The density disturbance, valve wear, valve stiction and pump impeller wear detection results are provided in Figure 6.10. The solids build-up in cooling coil, peristaltic pump tube failure, sulphuric acid controller misuse and bubbler level sensor failure detection results are provided in Figure 6.11. Mean detection results are shown, while standard deviations observed from replicates are indicated with error bars.

The density disturbance (valve blockage) fault detection results are shown in Figure 6.10 (i). The density disturbance occurs right at the start of the process and has little impact on the process. It is therefore expected that the fault will be difficult to detect as it propagates through the process. Both univariate and KPCA were unable to detect the fault. Both PCA detection diagnostics were able to detect the fault in five of the ten replicates. The PCA detection diagnostics large standard deviations confirm the inconsistent detection delays. False alarm rates are below 4% for both PCA and KPCA.

The post hoc analysis showed a significant difference in both PCA detection delays when compared to KPCA and univariate. A significant difference in the PCA SPE false alarm rate was noted when compared to univariate and KPCA SPE. The false alarm rate is, however, still acceptable below 5%. The PCA SPE offered the best AUC, while both KPCA and univariate have AUCs below 0.5, which is expected when considering the poor detection delays (AUC results reported in Appendix D).

Both PCA detection diagnostics achieved the lowest missing alarm rates. This is expected when considering the detection delays shown in Figure 6.10 (i). The KPCA T^2-statistic missing alarm rate indicates that some alarms were triggered under fault conditions. However, the alarms were not triggered consecutively resulting in no registered detection delay. The post hoc analysis confirmed this observation with no significant difference in missing alarm rates observed between PCA and KPCA.

The valve wear detection results are shown in Figure 6.10 (ii). A transition time of 504 hours (3 weeks) was used to more accurately simulate the fault occurrence and evaluate the fault impact. The valve wear changes the valve characteristic from linear to quick opening; however process controllers are able to deal sufficiently with the valve wear. It is therefore expected that the fault will be difficult to detect significantly early.

Figure 6.10 (ii) shows that a univariate variable has the smallest mean detection delay. The fault is detected through the third residue offline sample. The fault is next detected by the KPCA T^2-statistic and closely followed by the PCA T^2-statistic. Large standard deviations are observed for the detection

delay results. The post hoc analysis however, did not show a significant difference in detection delays when comparing the T^2-statistic results to the univariate results. This is expected considering the large standard deviations observed.

The KPCA T^2-statistic has the lowest mean missing alarm rate as shown in Figure 6.10 (ii). However, the post hoc analysis did not show any significant difference in the missing alarm rates. This is again expected when considering the large standard deviations observed and no significant difference in detection delays.

The valve stiction detection results are shown in Figure 6.10 (iii). A transition period of 504 hours (3 weeks) was used to more accurately simulate the fault occurrence and evaluate the fault impact. The valve stiction results in large valve oscillatory behaviour. It is therefore expected that the fault will be easier detected when compared to the valve wear.

Figure 6.10 (iii) clearly shows the PCA SPE detecting the fault prior to both KPCA and univariate. This is confirmed by the post hoc analysis. The KPCA SPE mean detection delays are also smaller than any mean univariate detection delay. The fourth compartment residue sample has the smallest mean detection delay. Large standard deviations are observed in both KPCA detection diagnostics.

The large standard deviation in PCA SPE false alarm rate is also noted. The false alarm rate is within ISA standards; however it is still far outside the 1% limit set through the verification data (refer to Appendix D for univariate control limit selection methodology).

It is expected that the PCA SPE will have the smallest mean missing alarm rate considering the results observed in Figure 6.10 (iii). The post hoc analysis confirmed that the PCA SPE missing alarm rate is significantly lower than the univariate missing alarm rate, but not the KPCA SPE missing alarm rate.

The pump impeller wear detection results are shown in Figure 6.10 (iv). The fault was simulated with a 504 hour (3 weeks) transition period. Once the impeller is fully worn, the flow to the autoclave significantly drops. The fault has a significant impact on the process. It is therefore desired that the fault should be detected prior to the impeller being fully worn.

Figure 6.10 (iv) show that the KPCA T^2-statistic has the best mean detection delay. Both KPCA and PCA detection diagnostics mean detection delays are below univariate. The post hoc analysis confirmed only the KPCA T^2-statistic detected the fault significantly earlier than univariate.

The fault was univariate detected through the second stage product mixing tank level. The PCA SPE shows the lowest missing alarm rate. Again, this indicates the lack of consecutive alarms being triggered, when considering the detection delay results.
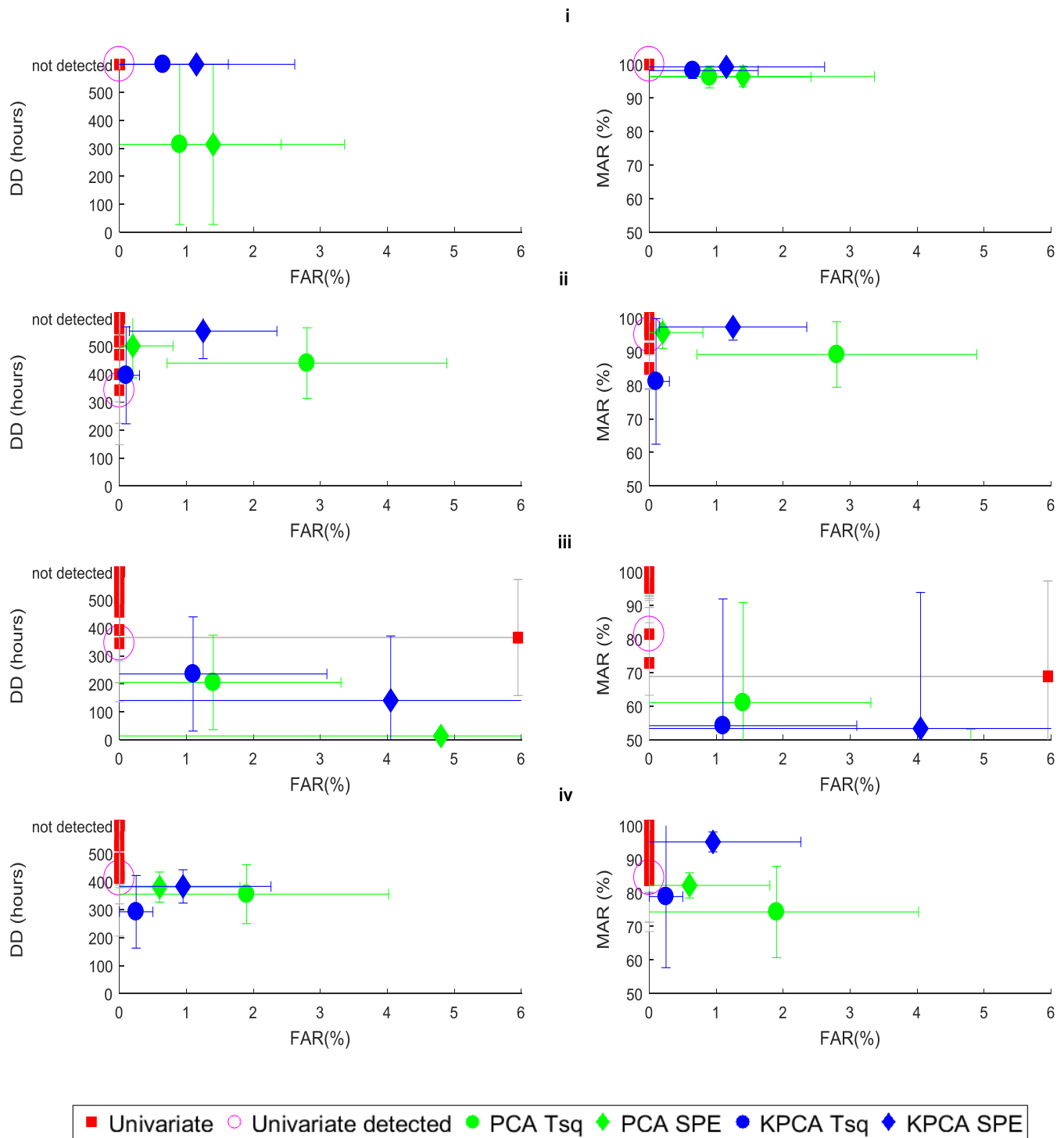
Figure 6.10: Fault detection false alarm rate, detection delay and missing alarm rate results: i) density disturbance, ii) valve wear, iii) valve stiction, iv) pump impeller wear. Mean results are shown, with error bars indicating standard deviations. Univariate variable detected indicated in pink.

The solids build-up-in-cooling coil results are shown in Figure 6.11 (i).The solids build-up in cooling coil is an incipient fault with a transition time of 50 hours. Once the second compartment cooling coil is blocked, the temperature of the compartment quickly rises. It is therefore crucial that the fault is detected prior to when the cooling coil is completely blocked.

From Figure 6.11 (i) it is clear that both PCA detection diagnostics have the lowest mean detection delay. Both KPCA detection diagnostics do not perform better than the best univariate detection variable. The post hoc analysis confirms that both PCA detection diagnostics have significantly lower detection delays when compared to both univariate and KPCA.

The third compartment temperature is the first univariate variable to detect the fault. This detection time also indicates the time at which the cooling water flow controller can no longer deal with the decreased flow. The approximately 9 hours which PCA detects the fault prior to this is significant since it allows intervention prior to a total loss of cooling water flow.

It is expected that both PCA detection diagnostics provide the smallest missing alarm rate. This observation is confirmed by the post hoc analysis for the PCA SPE statistic. However, the KPCA again does not perform better than the univariate detection variable.

Peristaltic pump tube failure detection results are provided in Figure 6.11 (ii). The peristaltic pump tube failure is an abrupt fault. The pump failure results in an immediate drop of first stage residue flow. The fault has a significant and immediate impact on the process. It is therefore desired that the fault is detected as soon as possible.

Figure 6.11 (ii) shows that all detection methods have a mean detection delay below 2 hours. The post hoc analysis confirms that the PCA SPE statistic detects the fault significantly earlier than both KCPA and univariate.

The early PCA SPE detection delay could contribute to process safety when considering the high mitigation priority and immediate impact of the fault. Following on the detection results, it is expected that PCA SPE has the lowest missing alarm rate. This is confirmed by the post hoc analysis.

Although the KPCA SPE has a smaller mean detection delay than univariate, a much larger mean missing alarm rate is observed. This could indicate the fault 'collapsing' into the reduced feature space after it has been detected.

Sulphuric acid controller misuse detection results are provided in Figure 6.11 (iii). The sulphuric acid controller misuse is an abrupt fault which lasts for one hour. The fault has a lesser impact on the process, with process controllers being able to deal with the impact. Increased number of PGMs in

the filtrate is expected with the increase in sulphuric acid. It is therefore desired to detect the fault as early as possible to decrease the number of recycled PGMs.

From Figure 6.11 (iii) it is clear that univariate is unable to successfully detect the fault. Univariate only detected the fault once in all ten replicates. Although both KPCA and PCA has clearly smaller mean detection delays, large standard deviations are observed for both methods. This is due to PCA only detecting the fault in five of the ten replicates, while KPCA only detected the fault in three of the ten replicates. The post hoc analysis confirms that only the PCA T^2-statistic has a significantly different detection delay.

The missing alarm rate trends in Figure 6.11 (iii) are similar to the detection delay results. The post hoc analysis confirmed the PCA T^2-statistic missing alarm rate to be only significantly different to that of univariate.

Bubbler level sensor bias detection results are provided in Figure 6.11 (iv). The bubbler level sensor bias is an abrupt fault. The fault causes the level reading of the fourth compartment to be biased. It is therefore expected that the fault will be difficult to detect, since the actual level measurement of the compartment is not available.

Similar to the sulphuric acid controller misuse fault, the fault was not detected with each replicate. Although the KPCA SPE has the smallest mean detection delay, the post hoc analysis concluded that there is no significant difference in detection delay results.

Univariate offline samples and PCA detected the fault in three of the ten replicates. KPCA detected the fault in six of the ten replicates. Figure 6.11 (iv) shows large deviations in most missing alarm rates. The post hoc analysis confirmed this observation with showing no significant difference in missing alarm rates.
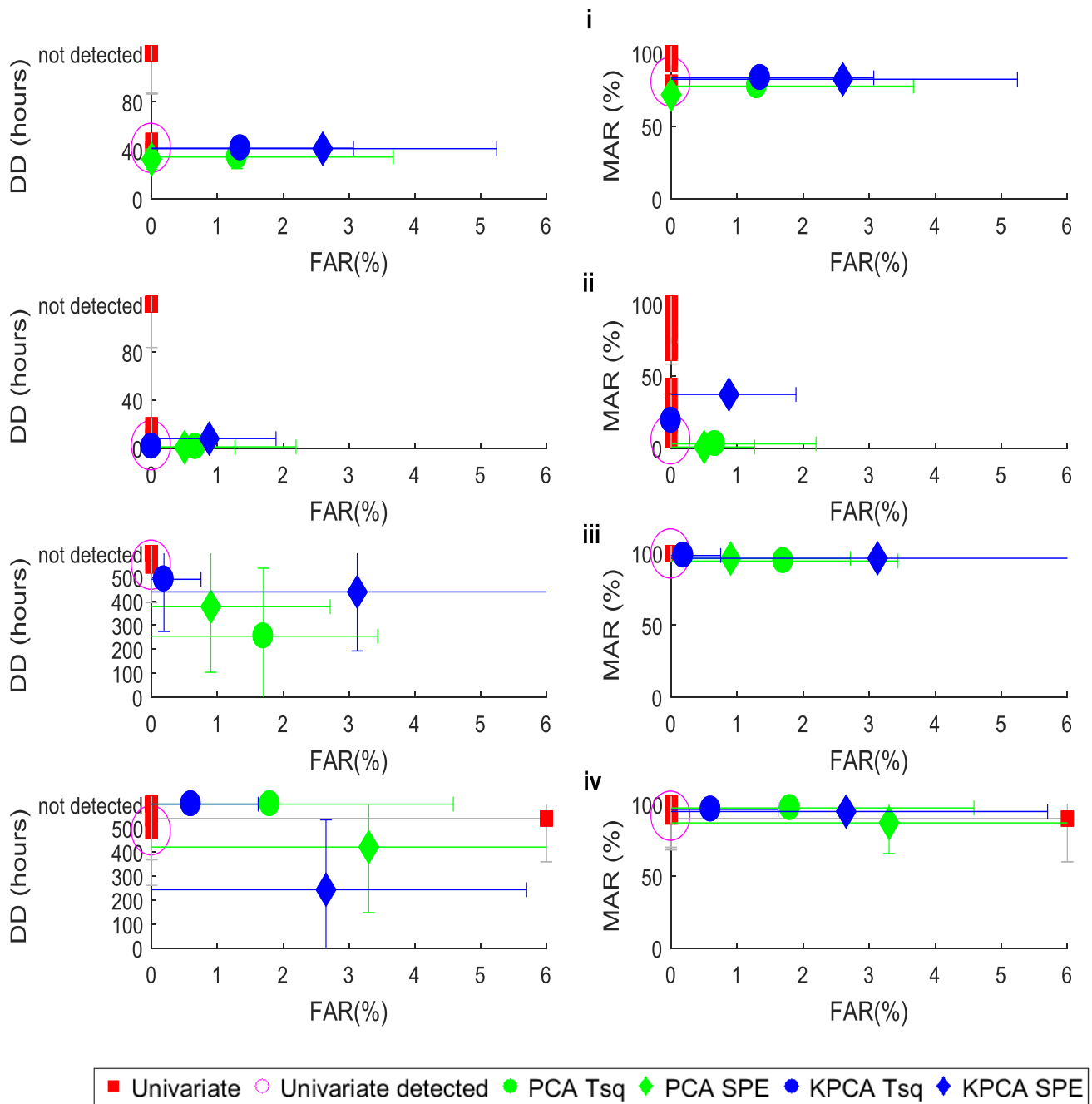
Figure 6.11: Fault detection false alarm rate, detection delay and missing alarm rate results: i) solids build up, ii) peristaltic pump tube failure, iii) sulphuric acid controller misuse, iv) bubbler level sensor failure. Mean results are shown, with error bars indicating standard deviations. Please note the difference in detection delay results scale for both figures i and ii. Univariate variable detected indicated in pink.

Large standard deviations are observed in both PCA and KPCA results provided in Figures 6.10 and 6.11. The variations again emphasises the significant impact of the input random walks. Acceptable false alarm rates are also observed (below 5% and below ISA standards provided in Appendix C). The false alarm rates indicate that both PCA and KPCA training models can adequately handle the input variations from the replicates.

Figures 6.10 and 6.11 clearly indicate that multivariate methods can successfully detect process faults. Once a fault is detected, the correct fault location needs to be identified. The fault identification results are provided and discussed in section 6.3.

6.3 Fault identification

The following section provides the fault identification results for each individual fault. Only significant process variable contributions are provided and discussed. Contribution plots relating to the detection diagnostic with the smallest mean detection delay are investigated for both PCA and KPCA. The significant contribution plots are provided in Appendix E.

6.3.1 PCA

The PCA fault identification results are summarised in Tables 6.1 and 6.2. Process variables with significant relative contributions are provided in the tables. The first variable provided, is the correct fault location. The variable is shown in green if it was identified and red if the location variable was not identified. The remaining variables are all symptoms of the fault which were identified. Results for both traditional- and reconstruction based -contributions (RBC) are considered.

Table 6.1 clearly show only fault symptoms were identified for faults 1 – 4. It is expected that correct fault location identification will be challenging when considering the 504 hour fault transition periods and the small impact of the density disturbance (valve blockage) fault.

The large density disturbance fault detection delays observed in Figure 6.10(i) indicated that fault symptoms triggered alarms instead of the fault location. The fourth compartment level should indicate the correct valve wear location. However, only offline samples are identified. This is again due to process controllers being able to deal with the fault and therefore hide its location. Similar observations are made for the pump impeller wear and valve stiction faults. RBC was generally unable to decrease the fault smearing when compared to the traditional contributions. However, RBC did provide less significant offline sample contributions.

Table 6.1: PCA fault identification results. The detection diagnostic with the smallest detection delay is considered. Process variables providing significant contributions are indicated using either traditional or reconstruction based contribution plots. Fault location correctly identified is shown in green. Fault location not identified is indicated in red.

#	Fault name	Detection diagnostic	Traditional contributions	RBC
1	Density disturbance (Valve blockage)	SPE	• Preparation tank residue feed flow • Flash recycle tank feed flow • Pressure leach preparation tank temperature • Third compartment residue • First stage residue • Fourth compartment residue	• Preparation tank residue feed flow • Recycle mixing tank temperature • Third compartment solid/liquid separator level • Third and fourth compartment residues • Third and fourth compartment filtrate
2	Valve wear	T^2	• Fourth compartment outlet flow and level • Fourth and first compartment residue	• Fourth compartment outlet flow and level • Third and fourth compartment residue • Third compartment filtrate
3	Valve stiction	SPE	• Preparation tank spent electrolyte feed • Third compartment solid/liquid separator level • Third and fourth compartment filtrate	• Preparation tank spent electrolyte feed • Third compartment solid/liquid separator level • Fourth compartment filtrate
4	Pump impeller wear	T^2	• First compartment feed flow	• First compartment feed flow

Table 6.1 (*cont.):* PCA fault identification results. The detection diagnostic with the smallest detection delay is considered. Process variables providing significant contributions are indicated using either traditional or reconstruction based contribution plots. Fault location correctly identified is shown in green. Fault location not identified is indicated in red.

			• Fourth compartment residue	• Third and fourth compartment residues • Third compartment filtrate

Legend:

Fault location identified	██████
Fault symptom not identified	██████

Both identification methods identified the second compartment temperature as the correct location variable for the solids build-up in cooling coils fault. RBC successfully identified the sulphuric acid controller misuse location variable. Both identification methods were unable to identify the correct location variables for both the peristaltic pump tube failure and bubbler level sensor failure faults. It is expected that the bubbler level sensor fault identification will be difficult to identify, considering the measurement showing no change in level.

Table 6.2: PCA fault identification results. The detection diagnostic with the smallest detection delay is considered. Process variables providing significant contributions are indicated using either traditional or reconstruction based contribution plots. Fault location correctly identified is shown in green. Fault location not identified is indicated in red.

#	Fault name	Detection diagnostic	Traditional contributions	RBC
5	Solids build-up in cooling coils	SPE	• Second compartment temperature • Third and fourth compartment filtrate	• second compartment temperature • Third and fourth compartment filtrate • Flash recycle tank temperature
6	Peristaltic pump tube failure	SPE	• Preparation tank residue feed flow • Preparation tank flow	• Preparation tank residue feed flow • Preparation tank flow

Table 6.2 (*cont.*): **PCA fault identification results. The detection diagnostic with the smallest detection delay is considered. Process variables providing significant contributions are indicated using either traditional or reconstruction based contribution plots. Fault location correctly identified is shown in green. Fault location not identified is indicated in red.**

			recycle • Third compartment recycle tank temperature • Third compartment solid/liquid separator level	recycle • Preparation tank level • Third compartment level • Second compartment temperature • Third compartment temperature • First compartment level • Autoclave pressure • Third compartment recycle tank level
7	Sulphuric acid controller misuse	T^2	• Flash recycle tank sulphuric acid flow • Second compartment temperature • Fourth compartment residue	• Flash recycle tank sulphuric acid flow
8	Bubbler level sensor bias	SPE	• Third compartment level and outlet flow • Third compartment recycle tank level • Third and fourth compartment residue • Third and fourth compartment filtrate	• Third compartment level and outlet flow • Third and fourth compartment residue • Third and fourth compartment filtrate

<u>Legend:</u>

Fault location identified	█████
Fault location not identified	█████

6.3.2 KPCA

The KPCA fault identification results are summarised in Tables 6.3 and 6.4. Results are again presented as with PCA, however only traditional contribution plots were considered.

The traditional contribution plot results for the first four faults are provided in Table 6.3. The correct fault locations were not identified. This is again due to the significant transition periods. Fault identification results are not available for the density disturbance (valve blockage) fault, since the fault was not detected as shown in Figure 6.10.

Table 6.3 also indicates that KPCA suffered increased fault smearing when compared to the PCA traditional contribution plot results in Table 6.1. This is expected, considering the general increased detection delays observed in Figure 6.10. The increased detection delay allows for more fault symptoms to be developed.

Table 6.3: KPCA fault identification results. The detection diagnostic with the smallest detection delay is considered. Process variables providing significant contributions are indicated using traditional contribution plots. Fault location correctly identified is shown in green. Fault location not identified is indicated in red.

#	Fault name	Detection diagnostic	Traditional contributions
1	Density disturbance (Valve blockage)	SPE	Fault not detected
2	Valve wear	T^2	• Fourth compartment outlet flow and level • Third compartment recycle tank level • Third compartment recycle tank temperature • Third and fourth compartment residue • Third and fourth compartment filtrate
3	Valve stiction	SPE	• Preparation tank spent electrolyte feed • First compartment recycle flow • Second compartment O_2 flow • Second compartment temperature • Autoclave pressure • Third and fourth compartment residue • Third and fourth compartment filtrate
4	Pump impeller wear	T^2	• First compartment feed flow • Flash recycle tank temperature

Table 6.3 (*cont.*): KPCA fault identification results. The detection diagnostic with the smallest detection delay is considered. Process variables providing significant contributions are indicated using traditional contribution plots. Fault location correctly identified is shown in green. Fault location not identified is indicated in red.

			• First compartment recycle flow
			• Second compartment O$_2$ flow
			• Second compartment temperature
			• Third compartment recycle tank level
			• Third compartment recycle tank temperature

Legend:

Fault location identified	🟩
Fault symptom not identified	🟥

The KPCA traditional contribution plots for the remaining faults are provided in Table 6.4. The solids build-up in cooling fault location was successfully identified. The peristaltic pump tube failure and sulphuric acid controller misuse fault locations were not identified. The bubbler level sensor was not considered, since the fault was not detected. The peristaltic pump tube failure suffered from significant fault smearing considering the number of fault symptoms identified. This is expected, when considering the immediate impact of the fault and the increased detection delay when compared to PCA.

Table 6.4: KPCA fault identification results. The detection diagnostic with the smallest detection delay is considered. Process variables providing significant contributions are indicated using traditional contribution plots. Fault location correctly identified is shown in green. Fault location not identified is indicated in red.

#	Fault name	Detection diagnostic	Traditional contributions
5	Solids build-up in cooling coils	SPE	• Second compartment temperature • Second compartment O_2 flow • Third and fourth compartment filtrate • Third and fourth compartment residue
6	Peristaltic pump tube failure	SPE	• Preparation tank residue feed flow • Preparation tank level • Flash recycle tank level • Flash recycle tank temperature • Second compartment O_2 flow • Third compartment level • Second compartment temperature • Third compartment recycle tank level • Third compartment recycle mixing tank level • Third compartment recycle mixing tank temperature
7	Sulphuric acid controller misuse	T^2	• Flash recycle tank sulphuric acid flow • Second compartment O_2 flow • Third compartment O_2 flow • Second compartment temperature • Third and fourth compartment residue • Third and fourth compartment filtrate
8	Bubbler level sensor bias	SPE	Fault not detected

Legend:

Fault location identified	■
Fault symptom not identified	■

6.4 Summary

The following section will provide a summary of the results discussed in sections 6.1 – 6.3. Both PCA and KPCA models were successfully trained. The training models were robust to input disturbances, offering acceptably low false alarms. The detection results can therefore be considered realistic for a real-world application. The fault detection and post hoc analysis results are summarized in Table 6.5.

Table 6.5: Fault detection results summary. Post hoc analysis results are indicated.

#	Fault	Univariate	PCA	KPCA
1	Density disturbance	✖	✓	✖
2	Valve wear	✓	✓	✓
3	Valve stiction	✓	✓	✓
4	Impeller wear	✓	✓	✓
5	Solids build-up in cooling coil	✓	✓	✓
6	Peristaltic pump tube failure	✓	✓	✓
7	Sulphuric acid controller misuse	✖	✓	✓
8	Bubbler level sensor bias	✓	✓	✓

Legend:

Fault detected	✓
Fault not detected	✖
Method detected fault significantly earlier than univariate	
Method detected fault significantly earlier than univariate and PCA/KPCA	

Table 6.5 clearly indicates that PCA out performed both KPCA and univariate methods. KPCA did not show significantly improved detection results when compared to univariate. This confirms observations made from the KPCA training results. The large kernel width selected indicated that input space linear correlations only needed to be taken into account. Furthermore, the sub-sampled training set resulted in higher detection diagnostic thresholds.

The early fault detection of both the solids build-up in cooling coil and peristaltic pump tube failure is of significance in terms of possible process safety. Both faults can have a significant immediate impact on process safety, adding an increased significance to the early fault detection results.

The input random walks incorporated by Miskin (2015) also clearly had a significant impact on the detection results. Large standard deviations were observed with the longer incipient faults, while faults were not always detected when considering the lower impact faults.

The fault identification results are summarized in Table 6.6.

Table 6.6: Fault identification results summary.

| # | Fault | PCA | | KPCA |
		Traditional contributions	RBC	Traditional contributions
1	Density disturbance	✘	✘	n.c
2	Valve wear	✘	✘	✘
3	Valve stiction	✘	✘	✘
4	Impeller wear	✘	✘	✘
5	Solids build-up in cooling coil	✔	✔	✔
6	Peristaltic pump tube failure	✘	✘	✘
7	Sulphuric acid controller misuse	✘	✔	✘
8	Bubbler level sensor bias	✘	✘	n.c

Legend:

Fault location identified	✔
Only fault symptoms identified	✘
Contribution plots not considered	n.c

The promising detection results were not supported by the fault identification results. Fault smearing was still observed for most faults. The PCA RBC only performed slightly better when compared to the PCA traditional contribution plots. KPCA traditional contribution plots provided similar results to that observed for PCA.

The tight process controller tuning is the main contributing factor for the poor fault identification results observed. The process controllers 'hide' the faults in order to preserve optimal operating conditions. This observation is in line with the conclusions made by Bin Shams (2010). In order to optimize a fault diagnosis strategy, the process controllers needs to detuned to allow for slightly more process variations. The detuned process controllers will allow for decreased detection delays and more accurate fault identification.

Chapter 7: Economic performance function development

Following the fault detection and identification results described in Chapter 6, the next objective needs to be addressed. Suitable economic indicators need to be identified for the pressure leach process followed by the development of economic performance functions (EPFs) in order to complete an economic impact assessment.

Chapter 7 describes the EPF development. The EPF development methodology developed by Wei (2010), discussed in Chapter 3, section 3.5.2, is followed to develop EPFs specific to the BMR. The methodology follows the five steps set out in Figure 3.11. The steps are described in sections 7.1- 7.5.

Two EPFs are developed: The first EPF focus on potential PGE losses in the process and the second EPF focus on potential PGE build-up in the process. The Chapter is summarized in section 7.6.

7.1 Information required

The goal of the first step is to determine the information required for the economic performance functions development. An understanding of process operations was developed from previous studies conducted on the base metal refinery (BMR). The work completed by Miskin (2015) and Knoblauch (2015) were used to develop an in-depth knowledge of the control strategy and process control systems present at the BMR. A site visit was conducted to develop an understanding of the process economics and identify the main economic objectives/key indicators. Expert knowledge identified the main objective as the Platinum group element (PGE) production rate with a specific focus on minimizing PGE losses (N.M. and J.B. 2016).

Unwanted variations in the PGE residue composition can be caused be either under- or over – leaching. Under-leaching occurs when the base metals are not sufficiently removed from the PGE-containing residue. Over-leaching results in excess PGEs being removed from the PGE-containing residue, alongside the base metals. The PGEs are then sent to the copper electrowinning circuit as second and third stage filtrate.

Figure 7.1 provides a basic flowsheet of the copper electrowinning circuit. The pressure leach filtrate is sent to the Se/Te removal unit followed by the copper electrowinning circuit. The spent electrolyte from the copper electrowinning circuit is recycled to the first stage atmospheric leach.
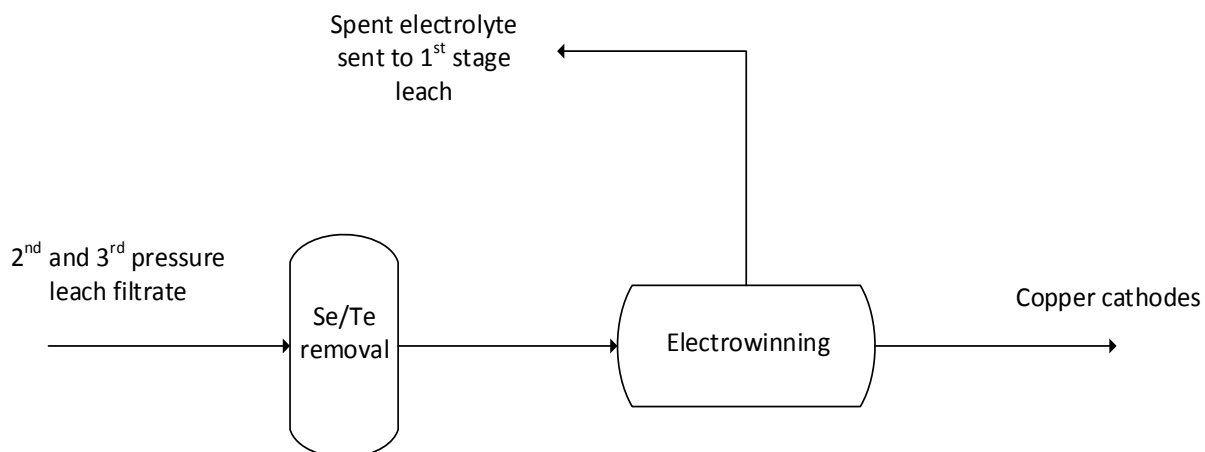
Figure 7.1: Copper electrowinning circuit. Second and third stage leach filtrate is first sent to Se/Te removal unit, followed by the copper electrowinning circuit.

Abnormal process conditions can lead to over-leaching. The over-leaching in turn results in increased PGMs reporting to the pressure leach filtrate product stream. These PGEs are then sent to the copper electrowinning circuit. Some of the PGEs are lost to the copper cathodes, while the remaining PGEs are recycled as spent electrolyte to the first stage atmospheric leach. The recycled PGEs are referred to as metals in process (MIP).

Although the MIP are not lost and will report back to the pressure leach in the first stage residue, any build-up of PGEs in the process is unwanted. Increased MIP also delays the PGE production rate further downstream (N.M. and J.B. 2016).

Under-leaching will result in an increased amount of base metals reporting to the pressure leach residue. The residue is then sent to an acid wash. The acid wash uses sulphuric acid in a batch process to remove the unwanted base metals. The spent electrolyte containing the base metals is then sent to the copper electrowinning circuit. The sulphuric acid required for the acid wash is not considered as an economic penalty. This is due to the overall sulphuric acid balance present in the BMR. The sulphuric acid used for the acid wash will therefore only result in a decreased amount of sulphuric acid required upstream. (N.M. and J.B. 2016).

Possible base metal losses are also not considered as an economic penalty. This is again due to the acid wash reducing any base metal losses. The copper production is not the main economic objective as identified by expert knowledge (N.M. and J.B. 2016).

7.2 Performance function information

Following section 7.1, potential over-leaching was identified as the main concern. Specific emphasis is placed on the potential increase in PGEs lost to the copper cathodes and the potential increase in MIP. The fractions of PGEs lost to the copper cathodes were gathered from the site visit. Fractions were calculated from historical plant operational data. The fraction of the copper electrowinning feed PGEs lost to the copper cathodes are provided in Table 7.1 (N.M. and J.B. 2016).

Table 7.1: Fraction of copper electrowinning feed PGEs lost to copper cathodes (N.M. and J.B. 2016).

PGE	Feed fraction lost to copper cathodes (%)
Rh	0.75
Ru	0.8
Ir	3
Pt	31
Pd	18

Table 7.1 clearly indicates significantly larger amounts of Pt and Pd is lost to the copper cathodes when compared to the remaining PGEs. However, it is important to note that the inlet Pt and Pd concentrations are relatively small when compared to the remaining PGEs concentration.

7.3 Performance measures

The strategy of the pressure leaching process is to produce a PGM rich residue. This strategy is reached through the removal of copper and the minimization of copper leaching. The key measurements are the operating condition control of the autoclave and the offline residue and filtrate samples.

7.4 Assumptions

The following assumptions are made when considering the economic performance function development. The assumptions relate to the either the PGE concentrations evaluated or the potential impacts of the simulated process faults not considered.

The assumptions relating to the PGE concentrations are:

- Prior to the copper electrowinning circuit, filtrate is first sent to a selenium and tellurium removal unit. Steenekamp and Dunn (1999) reported that some PGMs are recovered in the unit through precipitation. It is assumed that the precipitated PGEs recovered are negligible.
- Coetzee (2016) reported some small amounts of Ru and Ir reporting in the atmospheric leach filtrate. It is assumed that these PGE losses are negligible after consultation with expert knowledge (N.M. and J.B. 2016).
- The fractions of PGEs lost, provided in Table 7.1, are constant.
- All PGE prices are constant.

The assumptions relating to the impact of process faults are:

- According to expert knowledge, faults will not result in an emergency shutdown (N.M. and J.B. 2016).
- Increased cooling water and oxygen usage are negligible according to simulation data and expert knowledge (N.M. and J.B. 2016).
- Process recovery times are considered constant, irrespective of the detection delay.

7.5 Performance functions

Following sections 7.1 - 7.4, two EPFs are developed. The first performance function is the PGE losses to the copper electrowinning circuit. The performance function is provided in equation 7.1.

$$PGE \ losses \ (\$/hr) = \sum_{i=1}^{5} P_i f_i (F_i - F_{is}) \tag{7.1}$$

In the above equation F_i refers to the individual PGE inlet flow-rate to the copper electrowinning circuit. P_i is the current PGE price and f_i is the fraction of the PGE lost to the copper cathodes (Table 7.1).

The second EPF is the metals in process (MIP) function. The MIP performance function is the PGEs recycled to the first stage atmospheric leach. The performance function is provided in equation 7.2.

$$MIP \ (\$/hr) = \sum_{i=1}^{5} P_i (1 - f_i)(F_i - F_{is}) \tag{7.2}$$

It is important to note that the MIP performance function does not represent any monitory loss. The MIP performance function shows the delayed PGE production rate.

Figure 7.2 aims to illustrate the use of both EPFs. Both EPFs are linear performance functions and are dependent on the individual PGE flowrates to the copper electrowinning circuit. The NOC point is indicated in red. Abnormal (faulty) process conditions will lead to potential increases in the PGE flow to the copper electrowinning circuit, which in turn will result in an increased amount of PGEs lost and MIP. Reducing the operating time spent away from the NOC point, will decrease the PGEs lost and the MIP under abnormal (faulty) conditions.
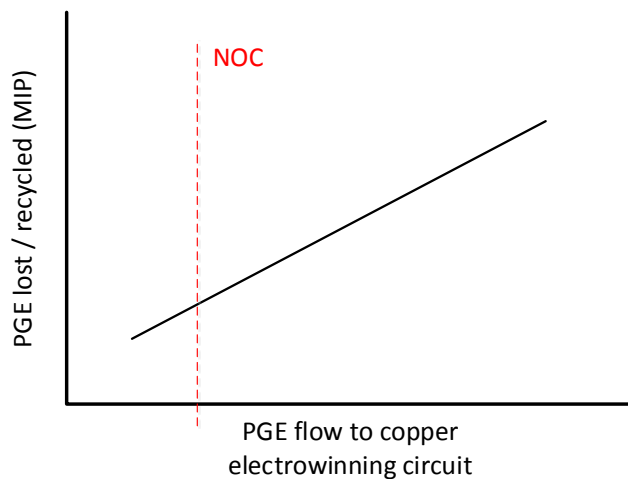
Figure 7.2: PGEs lost and MIP linear EPFs illustration. NOC operating conditions indicated in red.

The performance functions calculation methodology is shown in Figure 7.3. The NOC data are used to calculate the steady-state PGEs flow to the copper electrowinning circuit. The PGEs flow to the copper electrowinning circuit can then be calculated under abnormal process data. PCA, KPCA and univariate detection delays are then used to calculate the PGEs lost and MIP for each detection method. The potential economic benefit from early multivariate fault detection can then be evaluated.
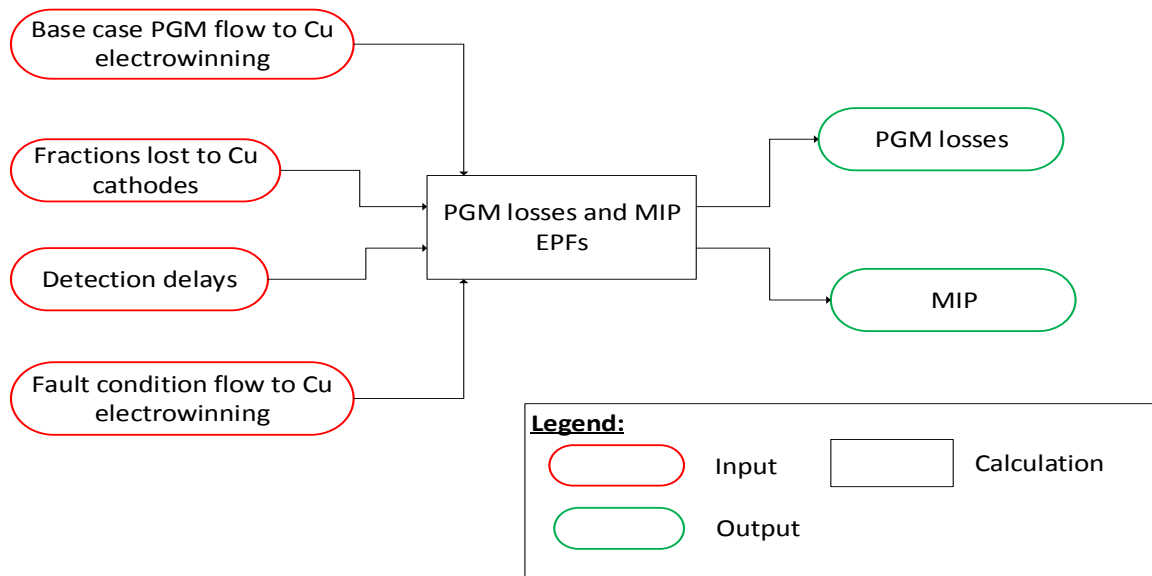
Figure 7.3: Performance function calculation methodology.

Pt and Pd concentrations are not predicted by the dynamic model as mentioned in Chapter 2, section 2.3. In order to include Pt and Pd in the EPFs, the concentrations are predicted using linear regression models. The linear regression models are developed from historical plant data. The models predict both the 2nd and 3rd stage filtrate Pt and Pd concentrations as a function of the combined Ir, Rh and Ru concentrations. The linear regression results are discussed and provided in Appendix G.

7.6 Summary

Two EPFs were successfully developed through consultation of previously published literature and expert knowledge from the BMR. The EPFs focus on the potential increases in PGEs lost and recycled due to over-leaching in the autoclave. A methodology is provided to evaluate the economic impact of the multivariate fault detection results provided in Chapter 6.

Chapter 8: Economic impact analysis results

The final project objective is addressed in Chapter 8, following the economic performance function development discussed in Chapter 7. The PGEs lost EPF results are discussed in section 8.1. The MIP EPF results are discussed in section 8.2. The economic impact assessment results are summarised in section 8.3.

The economic impact results for both PCA and KPCA are compared to the univariate economic impact results. Significant differences were determined with ANOVA followed by LSD post hoc analysis as described in Chapter 5, section 5.5.

All economic impact results are scaled between zero and ten. Ten was set as the monetary value of the maximum PGM production rate ($/hr).

8.1 PGEs lost

The PGEs lost EPF results are given in Table 8.1. It is clear that the significant decreased detection delays provided by PCA, observed in Chapter 6, did not translate in a significant decrease in PGE losses. The valve stiction early fault detection provided the only significant economic benefit. The largest losses were observed for the pump impeller wear, which is expected when considering the large detection delays observed in Chapter6, Figure 6.10, and the impact of the fault described in Chapter 3, section 3.1.3.4. The smallest losses are observed for the peristaltic pump tube failure, which is again expected when considering the immediate impact and detection of the fault.

It should also be noted that the scaled results are relatively small. The small losses observed firstly indicate the robustness of the process. It is clear that process controllers can mitigate fault symptoms to an extent to minimize the PGE losses to the copper electrowinning circuit. Secondly, it should also be noted that the univariate fault detection detects faults prior to any significant over-leaching occurs. This observation is especially evident for the solids build-up in cooling coils fault. The univariate detection delay detects the fault prior to autoclave temperatures increasing significantly, which will result in unacceptable levels of over-leaching.

Table 8.1: Scaled PGEs lost EPF results. Both mean and standard deviation results are provided. Significant differences between detection methods are indicated in green.

#	Fault Name	Univariate detection (x 10^{-3})		PCA detection (x 10^{-3})		KPCA detection (x 10^{-3})	
		μ	σ	μ	σ	μ	σ
1	Valve blockage	1.88	1.75	1.38	1.90	1.88	1.75
2	Valve wear	0.890	1.88	1.61	2.83	1.23	2.01
3	Valve stiction	5.00	4.56	0.573	0.486	2.07	1.59
4	Pump impeller wear	9.98	17.0	3.91	6.76	9.95	17.0
5	Solids build-up in cooling coils	0.299	0.379	0.191	0.257	0.299	0.379
6	Peristaltic pump tube failure	0.000107	0.000300	0.0000171	0.000500	0.0000714	0.000178
7	H$_2$SO$_4$ controller misuse	1.31	1.09	0.876	0.946	1.01	0.830
8	Level sensor blockage	4.36	2.31	3.06	2.62	2.62	2.75

Legend:

Significant economic benefit when compared to univariate	
Significant economic benefit when compared to univariate and PCA/KPCA	

8.2 Metals in process

The MIP EPF results are provided in Table 8.2. The results are similar to that observed to that in Table 8.1. This is expected when considering the linear relationship between the EPFs. Similar to the PGE losses, only the valve stiction fault provides a significant decrease in MIP. The reported values in Table 8.2, although larger than that observed in Table 8.1, are still relatively small. The increased PGE's recycled should not results in a significant build-up of PGEs, assuming univariate detection delays.

Table 8.2: Scaled PGMs lost EPF results. Both mean and standard deviation results are provided. Significant differences between detection methods are indicated in green.

#	Fault Name	Univariate detection (x 10^{-3})		PCA detection (x 10^{-3})		KPCA detection (x 10^{-3})	
		μ	σ	μ	σ	μ	σ
1	Valve blockage	19.4	18.1	14.2	19.6	19.4	18.1
2	Valve wear	9.27	19.6	16.3	24.3	12.5	20.9
3	Valve stiction	69.8	52.2	5.88	5.24	21.3	16.5
4	Pump impeller wear	108	175	42.3	175	103	175
5	Solids build-up in cooling coils	3.06	3.89	1.95	2.64	3.06	3.89
6	Peristaltic pump tube failure	0.000998	0.00316	0.000166	0.000524	0.000617	0.000183
7	H_2SO_4 controller misuse	13.3	11.4	8.96	9.75	10.3	8.64
8	Level sensor blockage	45.9	23.7	32.1	27.3	27.6	28.6

Legend:

Significant economic benefit when compared to univariate	
Significant economic benefit when compared to univariate and PCA/KPCA	

8.3 Summary

Economic impact assessment was successfully completed for PCA, KPCA and compared to univariate fault detection. The significant benefits in PCA detection delays observed in Chapter 6, section 6.4, did not translate in a significant economic benefit. The lack of a significant economic benefit is due to the robustness of the process and the univariate detection delays, detecting faults prior to significant increased variations in leaching performance.

Chapter 9: Conclusions and recommendations

Chapter 9 provides conclusions for the objectives set out in Chapter 1. Subsequent recommendations are made from the conclusions and are provided in sections 9.4 and 9.5.

9.1 Fault detection

A fault diagnosis approach was successfully designed specifically for the base metal refinery (BMR). Principal component analysis (PCA) and kernel PCA (KPCA) were utilized as linear and nonlinear feature extraction methods. Results were compared to a simple univariate fault detection approach to quantify potential benefits.

Robust simulated normal operating conditions (NOC) training data were collected through rigorous input disturbance modelling. The random walk input disturbances allowed for replicates of simulated faults, ten replicates were completed per fault. The replicates and robust training data set allowed for rigorous testing of both PCA and KPCA as fault detection methods.

Post hoc statistical analysis of detection delay results confirmed PCA outperformed KPCA and a base case univariate fault detection methodology. PCA provided a significant decrease in detection delay for six of the eight faults evaluated. KPCA did not provide improved results, due to the linearity of the NOC training data set, sub sampling of the NOC training data set and the kernel width selection process.

9.2 Fault identification

Traditional contribution plots were used to identify fault locations for both PCA and KPCA. Reconstruction based contributions (RBC) were used to address possible fault smearing for PCA. Only two of the eight faults were successfully identified using RBC, while traditional contribution plots only correctly identified a single fault for both PCA and KPCA. The poor identification results were mainly due to the significant fault smearing. The fault smearing was expected due to the significant fault transition periods and process controllers' supressing fault location symptoms.

9.3 Economic impact assessment

The key economic indicator was identified following a site visit and two Economic Performance Functions (EPFs) were subsequently developed. The significant decrease in detection times observed for PCA when compared to base case univariate detection, did not translate into a similar significant economic benefit. Only one fault showed a statistically significant economic benefit due to early fault detection from PCA.

Therefore it is concluded that the multivariate fault diagnosis methods tested here do not promise sufficient benefit over a simple univariate fault detection approach for the operating plant considered.

9.4 Recommendations for industrial application

9.4.1 BMR pressure leach plant

It is recommended that a multivariate fault diagnosis system is implemented at the operating plant, since the PCA fault detection results showed significant potential. If a multivariate fault diagnosis system is to be implemented, a more robust fault identification approach needs to be developed and implemented. Recommendations are made for industry in general and are provided in section 9.4.2.

9.4.2 General

The availability and selection of robust NOC training data will be a hindrance for real world application, due to clean NOC training data being not being readily available at an actual plant. It is recommended that expert knowledge is incorporated when selecting NOC data. Expert knowledge together with operators can determine whether the NOC data in question will be adequate for model training.

Another possible hindrance will be the fault identification method applied, specifically when aiming to apply a fully automated fault diagnosis system. The basic fault identification methods applied in this work will not offer satisfactory performance for an industrial application. It is recommended that more complex fault identification methods are investigated for industrial application. A possible improved method is using process causality for fault identification. Lindner (2014) investigated the use of process causality in several case studies.

A more supervised fault identification method can also be recommended for industry use. Expert operator knowledge can be used in conjunction with basic fault identification methods. Expert knowledge together with process operators can potentially identify fault locations from the triggered contribution variables.

An efficient and interactive interface would need to be developed which includes the fault detection and identification results. This will allow operators to more easily and readily determine the current process conditions and potential process abnormalities.

9.5 Recommendations for future work

Considering the work completed in this study, the main recommendation will be an increased focus on economic impact assessments for fault diagnosis applications. The economic performance related

literature reviewed for this study was mostly focused on advanced process controllers and not fault diagnosis systems. Considering the significant amount of work completed on especially fault detection methods, there needs to be an increased focus on economic performance to determine whether the increasingly more complex fault detection methods translates into a similar economic benefit.

Furthermore, these fault diagnosis methods need to be investigated on more complex real-life case studies or actual plant data. This will provide an opportunity to address the problems relating to NOC data selection and fault smearing.

References

Aldrich, C., Auret, L. 2013. *Unsupervised process monitoring and fault diagnosis with machine learning methods*. Springer, London.

Alves dos Santos, N., Savassi, O., Peres, A. and Martins, A. 2014. Modelling flotation with a flexible approach – Integrating different models to the compartment model. *Minerals Engineering*, 66-68, pp.68-76.

Auret, L. 2010. *Process Monitoring and Fault Diagnosis using Random Forests*. Ph.D. Stellenbosch University.

Bauer, M., Craig, I.K., Tolsma, E., de Beer, H., 2007. A profit index for assessing the benefits of process control. Industrial Engineering Chemistry, 46, pp. 5614 – 5623.

Bin Shames, M., 2010. *Observability and Economic aspects of Fault Detection and Diagnosis Using CUSUM based Multivariate Statistics*. Ph.D. University of Waterloo

Bin Shams, M., Budman, H., Duever, T., 2011. Finding a trade-off between observability and economics in the fault detection of chemical processes. Computers and Chemical Engineering, 35, pp. 319 – 328.

Coetzee, R.J., 2006. Platinum group metals behaviour during iron precipitation and goethite seeding in nickel sulphate solution. M.Eng. Stellenbosch University.

Cguang, L., Braatz, R., Chiang, L. and Russell, E. 2000. *Data-driven methods for fault detection and diagnosis in chemical processes*. New York: Springer-Verlag New York.

Cheng, C.Y., Hsu, C.C., Chen, M.C. 2010. Adaptive kernel principle component analysis (KPCA) for monitoring small disturbances of nonlinear processes. Industrial and engineering Chemistry Research, 49(5), pp. 2254 – 2262.

Cho, J.H.,Lee, J.M., Wook, C.S., Lee, D., Lee, I.B. 2005. Fault identification for process monitoring using kernel principle component analysis. Chemical Engineering Science, 60(1), pp. 279 – 288.

Craig, I.K., Bauer, M. 2008. Economic assessment of advanced process control – A survey and framework. *Journal of Process Control*, 18(1), pp.2-18.

Deng, X., Tian, X., Chen, S. 2013. Modified kernel principle component analysis based on local structure analysis and its application to nonlinear process fault diagnosis. Chemometrics and Intelligent Laboratory Systems, 127, pp. 195 – 209.

Duever, T., Budman, H. and Shams, M. 2011. Finding a trade-off between observability and economics in the fault detection of chemical processes. *Computers & Chemical Engineering*, 35(2), pp.319-328.

Dorfling, C., 2012. *Characterisation and dynamic modelling of the behaviour of platinum group metals in high pressure sulphuric acid/oxygen leaching systems*. Ph.D. Stellenbosch University.

Dorfling, C., Eksteen, J., Bradshaw, S., Akdogan, G. 2013. Modelling of an autoclave used for high pressure sulphuric acid/oxygen leaching of first stage leach residue, part 2: Model application. *Minerals Engineering*, 53, pp.213-219.

Dorfling, C., Eksteen, J., Bradshaw, S., Akdogan, G. 2013. Modelling of an autoclave used for high pressure sulphuric acid/oxygen leaching of first stage leach residue. Part 1: Model development. *Minerals Engineering*, 53, pp.220-227.

Faris, M., Moloney, M. and Pauw, O. 1992. Computer simulation of the Sherritt nickel-copper matte acid leach process. *Hydrometallurgy*, 29(1-3), pp.261-273.

Ge, Z., Yang, C., Song, Z. 2009. Improved kernel PCA-based monitoring approach for nonlinear processes. Chemical Engineering Science, 64(9), pp. 2245 – 2255.

Groenewald, J., Aldrich, C.and Coetzer, L. 2006. Statistical monitoring of a grinding circuit: An industrial case study. *Minerals Engineering*, 19(11), pp.1138-1148.

Haasbroek, A., and Lindner, B., (2015). *Reconstruction of a BMR MATLAB® model in Simulink®*. Stellenbosch University.

Horch, A. and Thornhill, N. (2007). Advances and new directions in plant-wide disturbance detection and diagnosis. *Control Engineering Practice*, 15(10), pp.1196-1206.

Isermann, R., 2005. Fault-diagnosis systems: an introduction from fault detection to fault tolerance. Springer, London.

Izadi, I., Chen, T., Shah, S., 2011. Alarm Systems: Quantitative Analysis and Design.

Jemwa, G.T., Aldrich, C., 2006. Kernel-based fault diagnosis on mineral processing plants. Minerals Engineering, 11, pp. 1149 – 1162.

Lindner, B., 2014. *Exploiting Process Topology for Optimal Process Monitoring*. M(Eng). Stellenbosch University.

Lee, J.M., Qin, S.J., Lee, I.B. 2008. Fault detection of nonlinear processes using kernel independent component analysis. The Canadian Journal of Chemical Engineering Science, 59(1), pp. 526 – 536.

Lee, J.M., Yoo, C., Choi, S.W., Vanrolleghem, P.A., Lee. I.B. 2004. Nonlinear process monitoring using kernel principal component analysis. Chemical Engineering 59. pp 223 -234.

Karelovic, P., Putz, E. and Cipriano, A. 2016. Dynamic hybrid modeling and simulation of grinding–flotation circuits for the development of control strategies. *Minerals Engineering*, 93, pp.65-79.

Kourti, T. 2002. Process analysis and abnormal situation detection: from theory to practice. Control Systems. IEEE 22, pp 10 – 25.

McAvoy, T. and Dong, D. 1996. Nonlinear principal component analysis—Based on principal curves and neural networks. *Computers & Chemical Engineering*, 20(1), pp.65-78.

M.N., B.J., 2016. *Site visit at BMR*. South Africa.

Mika, S., Scholkopf, B., Smola, A., Muller, K.R., Scholz, M., Ratsch, G. 1999. Kernel PCA and De-Noising in Feature Spaces. Advances in Neural Information Processing Systems, 11, pp. 536 – 542.

Miskin, J., Bradshaw, S., Dorfling, C., Auret, L., Lindner, B., 2016. Fault detection for simulated valve faults in a high pressure leaching process. *IFAC-PapersOnLine*, 49(7), pp.394-399.

Miskin, J., 2015. *Control performance assessment for a high pressure leaching process by means of fault database creation and simulation*. Master thesis. Stellenbosch University.

Muske, K.R., 2003. Estimating the economic benefit from improved process control. Industrial Engineering Chemistry, 42, pp. 4535 – 4544.

Olivier L.K. and Craig I.K., 2017. Should I shut down my processing plant? An analysis in the presence of faults. *Journal of Process Control*, 56, pp.35 – 47

Oosthuizen, D.J., Craig, I.K., and Pistorius, P.C. 2004. Economic evaluation and design of an electric arc furnace controller based on economic objectives, *Control Engineering Practice* 12, pp. 103 – 115.

Phillpotts, D., 2016. *Nonlinear fault detection and diagnosis using kernel based techniques applied to a pilot distillation column*. Master thesis. University of Pretoria.

PWC, 2016. SA's mining industry continuous to face tough times. [Online] Available at: https://www.pwc.co.za/en/press-room/sa-mining-face-tough-time.html [Accessed 27 July 2017].

Qin, S. 2012. Survey on data-driven industrial process monitoring and diagnosis. *Annual Reviews in Control*, 36(2), pp.220-234.

Qin, S. and Alcala, C. 2009. Reconstruction-based contribution for process monitoring. *Automatica*, 45(7), pp.1593-1600.

Quist, J. and Evertsson, C. 2016. Cone crusher modelling and simulation using DEM. *Minerals Engineering*, 85, pp.92-105.

Rademan, J., Lorenzen, L. & van Deventer, J., 1999. The leaching characteristics of Ni-Cu matte in the acid-oxygen pressure leach process at Impala Platinum. *Hydrometallurgy*, 52, pp. 231 – 52.

Russell, E., Chiang, L. and Braatz, R. 2000. *Data-driven methods for fault detection and diagnosis in chemical processes*. 1st ed. London [etc.]: Springer.

Salazar, J., Magne, L., Acuña, G. and Cubillos, F. 2009. Dynamic modelling and simulation of semi-autogenous mills. *Minerals Engineering*, 22(1), pp.70-77.

Salazar, J., Valdes-Gonzales, H., Cubillos, F., 2010. Advanced Simulation for Semi-Autogenous Mill Systems: A Simplified Models Approach. InTech, 2010, pp 148 – 156.

Sargent, R. 2005. *Verification and Validation of Simulation Models*. Proceedings of the 37th winter simulation conference, pp.130-142.

Schölkopf, B., Simola, A., Muller, K.R., 1998. Nonlinear Component Analysis as a Kernel Eigenvalue Problem. Neural Comput. 10, pp. 1299 – 1319.

Steenekamp, N. and Dun, G.M. 1999. Operations of and Improvements to the Lonrho Platinum Base   Metal Refinery. Proceedings of EPD Congress 1999, San Diego, California, Editor: Mishra, B. pp 365-378

Vamuza, K., Filzmoser, P. 2008. Introduction to Multivariate statistical analysis in Chemometrics. Boca Raton, FL, United States, Taylor & Francis.

Van Schalkwyk, R., 2011. *Leaching of Ni-Cu-Fe-S Pierce Smith converter matte: Effects of the Fe-endpoint and leaching conditions on kinetics and mineralogy*. Master Thesis. Stellenbosch University.

Venkatasubramanian, V., Rengaswamy, R., Kavuri, S., 2003. A review of process fault detection and diagnosis Part I: Quantitative model based methods. *Computers and Chemical Engineering* 27, pp. 293 – 311.

Venkatasubramanian, V., Rengaswamy, R., Kavuri, S., 2003a. A review of process fault detection and diagnosis Part II: Qualitative models and search strategies. *Computers and Chemical Engineering* 27, pp. 313 -326.

Venkatasubramanian, V., Rengaswamy, R., Kavuri, S., 2003b. A review of process fault detection and diagnosis Part III: Process history based methods. *Computers and Chemical Engineering* 27, pp. 327 – 346.

Wang, Z., Wiebe, S., Shang, H., 2016. Fault detection and diagnosis og an industrial copper electrowinning process. The Canadian Journal of Chemical Engineering, 94, pp. 415 – 422.

Wei, D. 2010. *Development of performance functions for economic performance assessment of process control systems*. Ph.D. University of Pretoria.

Wei, D., Craig, I.K., 2009. Economic performance assessment of two ROM ore milling circuit controllers. Minerals Engineering, 22, pp. 826 – 839.

Wu, M., She, J., Nakano, M., Gui, W., 2002. Expert control and fault diagnosis of the leaching process in a zinc hydrometallurgy plant. Control Engineering Practice, 10, pp. 433 – 442.

Zhang, Y., Qin, S.J. 2008. Improved nonlinear fault detection technique and statistical analysis. AIChe Journal, 54(12), pp. 3207 – 3220.

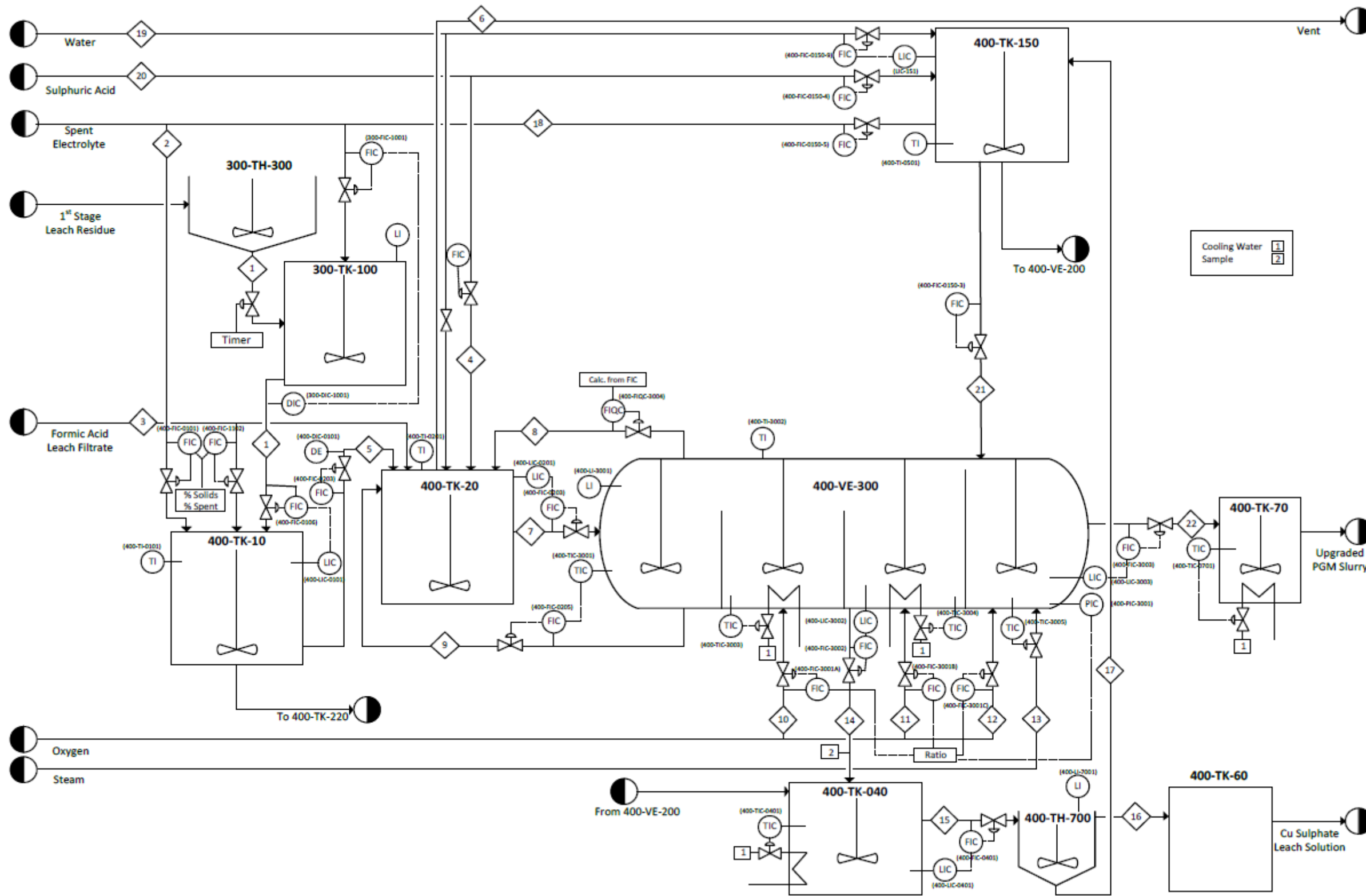# Appendix A: Process flow diagram and dynamic process model
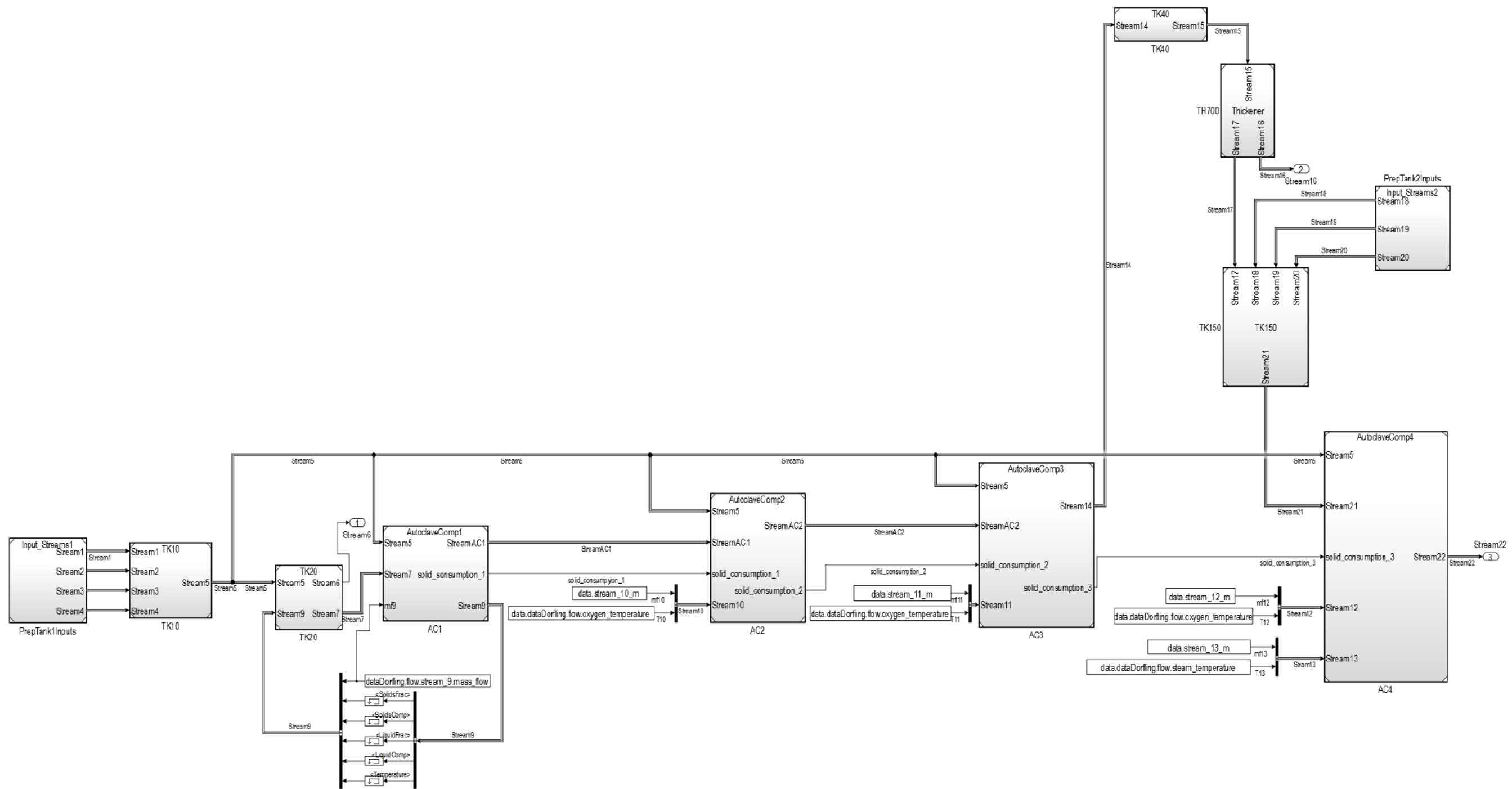

Figure A.1: Pressure leach process flow diagram.

Figure A.2: Dynamic pressure leach model Simulink® flow diagram.

Appendix B: Kernel width selection

Appendix B describes a proposed approach to optimal kernel-width estimation. The proposed method was used to select a kernel width from the normal operating conditions (NOC) training data set. The proposed method is based on the following requirements:

1. KPCA-based fault detection will be most optimal if projected data in the feature space are Gaussian.

2. Only NOC data should be used to estimate kernel-width, since fault data are typically scarce.

3. False alarms must be minimized by ensuring good generalization to unseen NOC data.

These requirements are used to develop an optimization objective function. The limitations to the proposed kernel width estimation method is discussed.

1. Kernel width effect demonstration

To demonstrate the effect of the kernel-width parameter, consider Figure B.1 and Figure B.2. Figure B.1 gives an example of two-dimensional input data: NOC used for training the KPCA projection; NOC used for verification (unseen during the training procedure); and test data representing a fault condition. Figure B.2 shows the projection of these three data sets into a two-dimensional KPCA feature space.
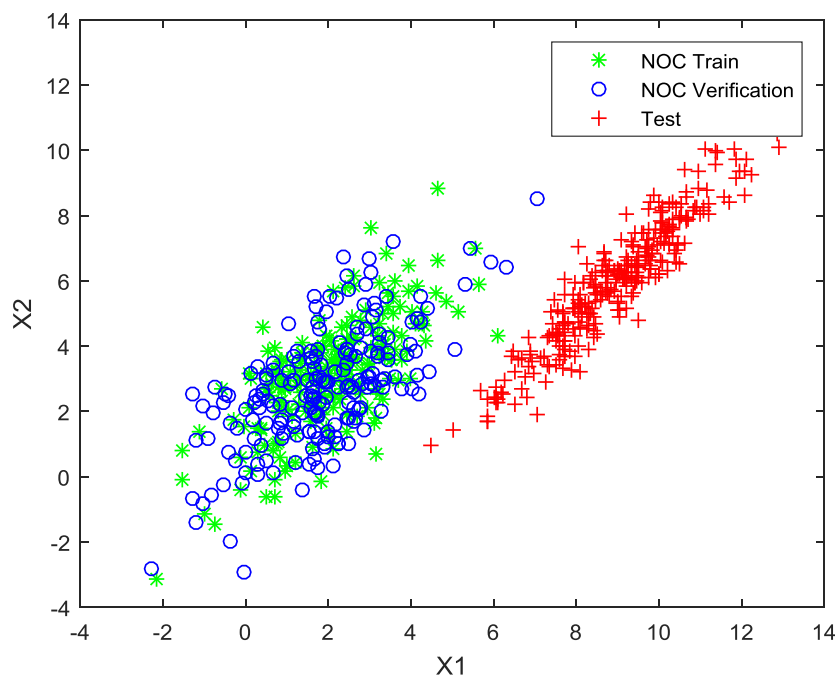

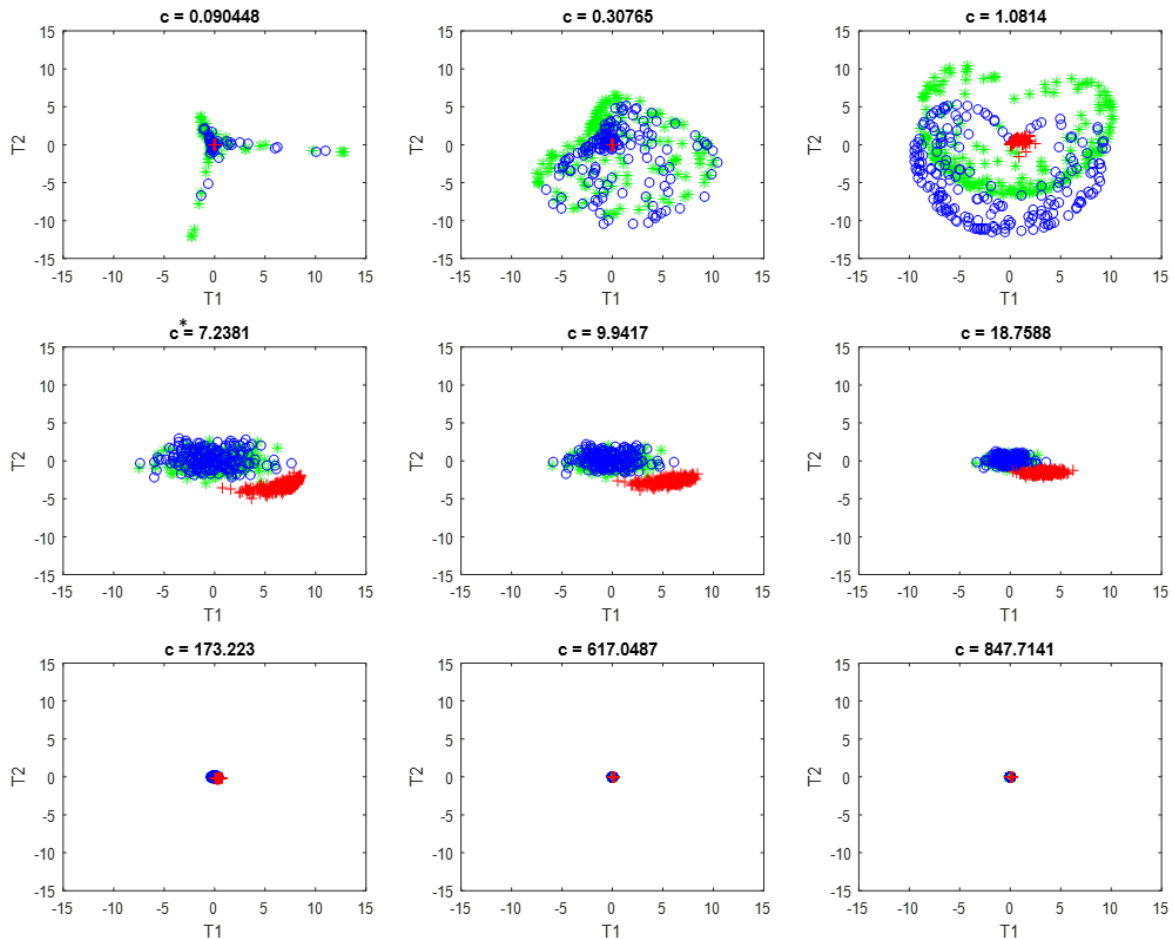**Figure B.1: Demonstration data: Two-dimensional input space**

Figure B.2: Demonstration data: Two-dimensional KPCA feature space for various values of the kernel-width c (green = training NOC; blue = validation NOC; red = test data). Note that the extent of the feature space has been kept the same for all plots.

Various interesting properties of KPCA is visible in Figure 2. If the kernel-width c is selected as too small, the projection of the training and verification NOC data sets do not follow Gaussian distributions, as expected. Strange artefacts arise due to the ill-conditioned kernel matrix resulting from too small a kernel-width.

As the kernel-width increases, the strange artefacts disappear, but there is still a noticeable difference between the NOC training and verification data, which should not be the case for good generalizability. When an optimal kernel-width is reach, training and verification NOC data are similar, and Gaussian. As the kernel-width increases beyond that, the extent of the projected features decreases (note the values of the feature space axes). For fault detection with the modified Hotelling's T^2 statistic, the statistical significance threshold is independent of kernel-width; these larger kernel-widths would make missing alarms more likely. If a percentile of the NOC[train] Hotelling's T^2 statistic is used as threshold, this issue is less important.

An automated search strategy is required to select an appropriate kernel-width: not too small (which would introduce artefacts and does not generalize to NOC verification data), and not too large (which would reduce the information content in the data).

2. Optimization objective function

From the requirements, the proposed kernel width estimation approach defines three criteria to be optimized: a feature space Gaussianity criterion, a generalizability criterion (ensuring that the projected training and verification NOC data are Gaussian) and the FARs.

2.1 Feature space Gaussianity

A Gaussian feature space will allow the modified Hoteling's T^2-statistic to be used effectively for fault detection in the feature space.

Two indices are defined to check the Gaussianity of the feature space projections: TC and VC (the NOC training and verification Gaussianity; larger values indicating increasing non-Gaussianity). These indices are calculated by comparing the feature space distance distributions of the NOC training and verification data to chi-squared distributions corresponding to Gaussian distance distributions (Vamuza and Filzmoser, 2008).

2.2 Only NOC data should be used

Unsupervised fault detection requires only the use of NOC data. Therefore only NOC data should be used when selecting the kernel width prior to any application to unseen fault data.

2.3 FAR should be minimized

The features for training NOC and verification NOC should be similar, to show good generalizability of the KPCA projection. An index, DC, is defined to assess the similarity of the NOC training and verification feature distributions. The feature space distance distributions are again used for comparison.

A constraint can also be placed on the maximal permissible false alarm rate (FAR) calculated on the verification NOC data. The constraint is set at 5%.

3. Methodology

The proposed optimal kernel-width estimation procedure is given here, for a range of considered kernel widths $c_{min} \leq c \leq c_{max}$:

1. Split NOC data set randomly into training and verification subsets, NOC^{train} and $NOC^{verification}$.

2. Set the required cumulative variance to be explained *v*.

3. Select kernel-width *c*.

4. Train KPCA on NOC[train] data, with Gaussian kernel and kernel-width *c*. Select *a* number of features to capture at least *v* cumulative variance. Store the features **T**[train], weight vectors {**α**^{a}}[train] and kernel matrix **K**[train].

5. Apply KPCA (with trained parameters *c*, *a*, {**α**^{a}}[train] and **K**[train]) to NOC[verification] data to determine the features **T**[verification].

6. Calculate the squared Mahalonobis distance distributions for the NOC training and verification features: {**d**^{2}}[train] and {**d**^{2}}[verification].

7. Calculate *TC* as the maximum absolute distance between the distribution of {**d**^{2}}[train] and the chi-squared distribution with *a* degrees of freedom.

8. Calculate *VC* as the maximum absolute distance between the distribution of {**d**^{2}}[verification] and the chi-squared distribution with *a* degrees of freedom.

9. Calculate *DC* as the maximum absolute distance between {**d**^{2}}[train] and {**d**^{2}}[verification].

10. Calculate the false alarm rate FAR for NOC[training]. FAR based on the Hotelling's T^2 statistic of the features **T**[train], where the upper limit for detection is ϑ^{T2} (typically chosen as some percentile of the NOC[verification] Hotelling's T^2 statistic).

11. Calculate the false alarm rate FAR for NOC[training] FAR based on the modified SPE statistic of the features **T**[train], where the upper limit for detection is ϑ^{SPE} (typically chosen as some percentile of the NOC[train] modified SPE).

12. Choose new *c*; repeat steps 3 to 10.

13. Optimal kernel-width c^* is given by:

$$c^* = \arg \min_c \{J(c) = TC + VC + DC\}$$

$$s.t. FAR_{SPE,T^2} < 0.05$$

4. Case Study

The proposed kernel width selection approach is applied to the well-known Tennessee Eastman benchmark problem (Russel *et al*. 2000).

An in depth process description is provided in Russel *et al*. 2000.

All training for the Tennessee Eastman process case study was done on the NOC data set (d00) and the NOC test data set (d00_te) combined, resulting in n = 1460 samples. A random split of 50% was selected to obtain NOC^{train} and NOC^{verification}.

The first set of results compares the proposed approach to results achieved by the KPCA implementation of Deng *et al*. (2013). The design aspects are given in Table B.1, and the comparison of true alarm rates and detection delays in Table B.2.

Table B.1. Design aspects for Deng *et al*. (2013) comparison

Design aspect	Deng *et al*. (2013)	This study
Feature space characterization	Kernel density function	Hotelling's T^2; ϑ based on 99th percentile
Number of input variables m	52	52
Cumulative variance explained v	90%	90%
Number of retained components a	30	32
Optimal kernel width c	1 040	92.32

The comparison with Deng *et al*. (2013) shows promising results: detection rates and detection delays are similar for most faults.

Table B.2. Comparison of true alarm rates and detection delays with Deng *et al*. (2013) and the proposed method. Extent of differences indicated with green and red.

Fault	True alarm rates						Detection delays					
	Deng et al. (2013)		Proposed method		Difference		Deng et al. (2013)		Proposed method		Difference	
	T^2	SPE	T^2	SPE	T^2	SPE	T^2	SPE	T^2	SPE	T^2	SPE
1	99.4	99.8	99.4	99.6	0.0	0.1	7	3	8	5	1	2
2	98.8	98.5	98.6	98.4	0.1	0.1	11	13	13	16	2	3
3	6.6	8.3	4.7	3.5	1.9	4.8	0	0	0	0	-	-
4	64.4	100.0	40.3	98.9	24.1	1.1	112	1	344	6	232	5
5	30.9	35.5	28.9	19.5	2.0	16.0	11	1	12	9	1	8
6	99.3	100.0	99.0	99.5	0.3	0.5	7	1	10	6	3	5
7	100.0	100.0	100.0	100.0	0.0	0.0	1	1	2	2	1	1
8	97.5	98.0	97.3	90.4	0.3	7.6	23	17	24	23	1	6
9	7.1	7.1	6.5	3.6	0.6	3.5	1	0	0	0	-	-
10	49.5	61.3	40.8	18.9	8.8	42.4	84	48	108	108	24	60
11	60.3	63.5	56.8	52.6	3.5	10.9	47	7	52	97	5	90
12	98.8	97.1	99.1	91.4	-0.4	5.8	7	3	8	23	1	20
13	94.6	95.6	94.9	94.9	-0.3	0.8	46	37	47	42	1	5
14	99.9	99.8	99.9	89.8	0.0	10.1	1	2	2	3	1	1
15	9.9	9.5	7.1	3.9	2.8	5.6	775	0	0	0	-	-
16	31.6	59.8	25.1	14.5	6.5	45.3	196	15	310	513	114	498
17	81.5	95.0	83.1	92.5	-1.6	2.5	29	22	28	26	-1	4
18	89.4	90.8	89.5	90.0	-0.1	0.8	89	84	90	85	1	1
19	15.9	24.8	15.6	6.0	0.3	18.8	0	0	0	0	-	-
20	42.3	56.8	41.4	47.6	0.9	9.1	87	85	86	88	-1	3
21	48.8	53.5	41.3	46.5	7.5	7.0	275	249	507	474	232	225

The second set of results compares the proposed approach to results achieved by the KPCA implementation of Lee *et al*. (2008). The design aspects are given in Table B.3, and the comparison of true alarm rates and detection delays in Table B.4.

Table B.3. Design aspects for Lee *et al*. (2008) comparison

Design aspect	Lee *et al*. (2008)	This study
Feature space characterization	Hotelling's T^2; ϑ based on $\alpha = 0.01$	Hotelling's T^2; ϑ based on 99th percentile
Number of input variables m	33	33
Cumulative variance explained v	88%	88%
Number of retained components a	11	32
Optimal kernel width c	90.825	25.27

The comparison with Lee *et al*. (2008) also shows acceptable results, except for three faults (2, 6 and 18) with poorer performance by the proposed approach. Although faults 2, 6 and 18 show poor performance for the proposed method, closer inspection revealed that the faults are detected early (see short detection delays), but that the faults are then "hidden" in the process soon after: the scores in the feature space collapse to the centre. If a reconstruction to the original input space was done to calculate the SPE statistic, this behaviour would have been classified as faulty.

Table B.4. Comparison of true alarm rates and detection delays with Lee *et al.* (2008) and the proposed method. Extent of differences indicated with green and red.

| Fault | True alarm rates | | | | | | Detection delays | |
| | Lee et al. (2008) | | Proposed method | | Difference | | Proposed method | |
	T^2	SPE	T^2	SPE	T^2	SPE	T^2	SPE
1	100.0	100.0	90.3	71.9	9.8	28.1	8	5
2	98.0	98.0	7.6	3.4	90.4	94.6	13	31
3	4.0	5.0	7.4	2.0	-3.4	3.0	0	0
4	9.0	100.0	33.9	99.9	-24.9	0.1	356	2
5	27.0	25.0	25.9	8.1	1.1	16.9	12	2
6	99.0	100.0	2.4	3.5	96.6	96.5	22	13
7	100.0	100.0	85.9	83.5	14.1	16.5	2	2
8	97.0	96.0	84.8	40.9	12.3	55.1	24	19
9	4.0	4.0	7.0	2.1	-3.0	1.9	0	0
10	43.0	51.0	35.5	9.4	7.5	41.6	145	126
11	24.0	81.0	55.9	54.3	-31.9	26.8	52	57
12	98.0	97.0	72.3	47.8	25.8	49.3	23	24
13	94.0	95.0	48.5	49.5	45.5	45.5	47	42
14	79.0	100.0	97.1	74.5	-18.1	25.5	2	11
15	8.0	6.0	9.0	1.9	-1.0	4.1	0	0
16	30.0	52.0	22.8	7.9	7.3	44.1	310	0
17	74.0	95.0	43.4	72.4	30.6	22.6	30	23
18	90.0	90.0	4.5	6.9	85.5	83.1	95	85
19	3.0	49.0	18.0	4.2	-15.0	44.8	0	0
20	41.0	52.0	38.3	49.0	2.8	3.0	87	88

5. Proposed approach limitations

There are some limitations with the proposed kernel width selection approach. These limitations are briefly discussed.

i)   Although the method requires FARs below a given threshold, smaller FARs will result in decreased detection rates. It is therefore important not to over-emphasise a low FAR.

ii)   The method does not provide a kernel width range selection approach. This could be problematic due to the computational expense of KPCA. Input space distance percentiles could be used as starting point.

iii) Only the first two feature space dimensions are used to estimate the linearity. The effect of other dimensions may also need to be considered since the feature space usually consist of several dimensions when considering chemical or metallurgical processes.

iv) The proposed kernel width selection approach is only compared to two previous studies. More comparisons may be required, including different process case studies to further improve and evaluate the proposed approach.

v) It is important to consider the training and verification set dimensionality to avoid model overfitting.

Appendix C: Univariate fault detection

Appendix C provides further information on univariate fault detection. Some background on the control limits selection is provided. The methodology for the control limit selection for the pressure leach is finally provided.

1. Background

Univariate fault detection considers each process variable individually. An upper and lower threshold is calculated for each process variable. Once a variable moves outside these predefined limits, it indicates potential fault conditions.

Russel *et al.* (2000) proposed a statistical univariate monitoring approach. The method is based on a cumulative standard normal distribution. The upper and lower thresholds are calculated from the variable mean μ and standard deviation σ.

$$Threshold = \mu \pm c_{\alpha/2}\sigma \tag{C.1}$$

$c_{\alpha/2}\sigma$ is the standard normal deviate for some level of significance α.

Thresholds can also be selected based on an upper and lower percentile. The selection of thresholds is crucial to avoid large FARs (Russel *et al*. 2000).The maximum amount of false alarms per hour can be calculated from the amount of operators typically present and the ISA standard.

$$Maximum\ FAR = ISA_{per\ operator}N_{operators} \tag{C.2}$$

The maximum amount of false alarms allowed can be used to evaluate the upper and lower control limit performance.

2. Pressure leaching process

The control limit selection process for the pressure leach process is described in the following section. The control limit selection process has two objectives:

1. Verification FAR should be as close as possible to 1%, to ensure detection results comparable to PCA and KPCA.
2. Offline thresholds should be robust in order to avoid FARs above the ISA standards.

The verification total false alarm rate calculated for univariate should be equal to 1%. This will ensure that the results are comparable to that of both PCA and KPCA. Since a total of 89 process variables are monitored, each individual false alarm rate should not exceed 0.011 %. This will allow for a total

false alarm rate of 1%. The 1% false alarm rate is also well below the maximum false alarm rate calculated from equation C.2.

As discussed in section 5.1.3, offline samples only get updated after a specific analysis time. All the offline analysis times exceed the five sample detection delay. Therefore, once an offline sample moves outside a threshold it will count towards a detection delay. It is therefore important that the offline sample thresholds do not result in any false alarms. An offline sample false alarm result in a false detection delay.

To ensure that offline sample thresholds are more robust, each threshold increased with a single sample standard deviation. The univariate detection training methodology is provided in Figure C.1.

Figure C.1 shows the percentile of the threshold selection being changed iteratively until the false alarm rate is set at 0.011 %. One standard deviation is then added to both upper and lower thresholds in order to allow for a more robust offline sample thresholds.
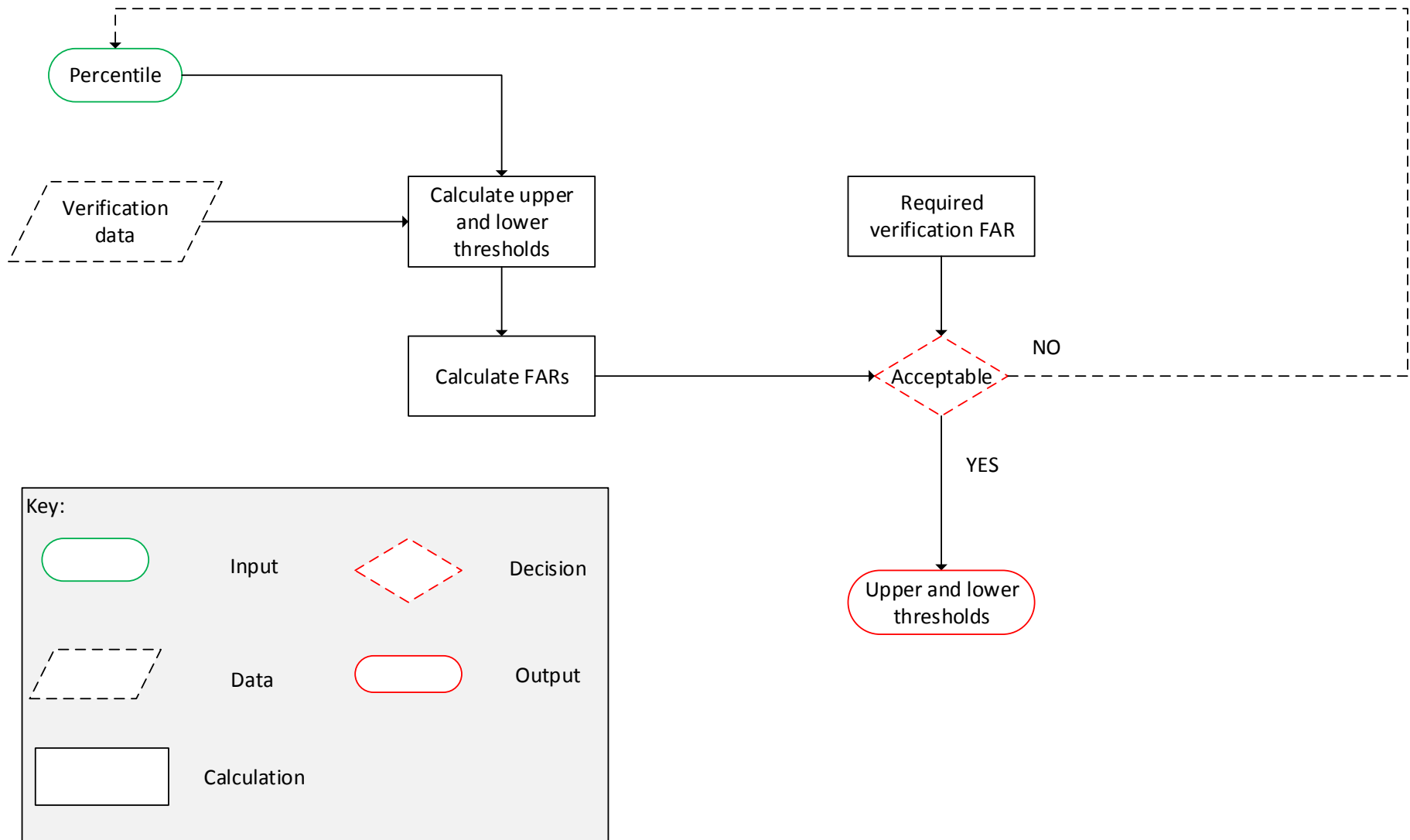
Figure C.1: Univariate fault detection threshold selection methodology.

Appendix D: Fault detection results

Appendix D provides the mean detection performance metric results for each fault. Significant differences are indicated following the ANOVA and LSD test results. The multivariate detection results are compared to the univariate variable who first detects the fault.

If a fault was not detected, a default detection delay of 800 hours was selected. This should be considered when observing the sometimes large standard deviations.

Legend:

LSD test significant difference from univariate detection	
LSD test significant difference from univariate and other multivariate method	
LSD test significant difference from only other multivariate method.	
ANOVA show insignificant difference in means	

1. Density disturbance (Valve blockage)

Performance metric	Univariate detection		PCA				KPCA			
	Best		T^2		SPE		T^2		SPE	
	$\overline{x}$	s	$\overline{x}$	s	$\overline{x}$	s	$\overline{x}$	s	$\overline{x}$	s
FAR	0.00	0.00	0.90	1.60	1.40	2.07	0.65	1.03	1.15	1.55
MAR	100	100	96.26	3.45	96.40	3.25	98.15	2.50	99.25	0.80
DD	N/D	-	401.40	4201.59	401.05	4201.59	800.00	0.00	800.00	0.00
AUC	0.63	0.03	0.48	0.10	0.78	0.21	0.48	0.16	0.29	0.13

2. Valve Wear

Performance metric	Univariate detection		PCA				KPCA			
	Best		T^2		SPE		T^2		SPE	
	$\overline{x}$	s	$\overline{x}$	s	$\overline{x}$	s	$\overline{x}$	s	$\overline{x}$	s
FAR	0.00	0.00	2.80	2.20	0.20	0.63	0.10	0.21	1.25	1.16
MAR	80.58	23.41	89.16	10.29	95.72	5.02	81.15	19.72	97.38	4.15
DD	232.970	208.903	265.923	368.22	420.087	400.508	475.540	283.480	713.620	185.407
AUC	0.89	0.16	0.66	0.12	0.84	0.07	0.74	0.16	0.29	0.14

3. Valve Stiction

Performance metric	Univariate detection		PCA				KPCA			
	Best		T^2		SPE		T^2		SPE	
	$\overline{x}$	s	$\overline{x}$	s	$\overline{x}$	s	$\overline{x}$	s	$\overline{x}$	s
FAR	0.00	0.00	1.40	2.01	4.80	13.13	1.10	2.11	4.05	4.54
MAR	76.28	19.66	61.05	31.40	24.60	30.05	54.19	39.79	53.35	42.73
DD	169.000	85.874	205.11	177.85	13.54	10.30	235.240	215.090	180.630	326.911
AUC	0.89	0.07	0.82	0.11	0.98	0.01	0.82	0.17	0.79	0.23

4. Impeller Wear

Performance metric	Univariate detection		PCA				KPCA			
	Best		T^2		SPE		T^2		SPE	
	$\overline{x}$	s	$\overline{x}$	s	$\overline{x}$	s	$\overline{x}$	s	$\overline{x}$	s
FAR	0.00	0.00	1.90	2.23	0.60	1.26	0.25	0.26	0.95	1.38
MAR	84.50	0.94	74.30	14.33	82.22	3.95	78.88	22.32	95.16	3.11
DD	412.150	43.24	355.10	110.91	380.42	56.84	292.120	136.721	382.930	62.727
AUC	0.54	0.01	0.65	0.20	0.78	0.23	0.59	0.22	0.27	0.14

5. Solids build-up in cooling coils

Performance metric	Univariate detection		PCA				KPCA			
	Best		T^2		SPE		T^2		SPE	
	$\overline{x}$	s	$\overline{x}$	s	$\overline{x}$	s	$\overline{x}$	s	$\overline{x}$	s
FAR	0.00	0.00	1.30	2.50	0.00	0.00	1.55	2.10	1.90	2.41
MAR	79.90	0.75	77.44	4.12	71.57	4.02	82.58	4.09	83.27	5.53
DD	41.330	3.83	34.52	10.03	32.77	8.77	41.950	8.83	41.650	5.442
AUC	0.80	0.01	0.69	0.11	0.91	0.09	0.60	0.11	0.62	0.03

6. Peristaltic pump tube failure

Performance metric	Univariate detection		PCA				KPCA			
	Best		T^2		SPE		T^2		SPE	
	$\overline{x}$	s	$\overline{x}$	s	$\overline{x}$	s	$\overline{x}$	s	$\overline{x}$	s
FAR	0.00	0.00	0.67	1.61	0.50	0.81	0.00	0.00	0.88	1.07
MAR	5.47	0.00	2.89	6.09	0.75	2.19	19.05	5.64	37.26	4.27
DD	1.60	0.00	1.02	1.21	0.61	0.47	1.280	1.336	7.900	0.645
AUC	0.98	0.01	0.98	0.02	0.99	0.00	0.86	0.04	0.77	0.05

7. Sulphuric acid controller misuse

Performance metric	Univariate detection Best		PCA T²		PCA SPE		KPCA T²		KPCA SPE	
	$\overline{x}$	s	$\overline{x}$	s	$\overline{x}$	s	$\overline{x}$	s	$\overline{x}$	s
FAR	0	0	1.70	1.83	0.90	1.91	0.19	0.59	3.13	4.99
MAR	99.2008	2.527295	94.60	6.71	96.29	6.15	98.41	2.12	96.49	3.68
DD	7284.5	2262.61	401.39	420.18	481.71	410.09	651.32	313.51	578.70	356.56
AUC	0.659033	0.097906	0.48	0.12	0.80	0.18	0.46	0.12	0.33	0.10

8. Bubbler level sensor blockage

Performance metric	Univariate detection Best		PCA T²		PCA SPE		KPCA T²		KPCA SPE	
	$\overline{x}$	s	$\overline{x}$	s	$\overline{x}$	s	$\overline{x}$	s	$\overline{x}$	s
FAR	0.00	0.00	1.80	2.94	3.30	5.44	0.60	1.07	2.65	3.21
MAR	83.83	31.88	97.34	5.33	86.98	22.48	96.34	4.40	94.86	3.16
DD	5693.50	3715.80	800.00	0.00	560.08	386.63	800.00	0.00	323.90	410.05
AUC	0.70	0.14	0.59	0.18	0.93	0.06	0.57	0.19	0.39	0.06

Appendix E: Fault identification results

Appendix E provides the fault identification contribution plot results summarised in Chapter 6, section 6.3. The significant contribution plots for each fault is provided and described. Contribution plot results representations are summarized from Chapter 5, section 5.3.

As discussed in Chapter 5, section 5.3, contribution plots are evaluated for each section of the plant. Specifically, the preparation-, recycle- and pressure leach –section. Offline samples are also considered separately.
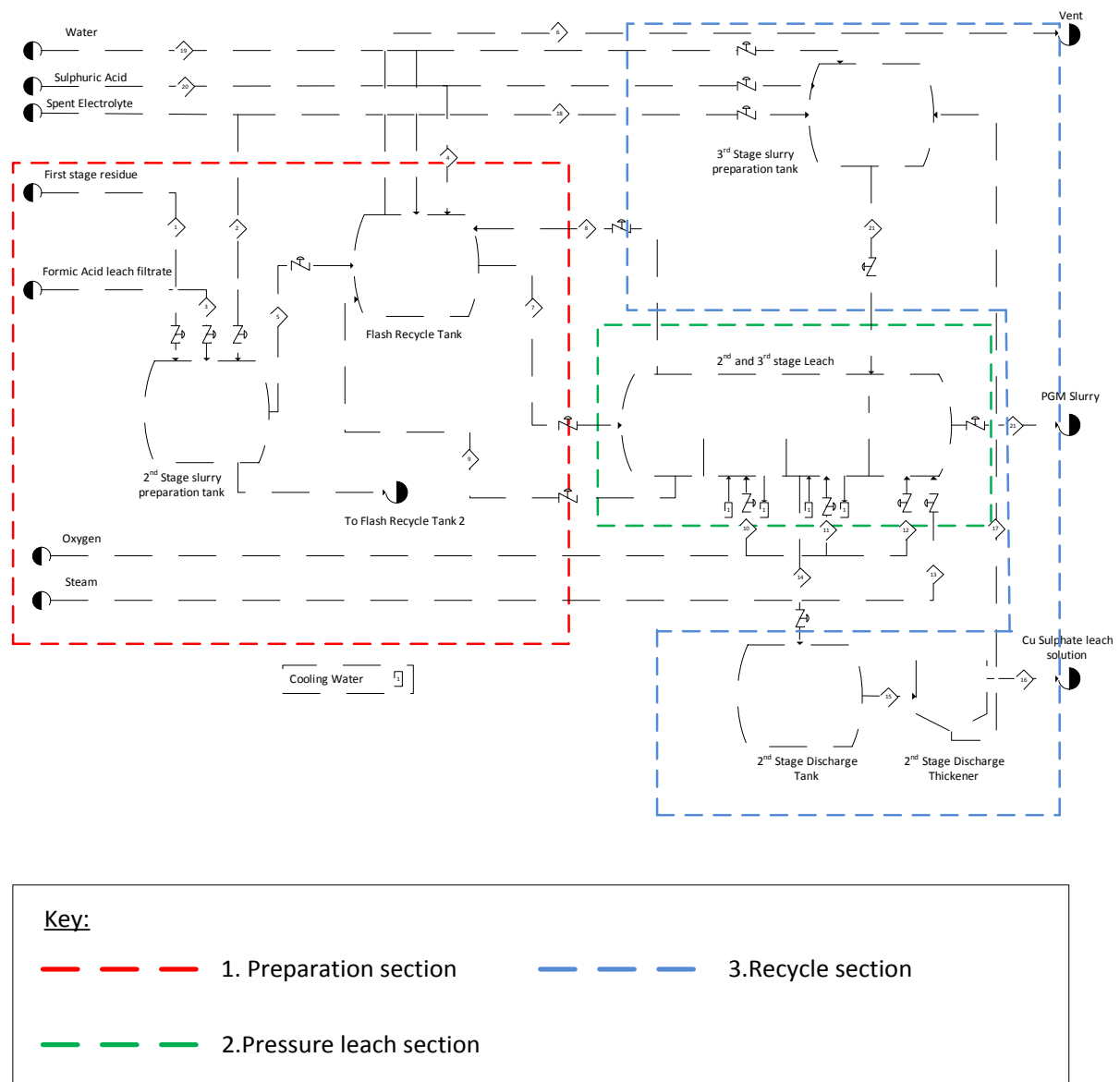
Figure E.1: Contribution plot sections. Preparation section indicated in red, pressure leach section indicated in green and recycle section indicated in blue.

Process variables are abbreviated as discussed in Chapter 5, section 5.3. The abbreviations are provided in Table E.1.

Table E.1: Fault identification process variable abbreviations.

Abbreviation	Definition
PT	Pressure leach preparation tank.
FR	Flash recycle tank.
AT#	Autoclave. # indicates the compartment number.
RT	Third compartment recycle tank.
SL	Third compartment recycle solid/liquid separator.
RM	Third compartment recycle mixing tank
F	Flow measurement
L	Level measurement
T	Temperature measurement.
OX	Oxygen
SE	Spent electrolyte
SA	Sulphuric acid
W	Water
PROD	Product
REC	Recycle

Offline sample compositions are provided in Table E.2. The fourteen residue species and seven filtrate species is shown. Note that the PGE oxides are not present in the first stage residue. Therefore, only eleven different species are presented in the first stage residue composition.

Table E.2: Residue and filtrate offline sample compositions.

Residue	Filtrate
NiS	Cu
Ni_3S_4	Ni
Cu9S5	Fe
CuS	Rh
$FeOHSO_4$	Ru
Rh_2S_3	Ir
Rh	H_2SO_4
RhO_2***	Cu
RuS_2	-
Ru	-
RuO_2***	-
Ir_2S_3	-
Ir	-
IrO_2***	-
***Compositions not detected in first stage residue	

Significant contribution plots are discussed in sections E.1 – E.8.

E.1 Density disturbance (Valve blockage)

The valve blockage (density disturbance) relative PCA SPE contribution plots are provided in Figure E.2.
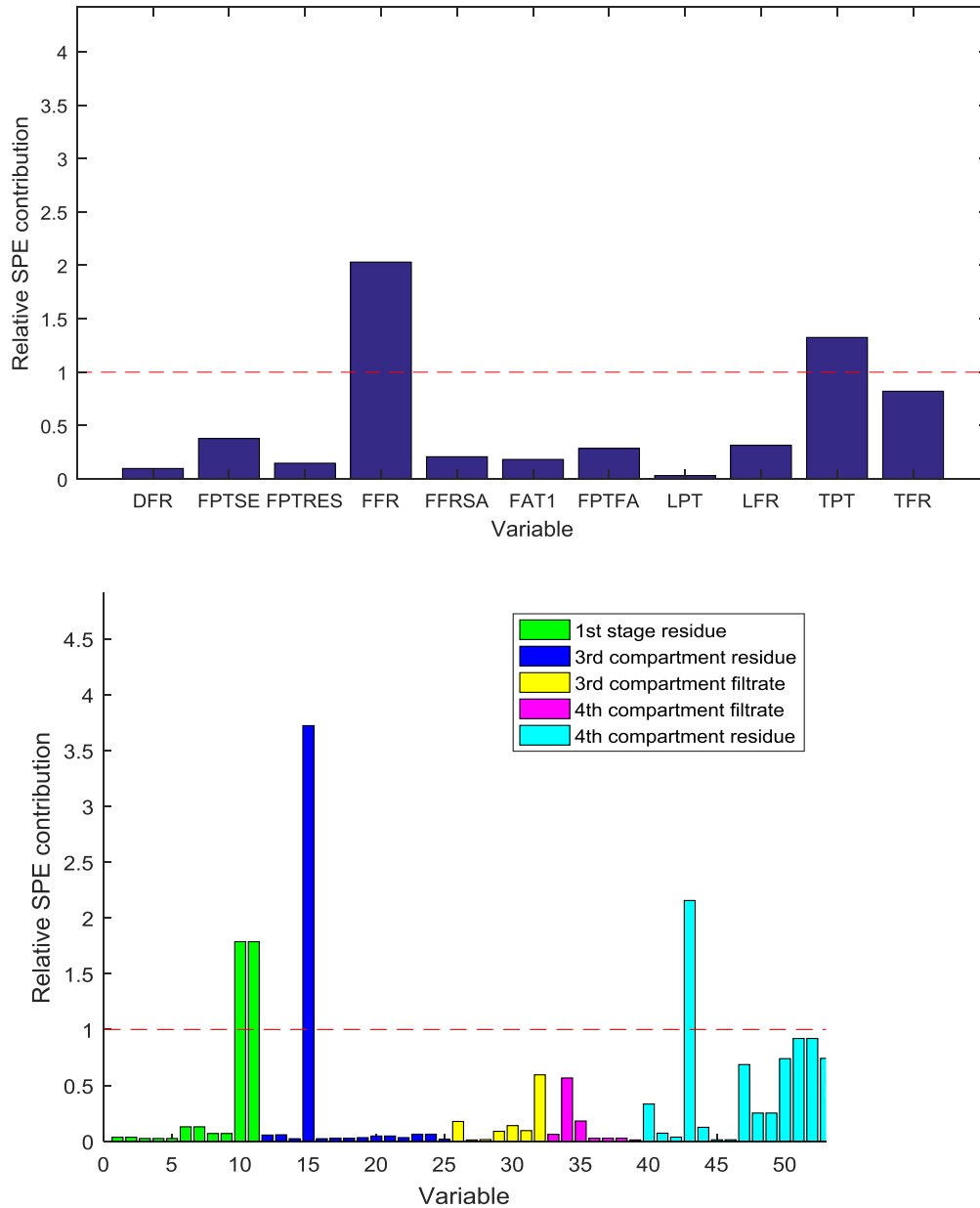
Figure E.2: Density disturbance PCA SPE relative contribution plots. The preparation section contributions are shown in the first plot and the offline sample contributions are shown the second plot.

The first contribution plot shows the flash recycle tank flow exceeding the contribution limit. This is a symptom of the fault, since the density disturbance causes some variation in the second stage preparation tank level. The feedforward controller subsequently reacts by changing the flow to the flash recycle tank.

Some minor deviations are observed in the offline residue samples. The CuS concentration show significant contributions for both the third and fourth compartment residues. This is expected, since the density disturbance causes a slight increase in base metal residue concentrations.
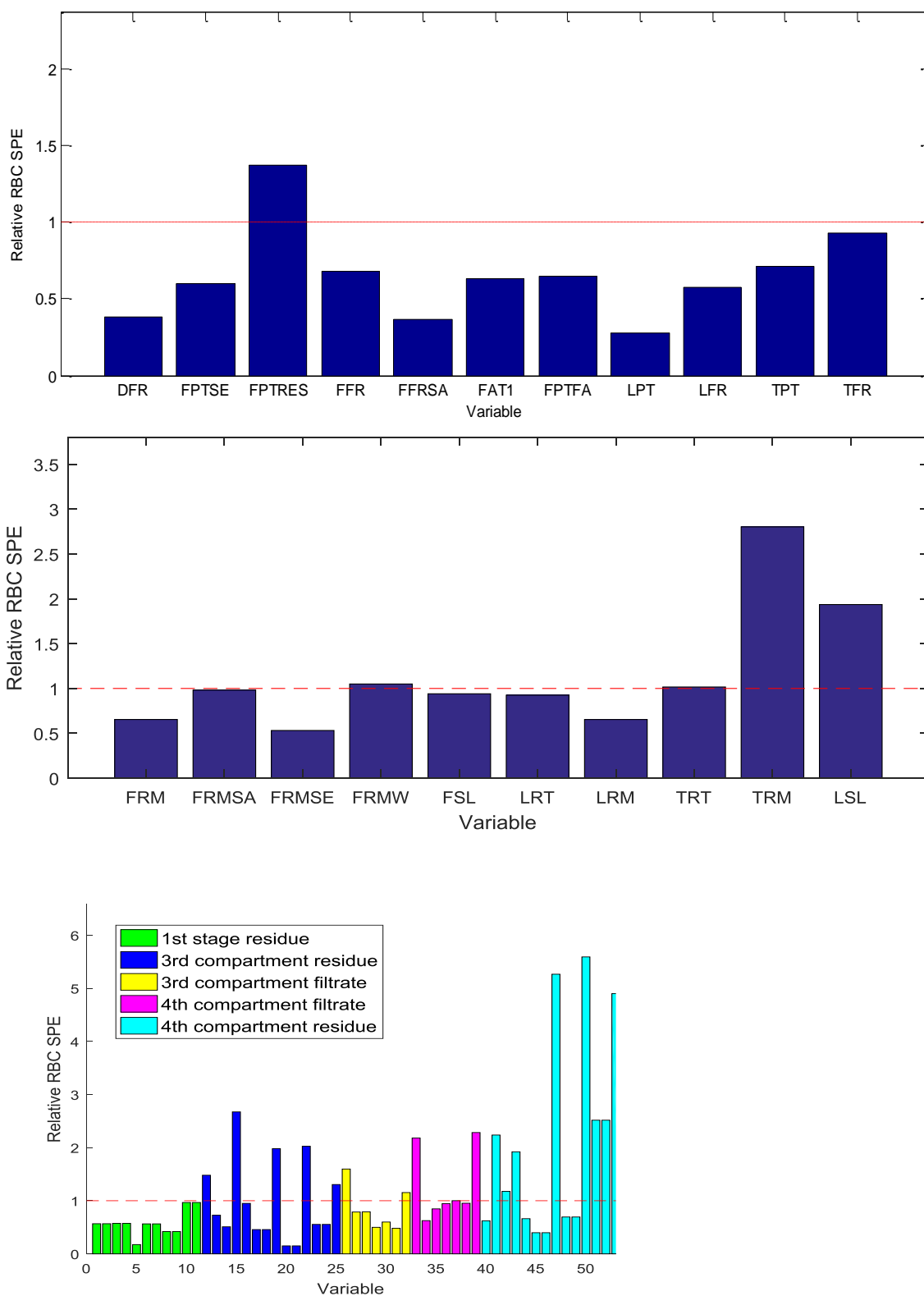
Figure E.3: Density disturbance SPE relative RBC plots. The preparation and recycle sections contributions are shown in the first two plots. Offline sample contributions are shown in the third plot.

Figure E.3 shows some deviations in the third stage recycle tank temperature. This is again only a symptom of the fault. The offline sample contribution plot shows deviations in all samples excluding the first stage residue. Larger deviations are observed in the fourth compartment residue. Both base metals and PGEs show significant contributions, indicating a specifically large deviation in the fourth compartment PGE concentrations.

Both the traditional and RBC emphasised the relatively small impact of the fault on the process. In conjunction with the relatively large detection delay, it will be difficult to diagnose and mitigate the fault prior to it propagating through the process. KPCA contribution plots are not considered, since KPCA was unable to detect the fault in any of the replicates.

E.2 Valve wear

The valve wear PCA relative T^2-statistic contribution plot is shown in Figure E.4.
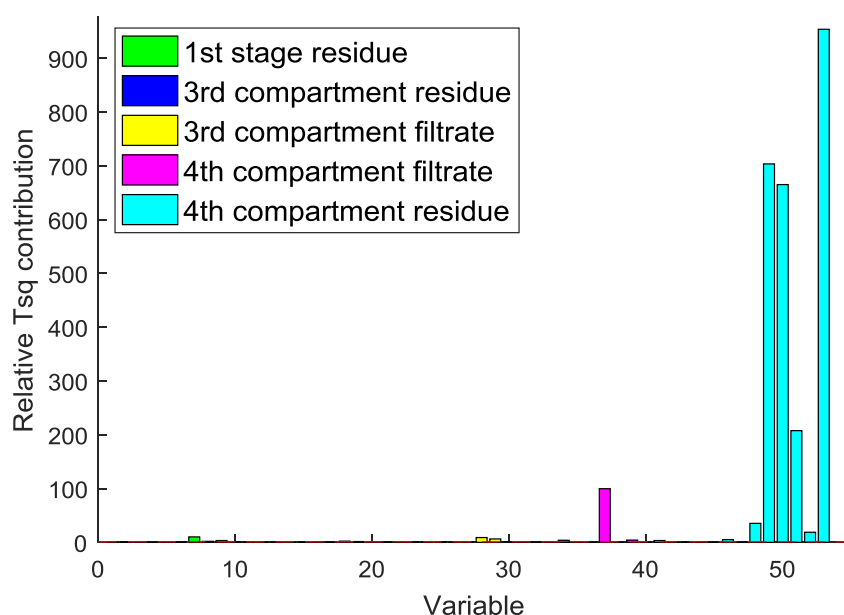
Figure E.4: Valve wear PCA relative T^2 contribution plot. Only offline samples provided significant contributions.

Large contributions were noted at the fourth compartment residue. The PGE concentration show large deviations in the fourth compartment residue. No significant contributions were noted in the first three fault identification sections. The fault is hidden by the process controllers resulting in poor fault identification results.

The valve wear PCA relative T^2-statistic RBC plot is shown in Figure E.5.
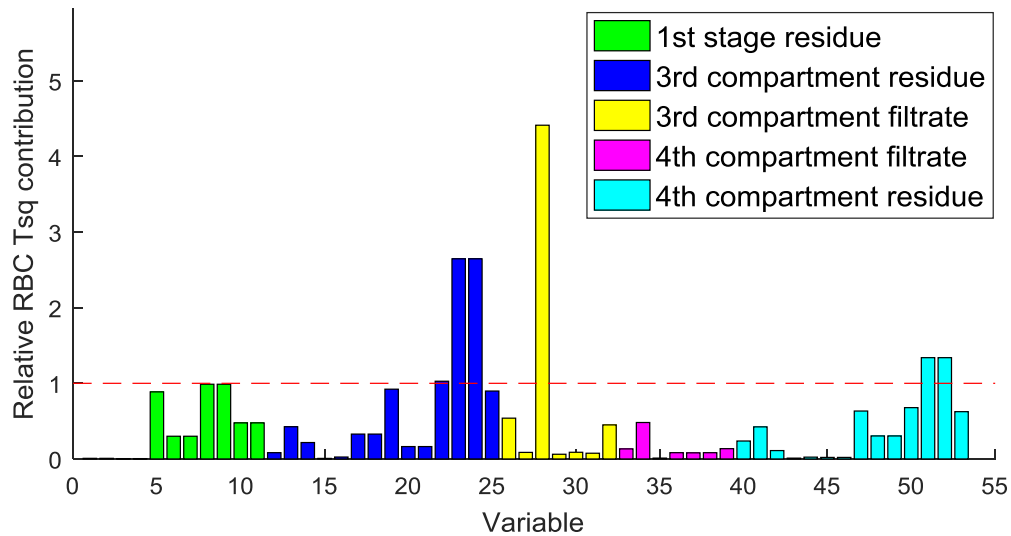
Figure E.5: Valve wear PCA relative RBC T² plot. Only offline samples provided significant contributions.

In contrast to Figure E.4, the largest contributions are noted at the third compartment residue and filtrate samples. However, the RBC similarly is unable to identify any significant contributions in the previous three sections.

The valve wear KPCA relative T²-statistic contribution plots are shown in Figure E.6.
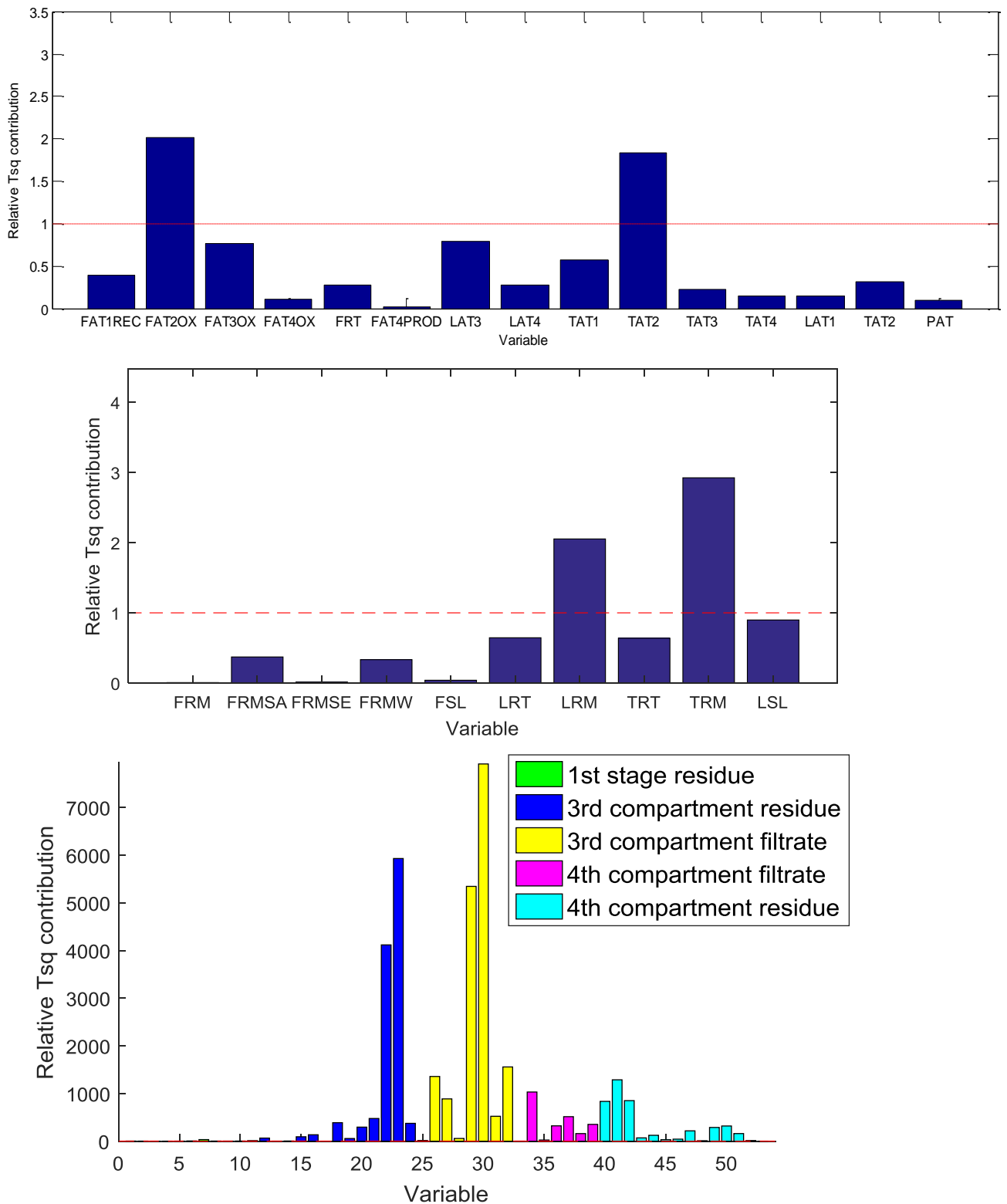
Figure E.6: Valve wear KPCA relative T² contribution plot. The recycling section contributions are shown in the first plot. Offline sample contributions are shown in the second plot.

Some deviations are noted in the third compartment mixing tank level and temperature. These contributions are considered to be symptoms of the fault. Large contributions are again noted at the third compartment filtrate and residue samples.

It is clear that none of the contribution plots identify the true fault location. This is primarily due to the process controllers hiding the impact of the fault as it propagates through the process. In conjunction with the poor detection delay results, the multivariate methods clearly offer no advantage to univariate when considering the valve wear fault.

E.3 Valve stiction

The valve stiction PCA relative SPE contribution plots are given in Figure E.7.
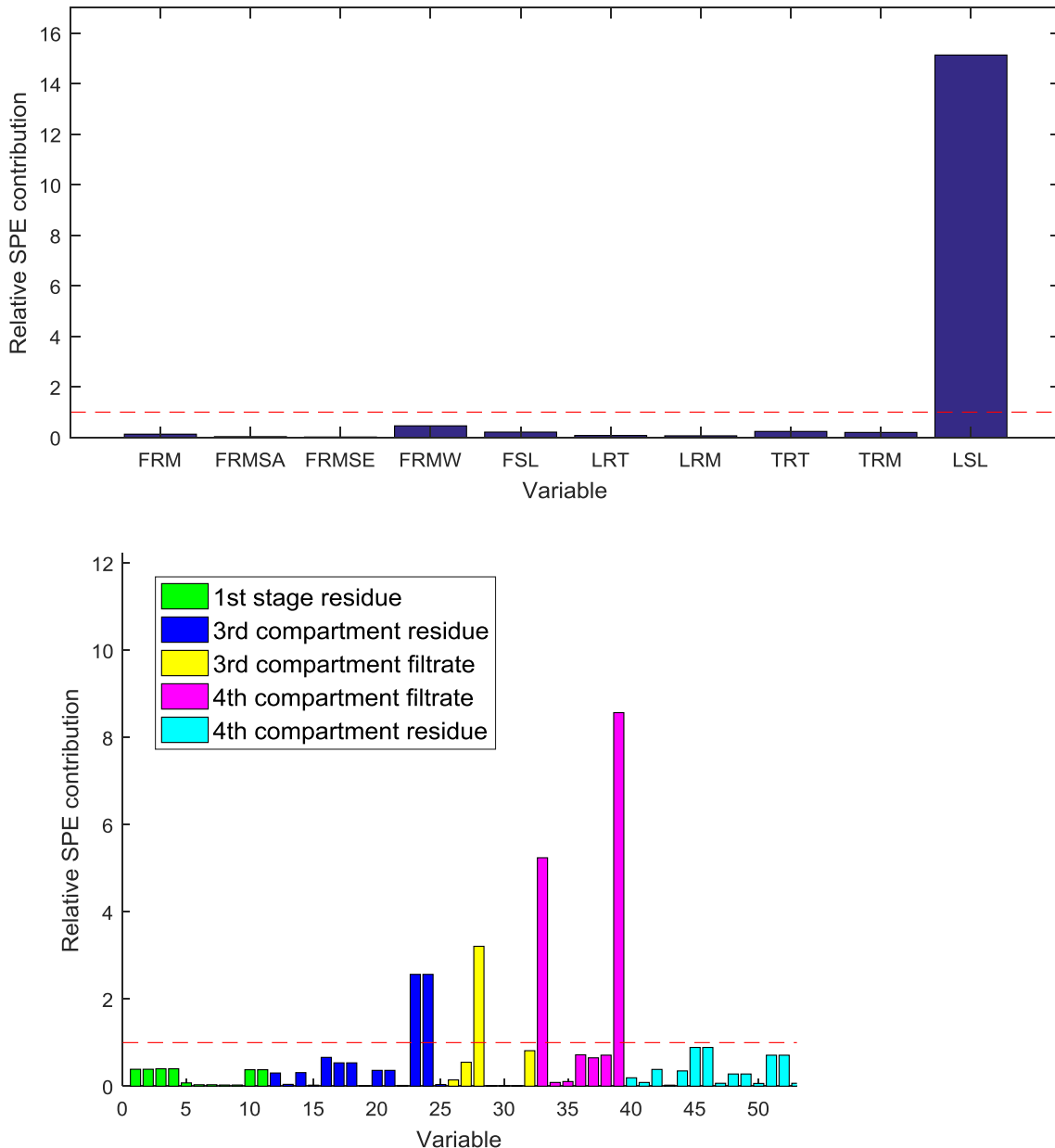
Figure E.7: Valve stiction PCA relative SPE contribution plot. The recycling section contributions are shown in the first plot. Offline sample contributions are shown in the second plot.

The largest contribution is noted at the third compartment solid/liquid separator level. Some deviations are also noted in third and fourth compartment filtrate. These contributions are all

symptoms of the fault. The PGEs show the largest deviations. Similar observations were made by Miskin (2015). The valve stiction results in lower concentration base metals present and therefore an increased rate of PGE leaching.

The valve stiction PCA SPE relative RBC plots are shown in Figure E.8.
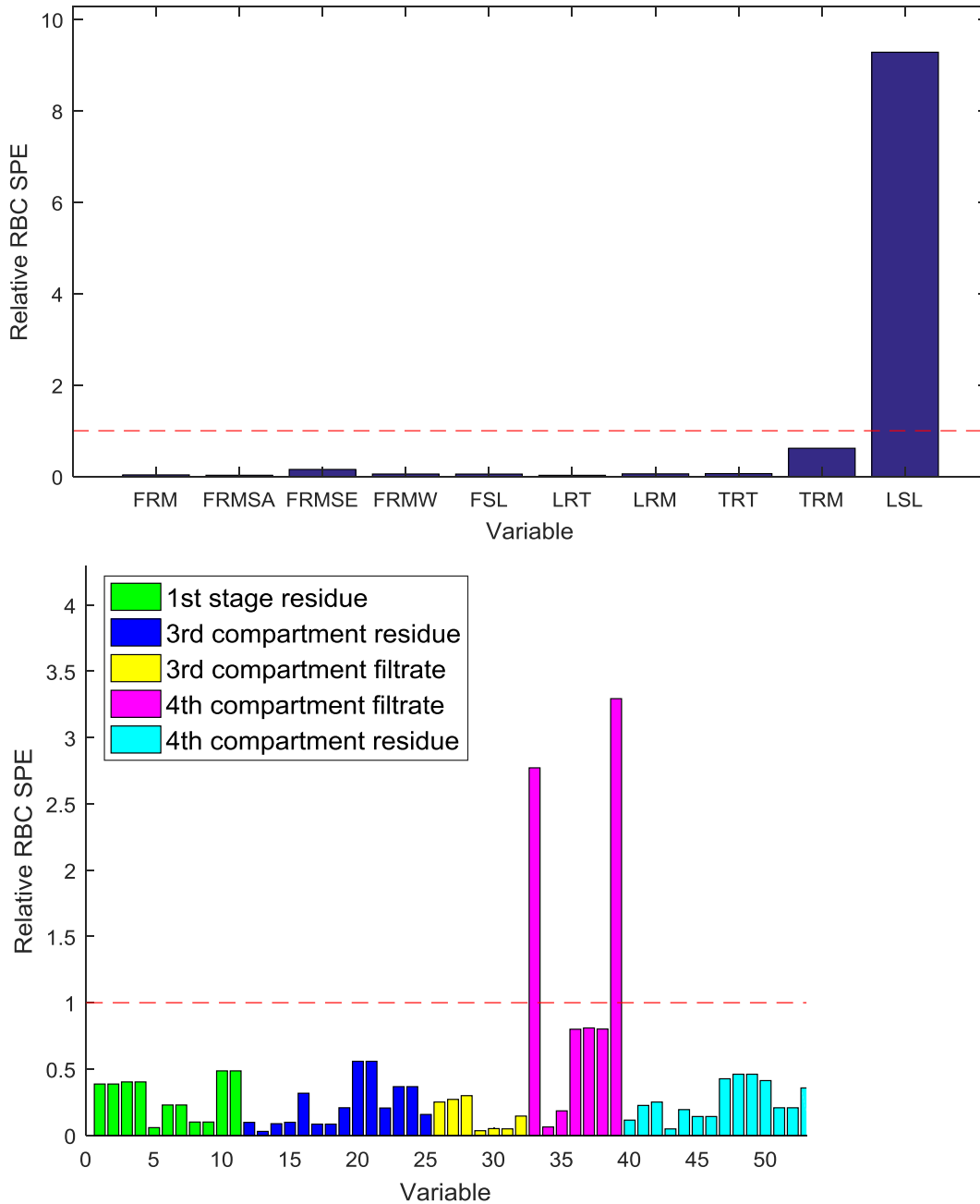
Figure E.8: Valve stiction PCA RBC SPE plot. The recycling section contributions are shown in the first plot. Offline sample contributions are shown in the second plot.

Similar contributions are noted with the RBC. Again only symptoms of the fault are identified. The same 4th compartment filtrate samples are again identified.

The valve stiction KPCA relative T^2-statistic contribution plots are shown in Figure E.9.
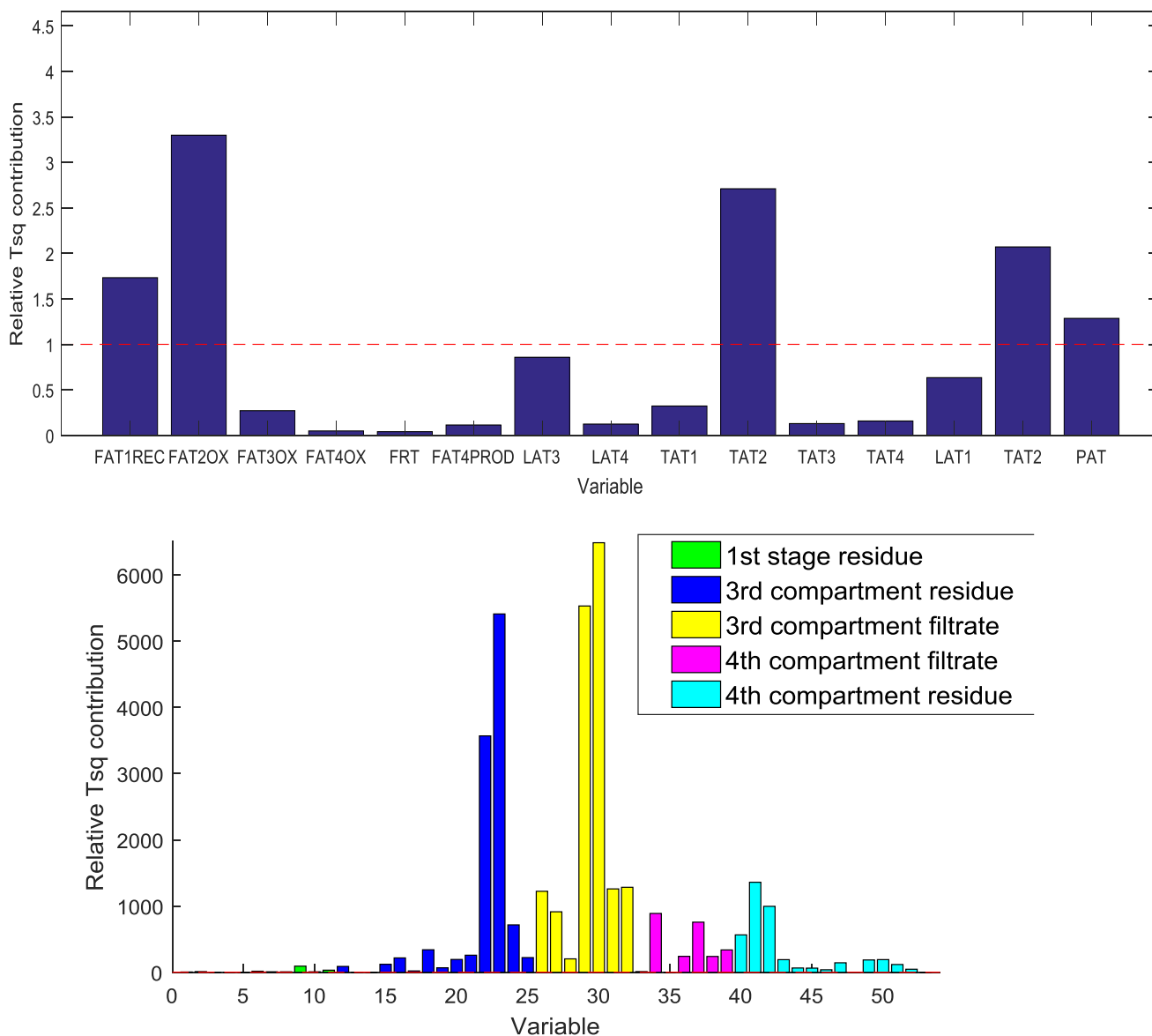
Figure E.9: Valve stiction KPCA relative T^2 contribution plot. The pressure leach section is shown in the first plot, followed by the offline samples plot.

Several significant contributions were noted in the autoclave section. Some variation in the second compartment temperature is noted, resulting in deviations in the oxygen feed rate. Some deviation in first compartment recycle is noted. These variations are again only symptoms of the fault. The fault results in density changes in the second stage preparation tank, which in turn affects the flash recycle tank level and flow-rates.

The detection results clearly indicate that valve stiction can be detected significantly early. However, the fault identification results show it will be more challenging to identify the correct fault location after the fault has been detected.

E.4 Pump impeller wear

The pump impeller wear PCA relative T^2-statistic contribution plot is shown in Figure E.10.
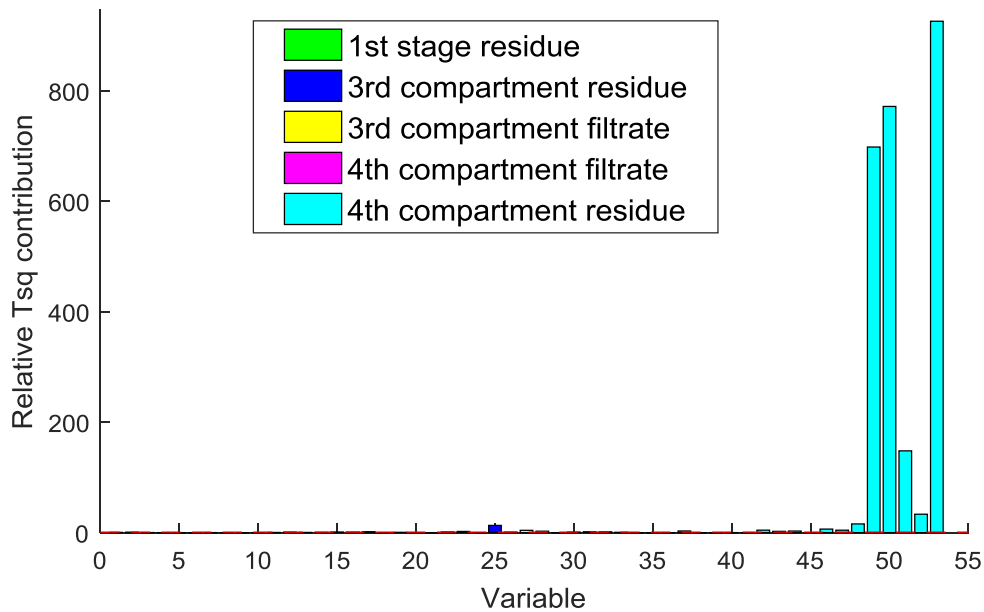
Figure E.10: Impeller wear PCA relative T^2 contribution plot. Only offline sample contributions are shown.

Significant contributions were only noted in the fourth compartment residue sample. Deviations in the both filtrate and residue samples are expected. The PGMs and PGEs provide the largest contributions for in the 4th compartment residue. The actual location of the fault is not identified.

The pump impeller wear PCA T^2-statistic RBC plot is shown in Figure E.11.
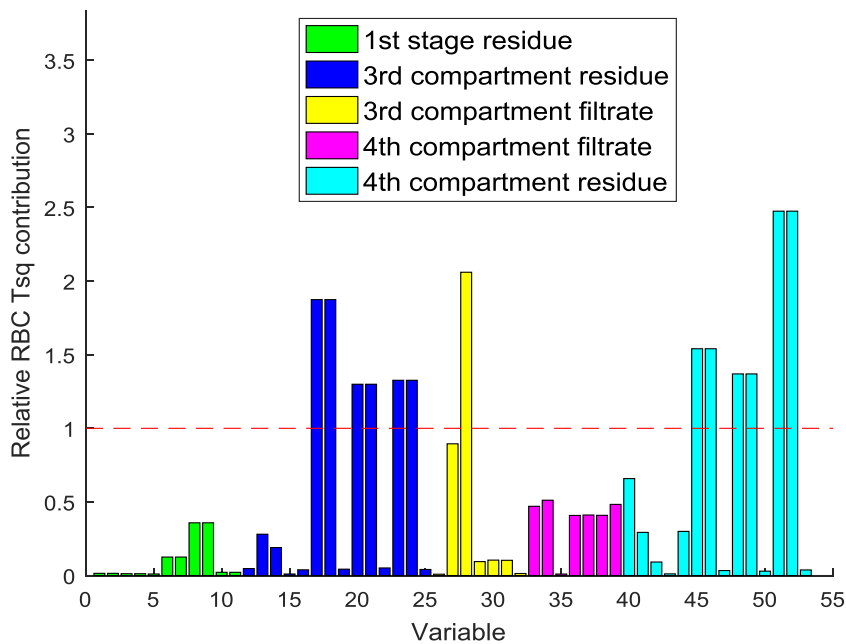
Figure E.11: Impeller wear PCA relative RBC T^2 plot. Only offline sample contributions are shown.

Again only significant contributions were noted in offline samples from Figure E.11. The RBC is also unable to identify the actual fault location. Similar deviations in both PGM and PGE compositions are noted for both the third and fourth compartment residue.

The pump impeller wear relative KPCA T^2-statistic contribution plots are shown in Figure E.12.
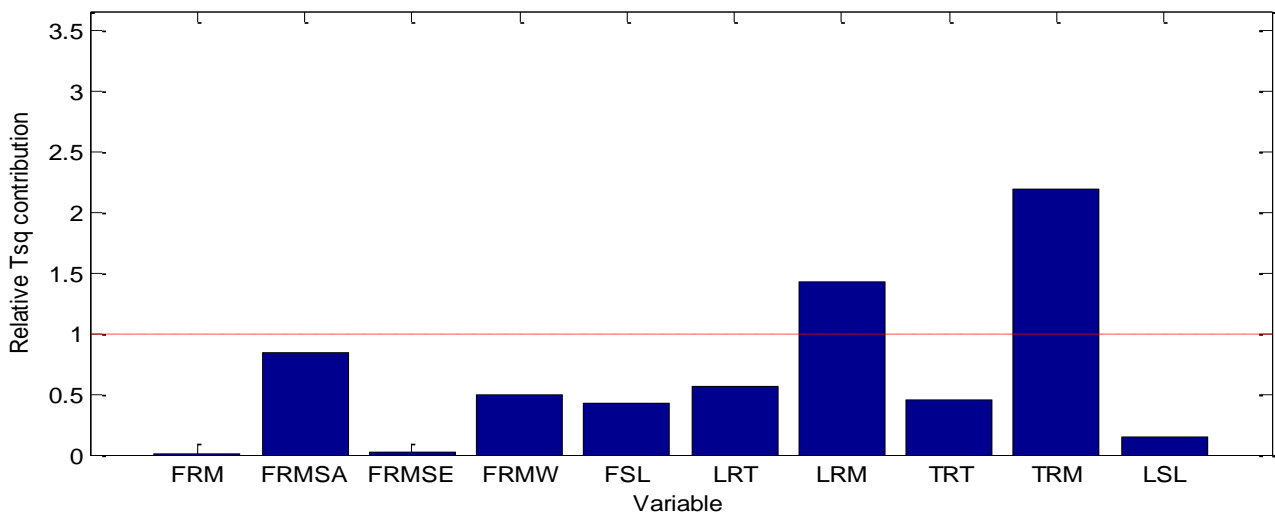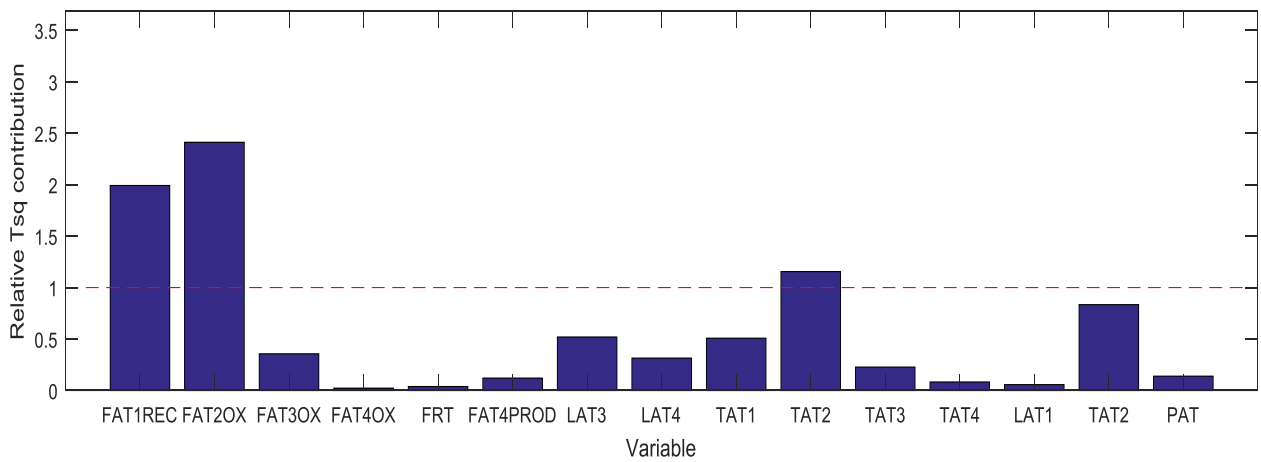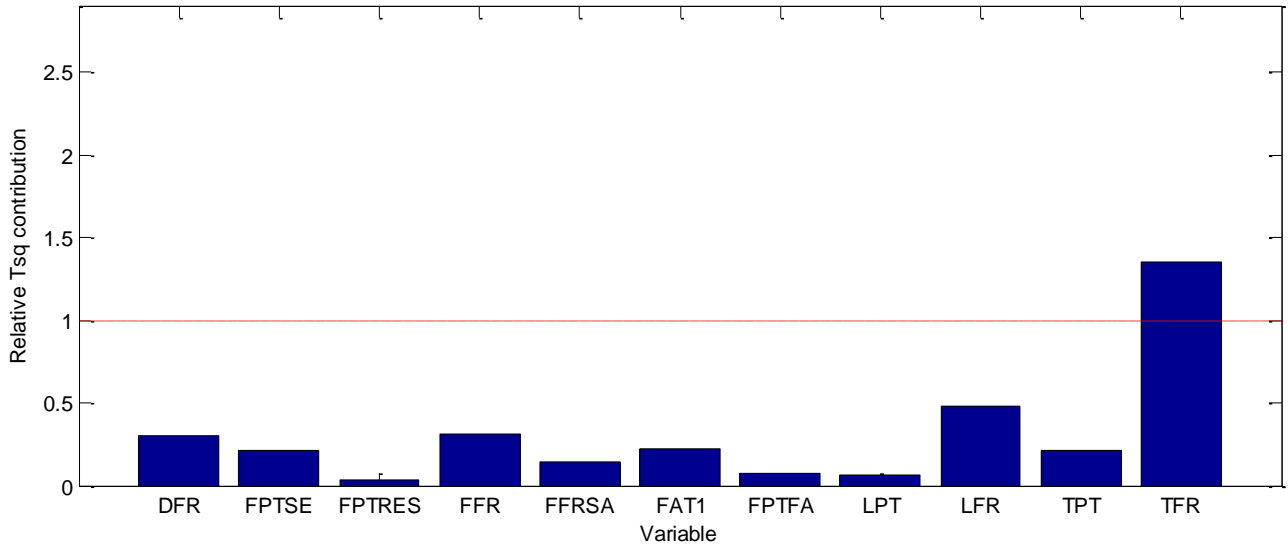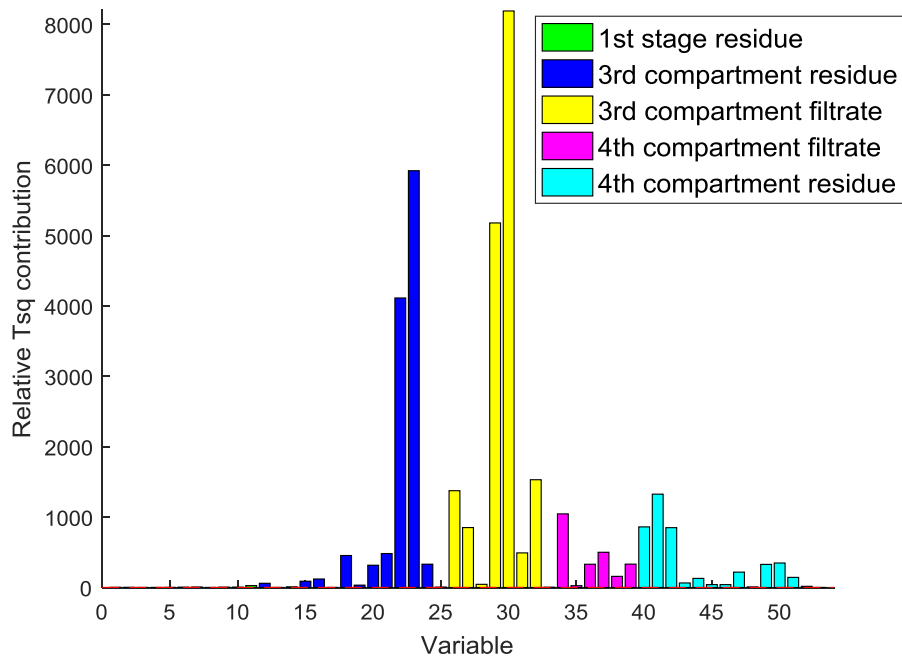
Figure E.12: Impeller wear KPCA relative T^2 contribution plot. The preparation-, pressure leach- and recycle – section contribution plots are shown followed by offline sample contribution plot.

Some minor significant contributions were noted in the autoclave. Since the fault occurs in the second stage feed, the first compartment recycle flow contribution can be considered to correctly identify the fault location.

Large contributions are noted in both third compartment offline samples. This is expected considering the temperature effect of the impeller wear.

E.5 Solids build-up in cooling coil

The solids build-up in cooling coil PCA relative contribution plots are given in Figure E.13.
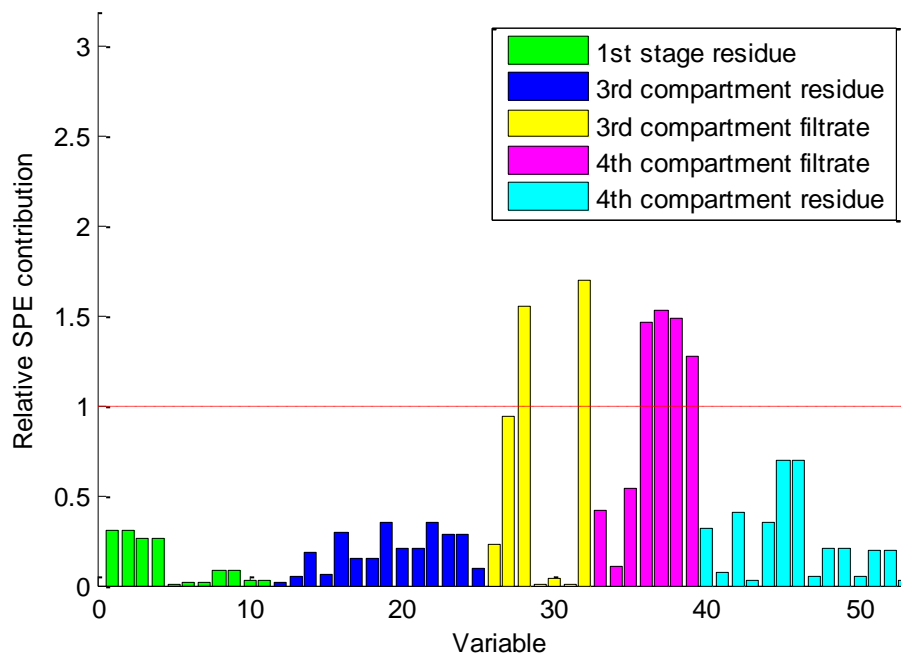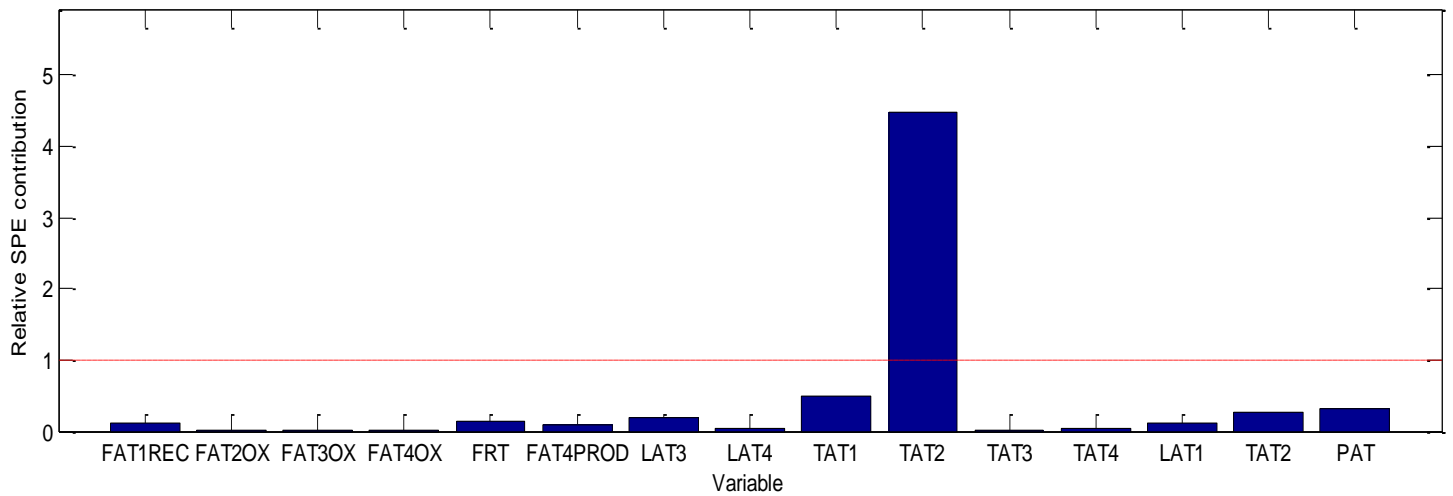
Figure E.13: Solids build up in cooling coils PCA SPE relative contribution plots. The pressure leach section and offline samples provided significant contributions.

The largest contribution is observed at the second compartment temperature. Some minor contribution variations are observed in the third and fourth compartment filtrate samples. The contribution plot therefore correctly identifies the fault location.

The solid build-up in cooling coil PCA relative RBC plots are given in Figure E.14.
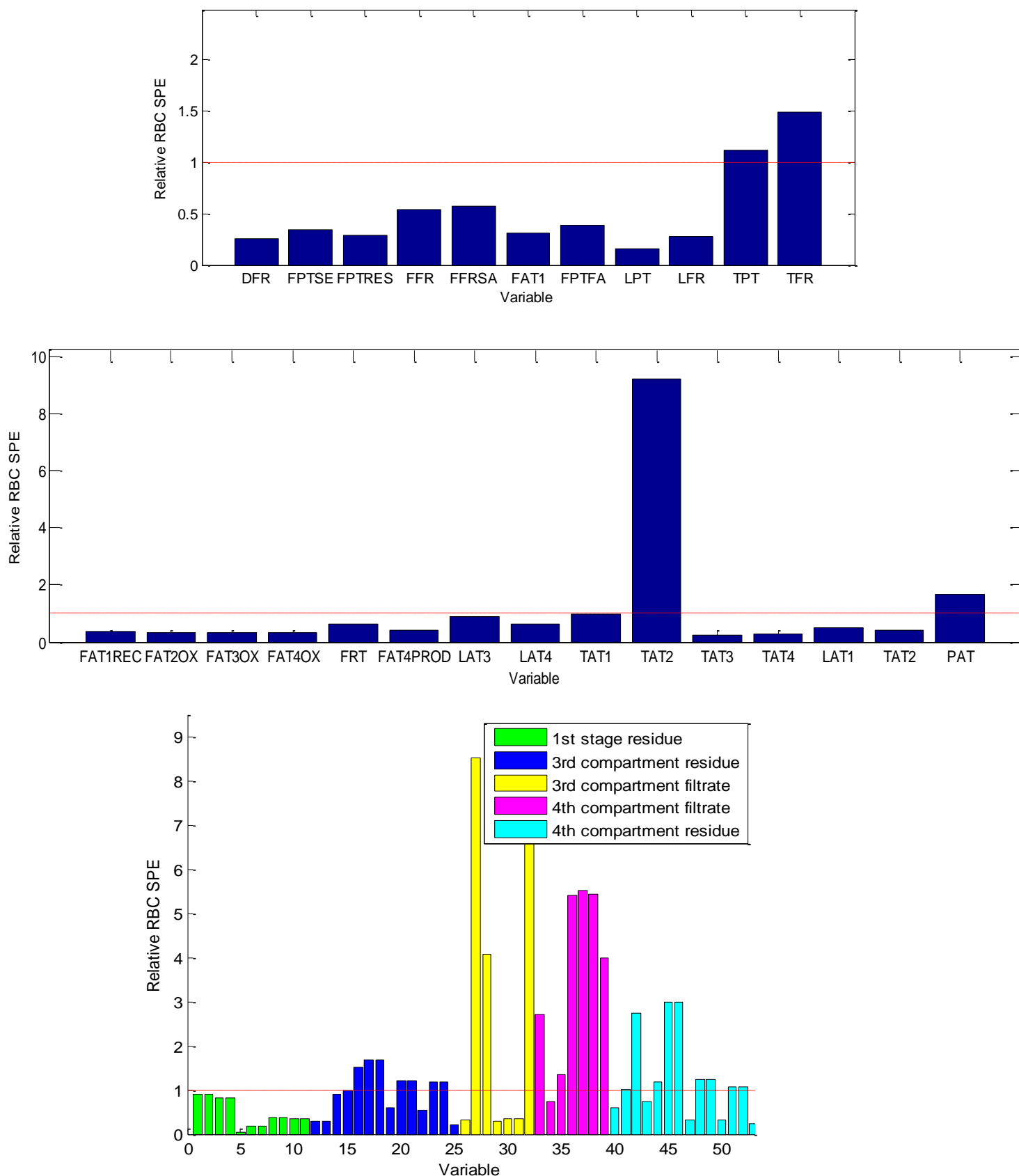
Figure E.14: Solids build up in cooling coils PCA SPE relative RBC plots. The preparation section, pressure leach section and offline samples provided significant contributions.

Similar to the traditional contribution plots, the second compartment temperature shows a large contribution. Larger contributions are observed for both the third and fourth compartment filtrate.
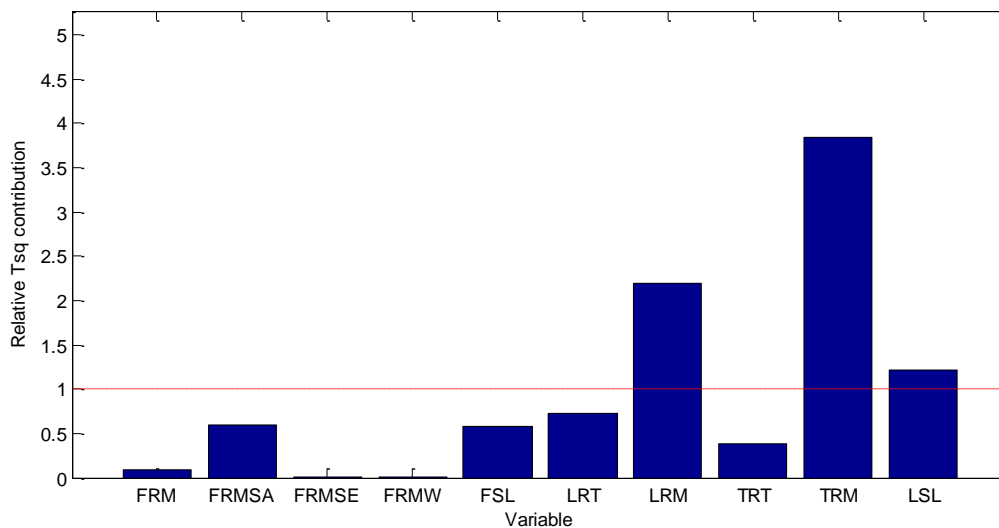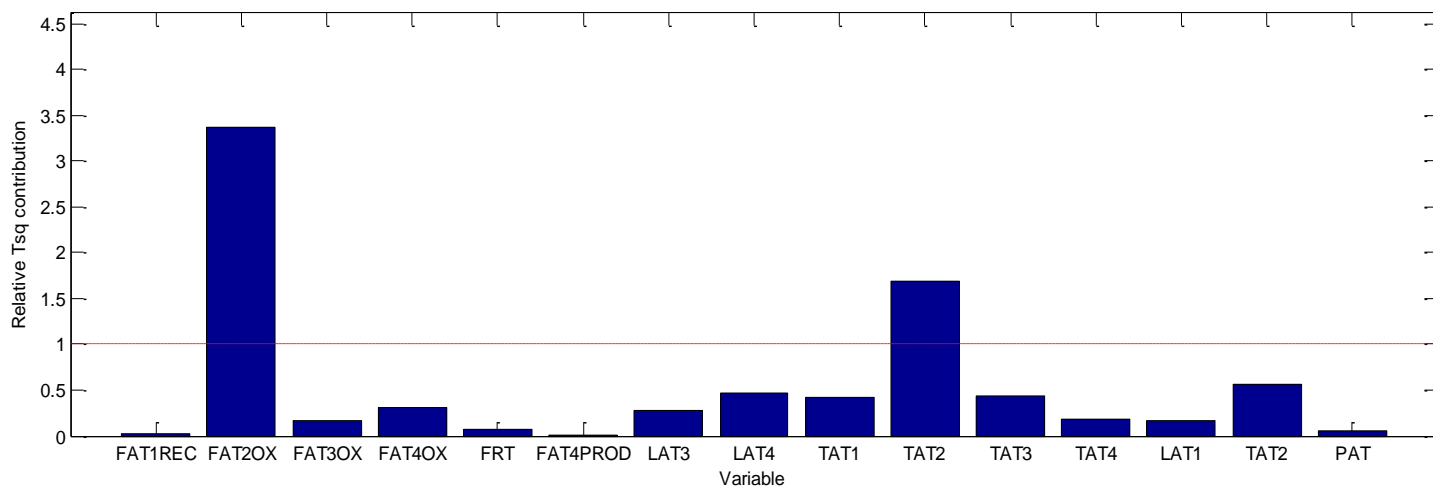
Figure E.15: Solids build up in cooling coils KPCA T²-statistic relative contribution plots. The pressure leach section, recycle section and offline samples provided significant contributions.
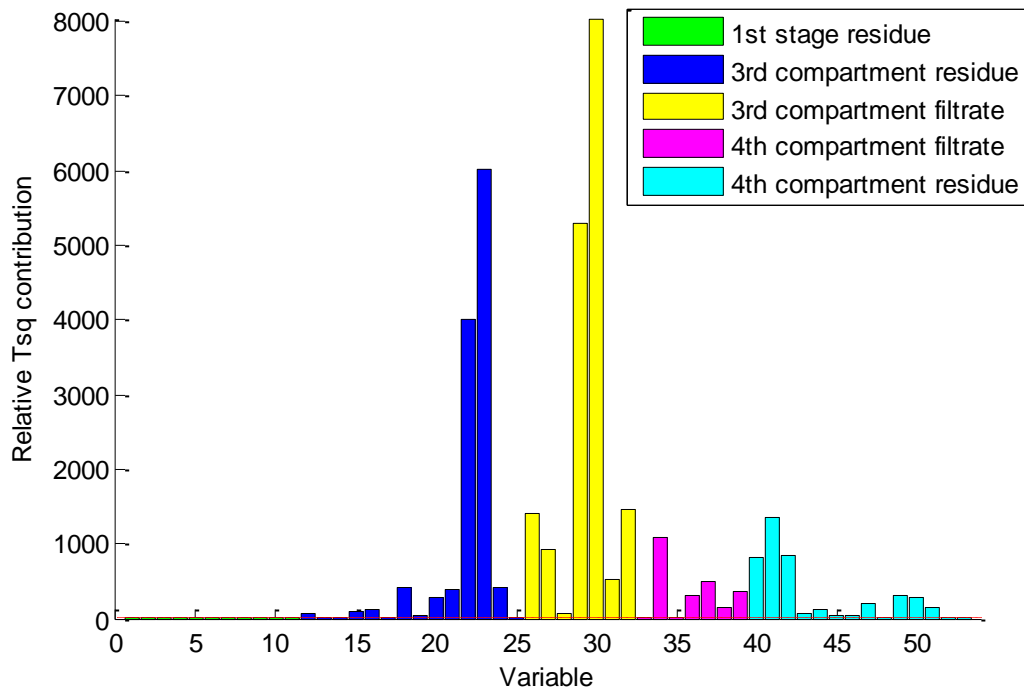
Figure E.15 *(cont.)*: **Solids build up in cooling coils KPCA T^2-statistic relative contribution plots. The pressure leach section, recycle section and offline samples provided significant contributions.**

Deviations in contributions are observed in the second compartment oxygen flow and second compartment temperature. The oxygen flow is reduced to accommodate for the increasing compartment temperature.

Significant contributions are also observed in the third and fourth compartment offline samples. The increase in temperature will also result in significant changes in sample compositions. However, due to the sampling time delay, it is expected that these changes should only be observed at a later period.

All contribution plots correctly identified the fault location. The offline sample contributions are however considered as incorrect.

E.6 Peristaltic pump tube failure

The peristaltic pump tube failure relative PCA SPE contribution plots are shown in Figure E.16.
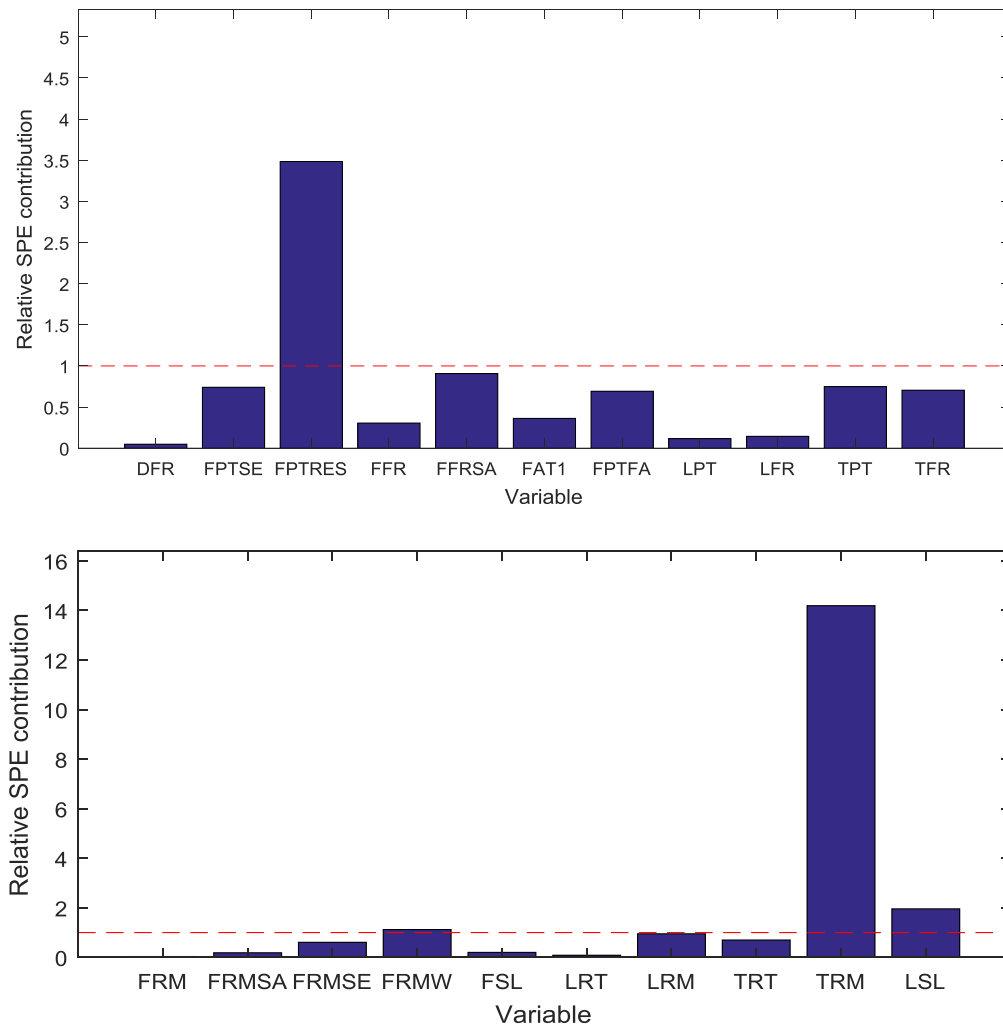
Figure E.16: Traditional PCA SPE contribution plots. The preparation section and recycle section provided significant contributions.

Due to the immediate impact of the fault, several variations in contributions are observed. The first is the preparation tank residue flow and level. This is expected, since the first stage residue flow towards the preparation tank immediately drops, which in turn results in an immediate drop in the level of the tank. Both these contributions are directly linked to fault location.

A large deviation is also observed in the level of the third compartment recycle mixing tank. This is a definite symptom of the fault and does not contribute to identifying the fault location.

The peristaltic pump tube failure PCA relative RBC plots are provided in Figure E.17.
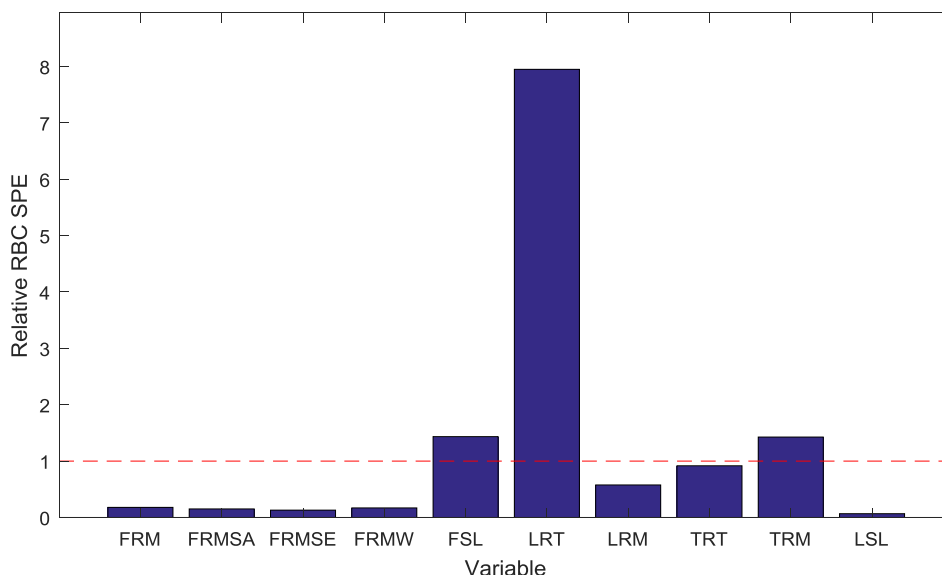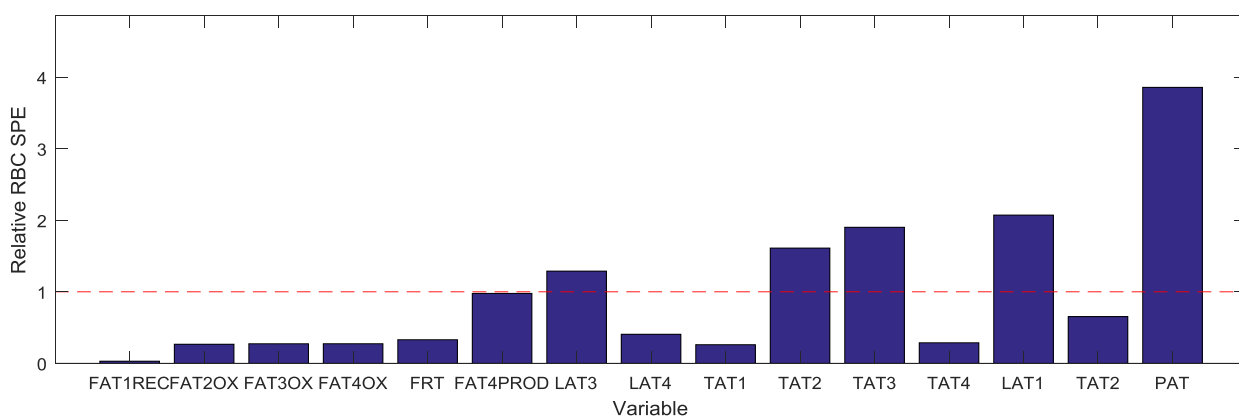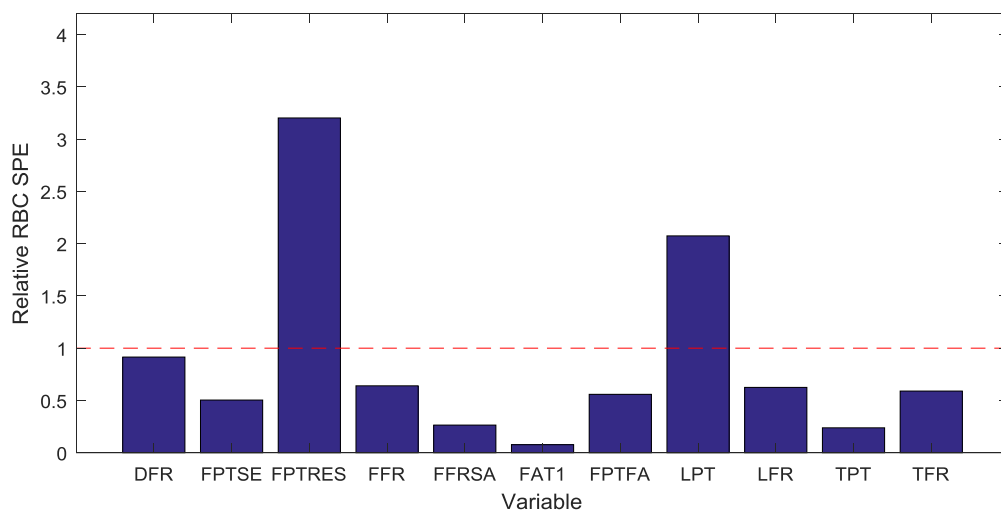
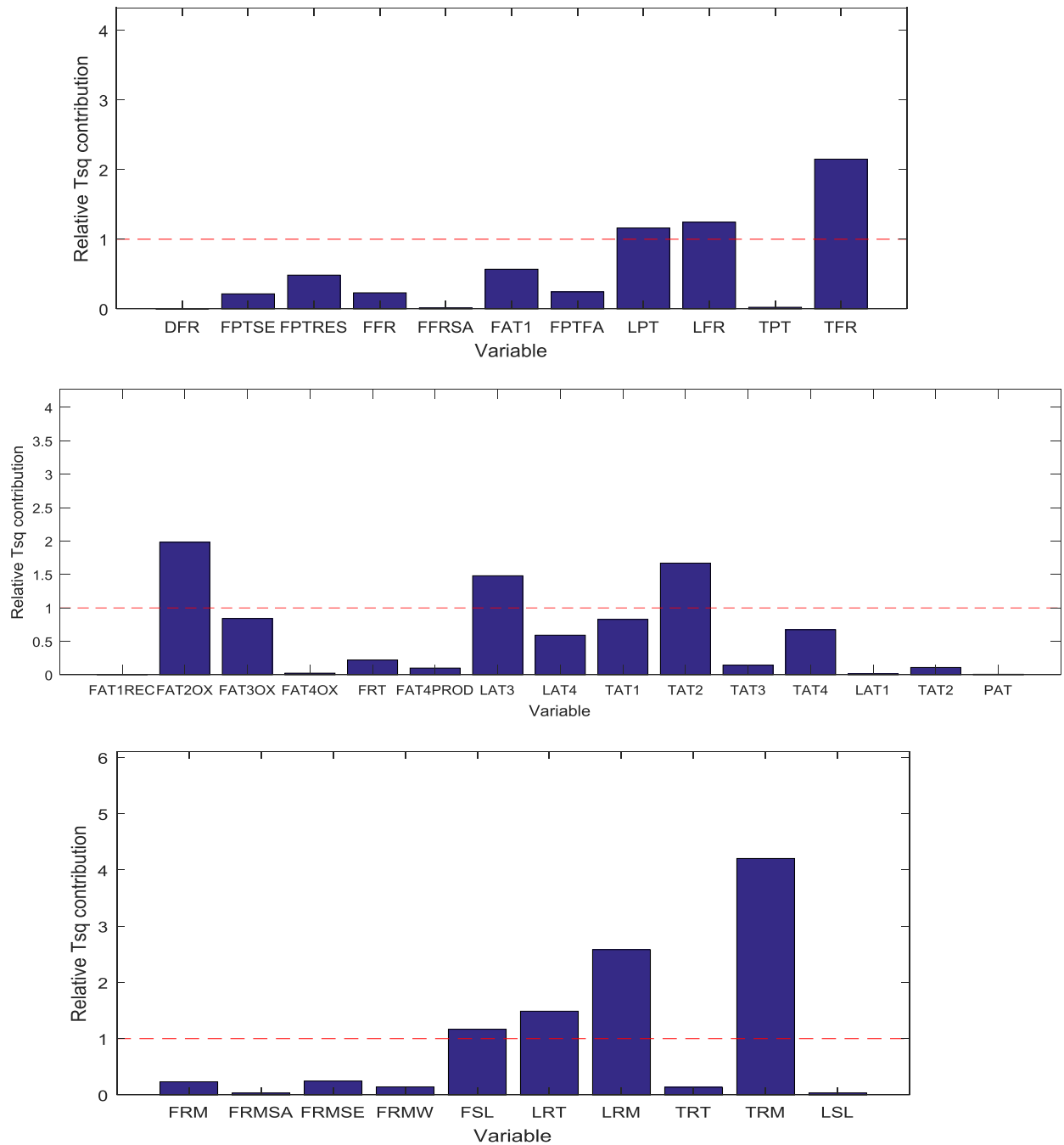**Figure E.17: Reconstruction based SPE contribution plots. The preparation section, pressure leach section and recycle section provided significant contributions.**

Similar deviations in contributions are observed at the second stage preparation tank. However, more symptoms are incorrectly identified. The loss in flow towards the autoclave results in temperature, level and oxygen flow deviations. A large deviation is consequently observed in the third compartment recycle tank level.

The RBC correctly identifies the location of the fault, but also fails to deal with the significant fault smearing observed in E.17 .The peristaltic pump tube failure KPCA relative T^2-statistic contribution plots are given in Figure E.18.

Figure E.18: KPCA T^2-statistic contribution plots. The preparation section, pressure leach section and recycle section provided significant contributions.

Similar fault symptoms are observed in the relative KPCA T^2-statistic contribution plots. Smaller deviations are observed at the second stage preparation tank section. The KPCA contributions therefore suffer more from fault smearing when trying to identify the peristaltic pump tube failure.

E.7 Sulphuric acid controller misuse

The sulphuric acid controller misuse PCA relative T^2-statistic contribution plot is given in Figure E.19.
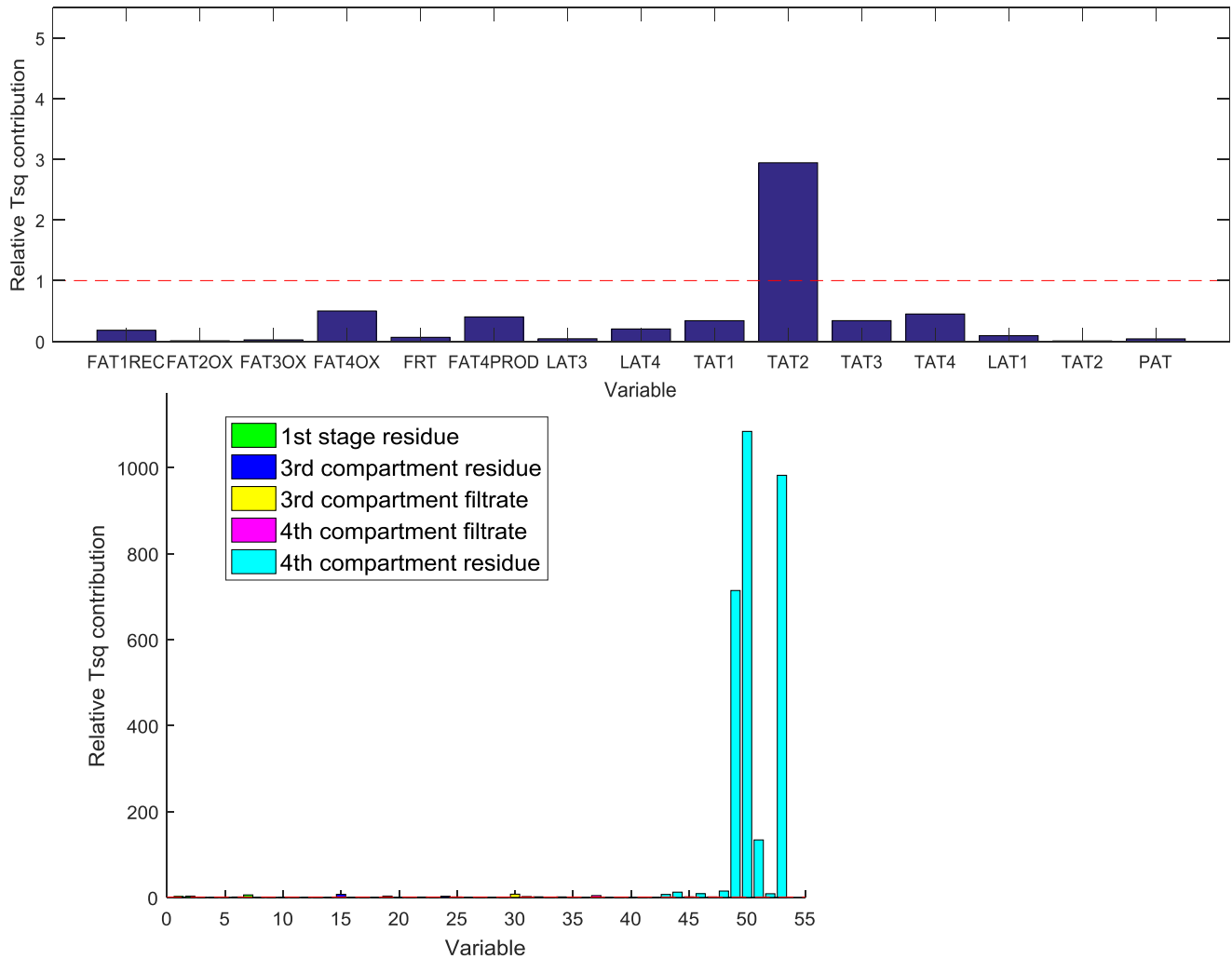
Figure E.19: Sulphuric acid controller misuse PCA relative T^2 contribution plot. The pressure leach section and offline samples provided significant contributions.

The only significant contributions are observed in the second compartment temperature and fourth compartment residue. Neither correctly identifies the location of the fault. The increased sulphuric acid results in minor disturbances to the autoclave temperatures.

The sulphuric acid controller misuse PCA relative T^2-statistic contribution plot is given in Figure E.20.
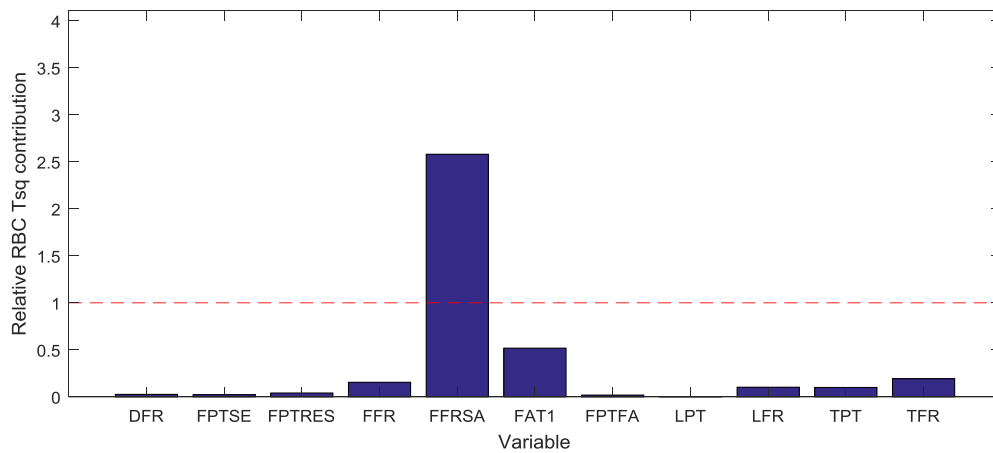
Figure E.20: Sulphuric acid controller misuse PCA relative RBC T^2 plot. The preparation section provided significant contributions.

The relative RBC plot in Figure E.20 shows the flash recycle tank sulphuric acid flow contributing to the T^2-statistic. The contribution correctly identifies the location of the fault.

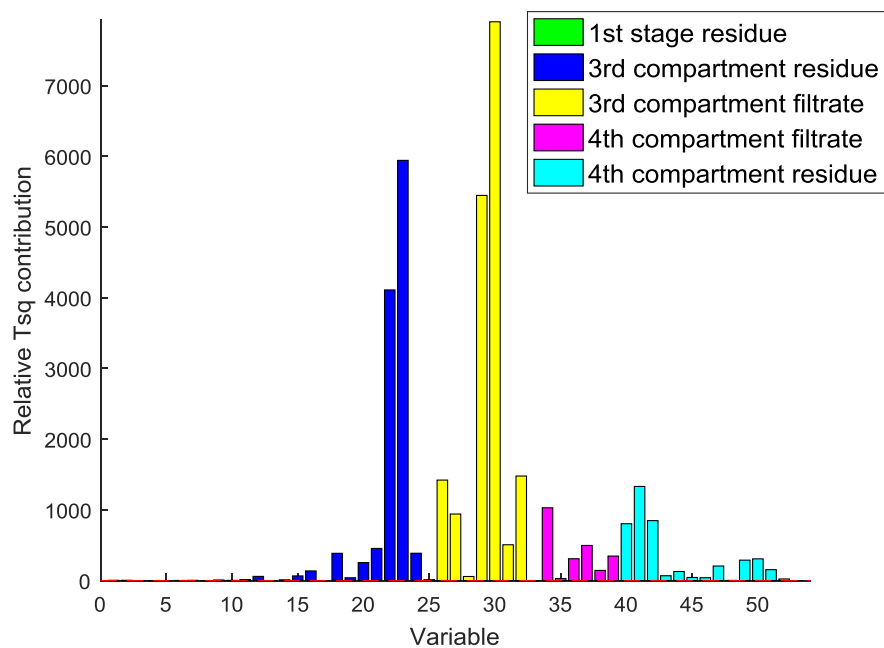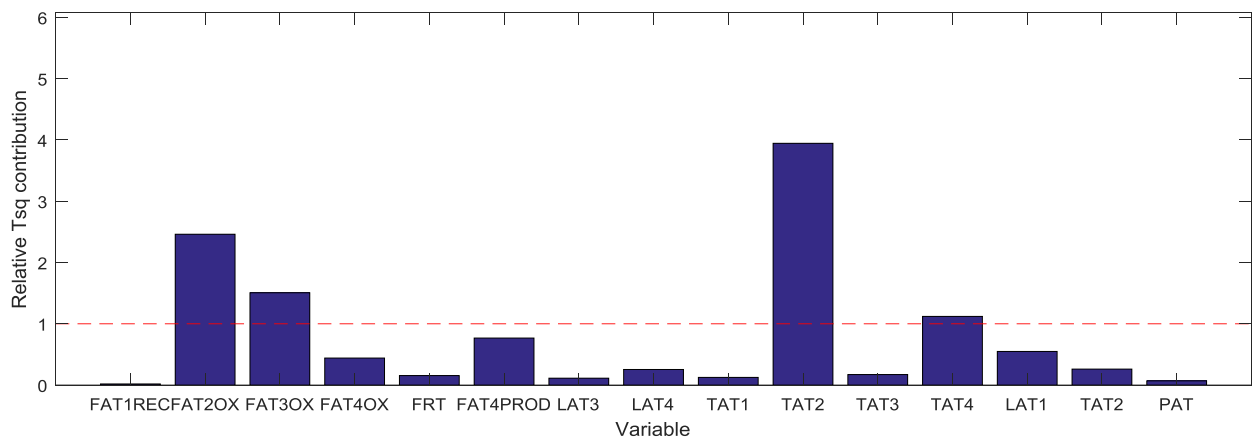The sulphuric acid controller misuse KPCA relative T^2-statistic contribution plots are given in Figure E.21.

Figure E.21: Sulphuric acid controller misuse KPCA relative T² contribution plot. The pressure leach section and offline samples provided significant contributions.

The KPCA contribution plots in Figure E.21 only identifies the symptoms of the fault. Large deviations are observed in the third and fourth compartment offline samples. This is due to the over-leaching occurring in both the third and fourth compartments.

E.8 Bubbler level sensor blockage

The PCA relative SPE contribution plots are given in Figure E.22.
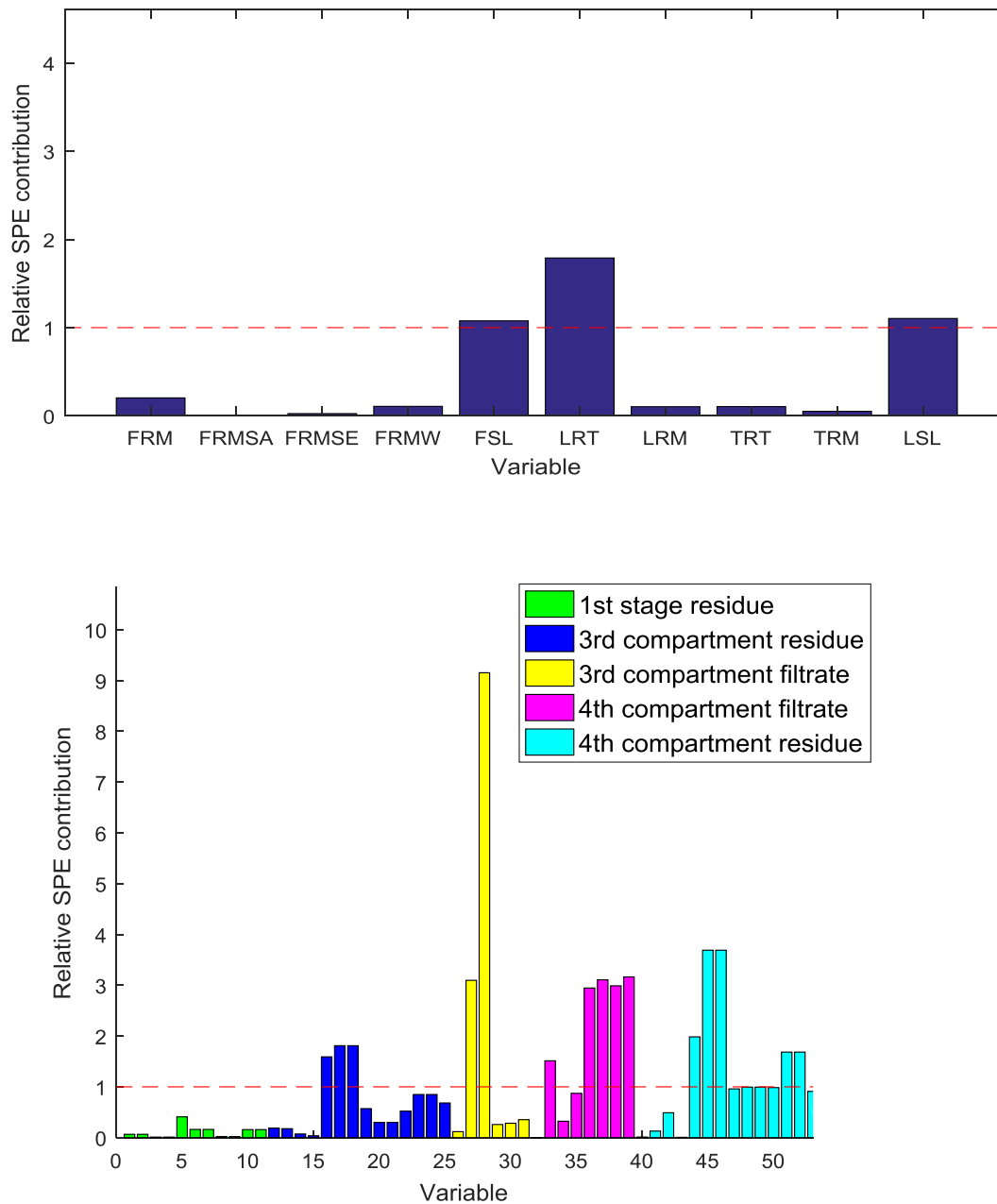
Figure E.22: Bubbler level sensor bias PCA SPE relative contribution plot. The recycle section and offline samples provided significant contributions.

Small deviations are observed in the third compartment recycle section. Deviations in contributions are also observed in both third and fourth compartment offline samples. All contribution deviations identify symptoms of the fault and not the location of the fault.

The relative PCA RBS plots are given in Figure E.23.
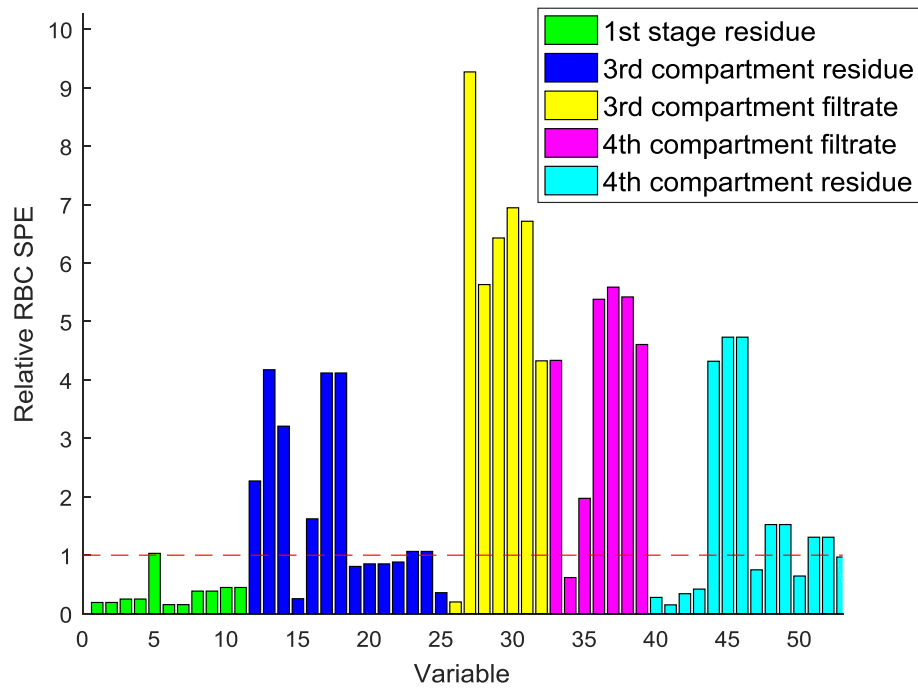
Figure E.23: Bubbler level sensor bias PCA relative SPE RBC plot. Offline samples provided significant contributions.

Large deviations are observed in both third and fourth compartment offline samples. The contributions again only identify the symptoms of the fault and not the true fault location. Since the KPCA T^2-statistic was unable to detect the fault, the KPCA T^2-statistic contribution plots are not considered.

Appendix F: Platinum and palladium concentration estimation

Appendix F discusses the estimation of both platinum and palladium concentrations. Linear regression is used to determine concentrations from iridium, rhodium and ruthenium concentrations. The estimated platinum and palladium concentrations were used in the economic impact analysis as described in Chapter 7. Historical plant data was used to develop linear regression models for both the second and third stage filtrate.

1. Second stage filtrate

Historical second stage filtrate composition data was used to build linear regression models for both platinum and palladium. The platinum concentration plant and estimated concentration is provided in Figure F.1. The estimated Pt concentration regression model provided a R^2 of 0.860.
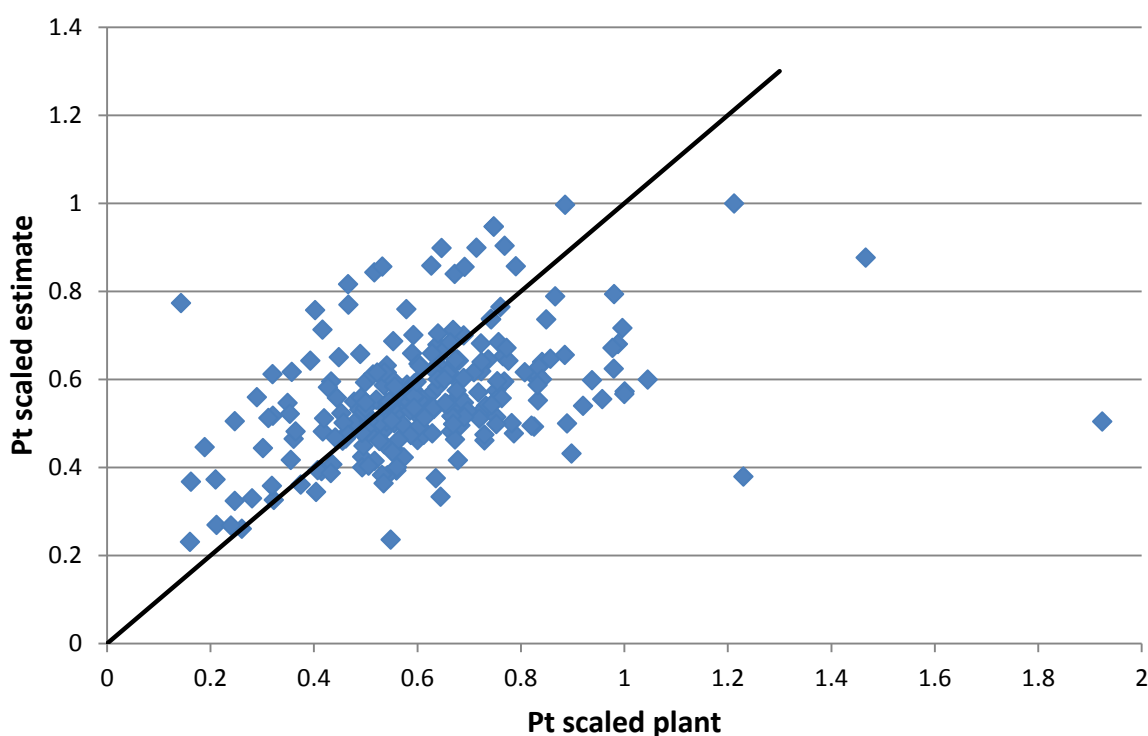

Figure F.1: Second stage filtrate scaled platinum concentration estimation comparison. The solid line represents perfect prediction.

The palladium concentration plant and estimated concentration is provided in Figure F.2. The estimated palladium concentration regression model provided a R^2 of 0.795.
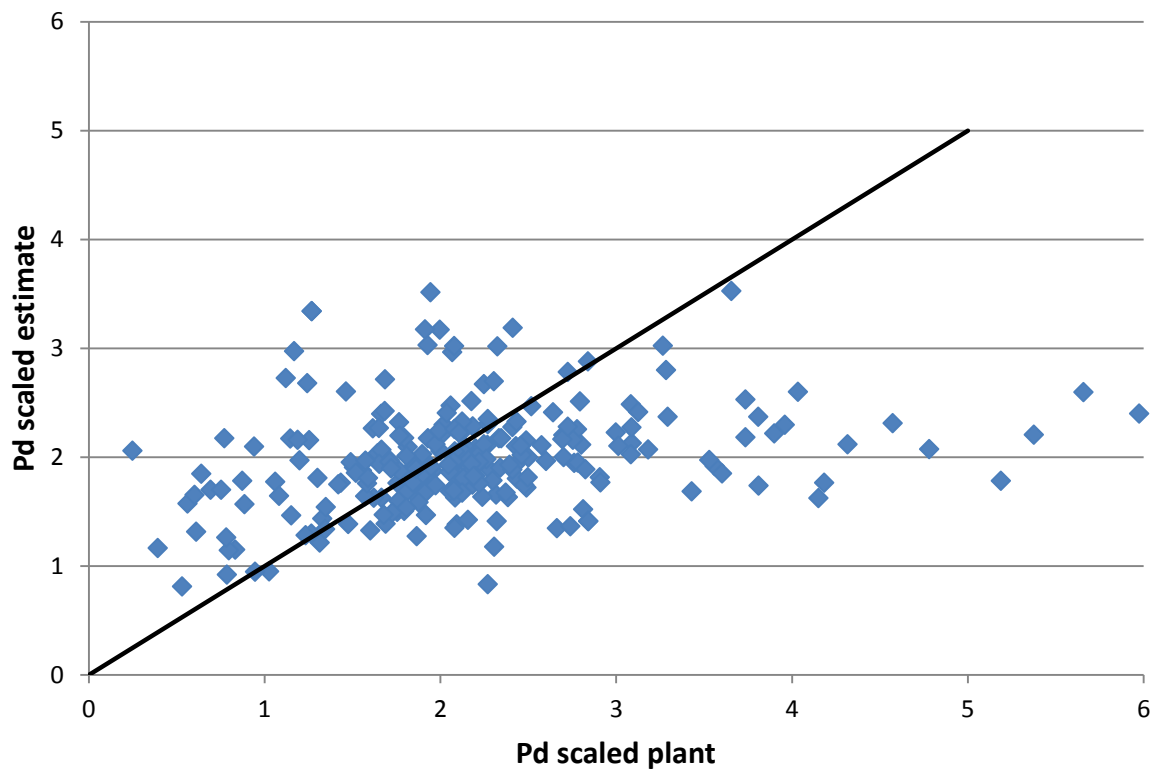
Figure F.2: Second stage filtrate palladium concentration estimation comparison. The solid line represents perfect prediction.

2. Third stage filtrate

Historical third stage filtrate composition data was used to build linear regression models for both platinum and palladium. The platinum concentration plant and estimated concentration is provided in Figure F.3. The estimated Pt concentration regression model provided a R^2 of 0.672.
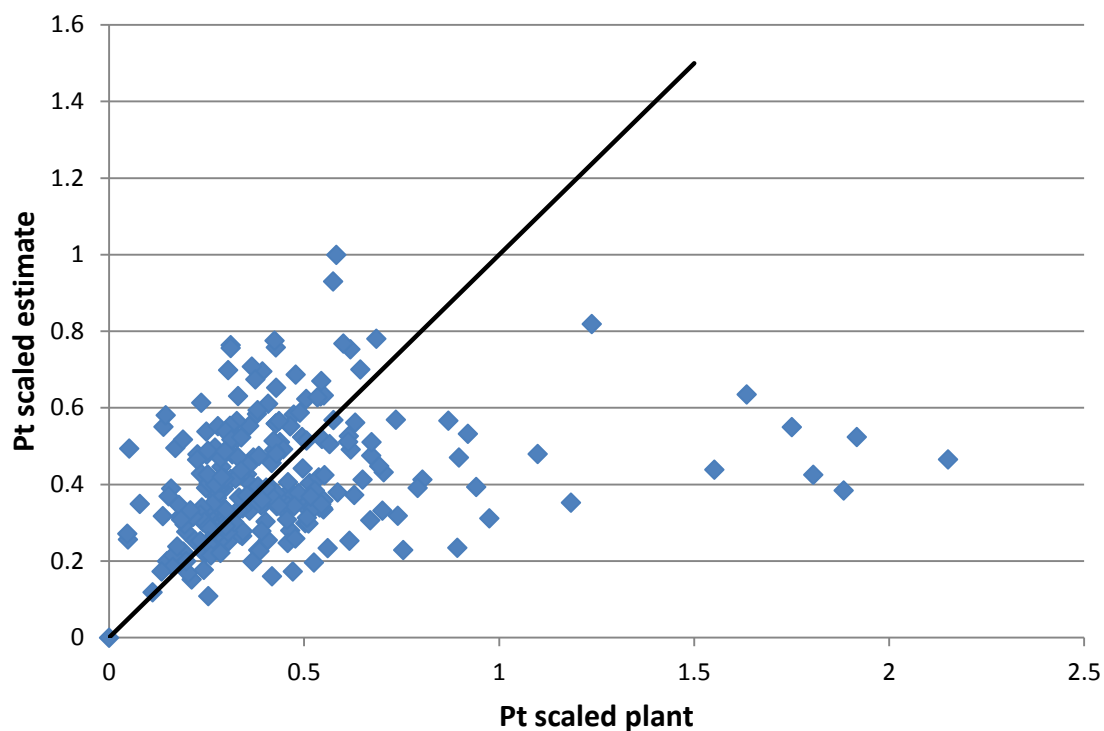
Figure F.3: Third stage filtrate scaled platinum concentration estimation comparison. The solid line represents perfect prediction.

The palladium concentration plant and estimated concentration is provided in Figure F.4. The estimated palladium concentration regression model provided a R^2 of 0.777.
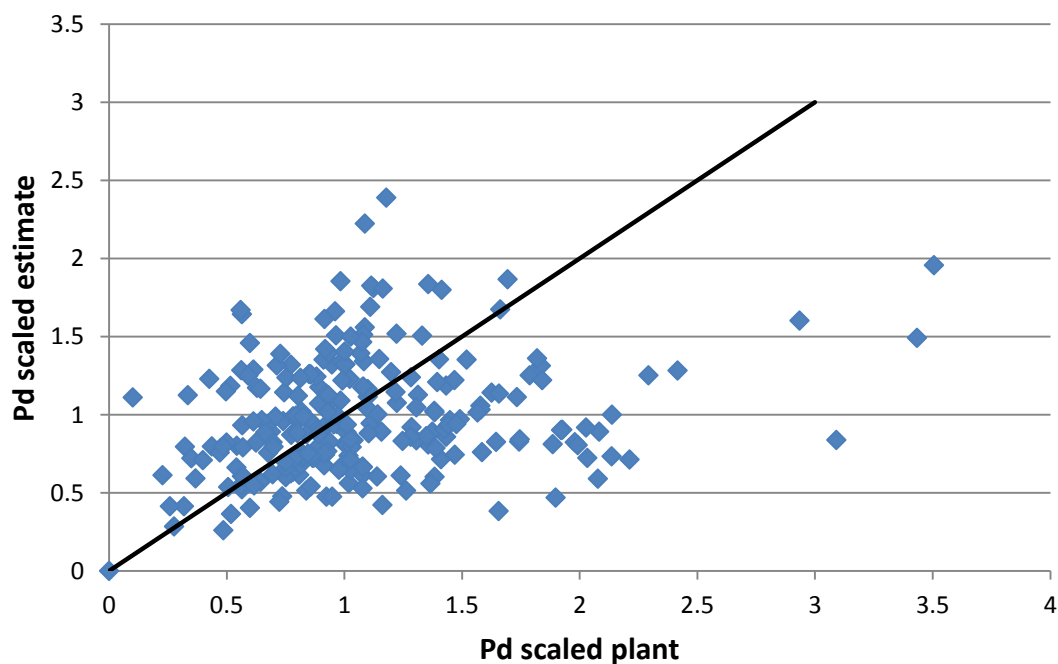

Figure F.4: Third stage filtrate palladium concentration estimation comparison. The solid line represents perfect prediction.

Appendix G: PCA and KPCA fault detection verification

Appendix G provides PCA and KPCA results compared to previously published literature. The objective of the section is to verify the PCA and KPCA fault detection methodologies developed in this work. The Tennessee Eastman process is used as the benchmark process for both PCA and KPCA.

PCA is verified with results published by Yin et al. (2012). KPCA is verified with results published by Aldrich and Auret (2012).

1. PCA verification

The PCA results obtained from Yin *et al.* (2012) is used as comparison. PCA was applied to the entire Tennessee Eastman data set and 9 principal components were retained.

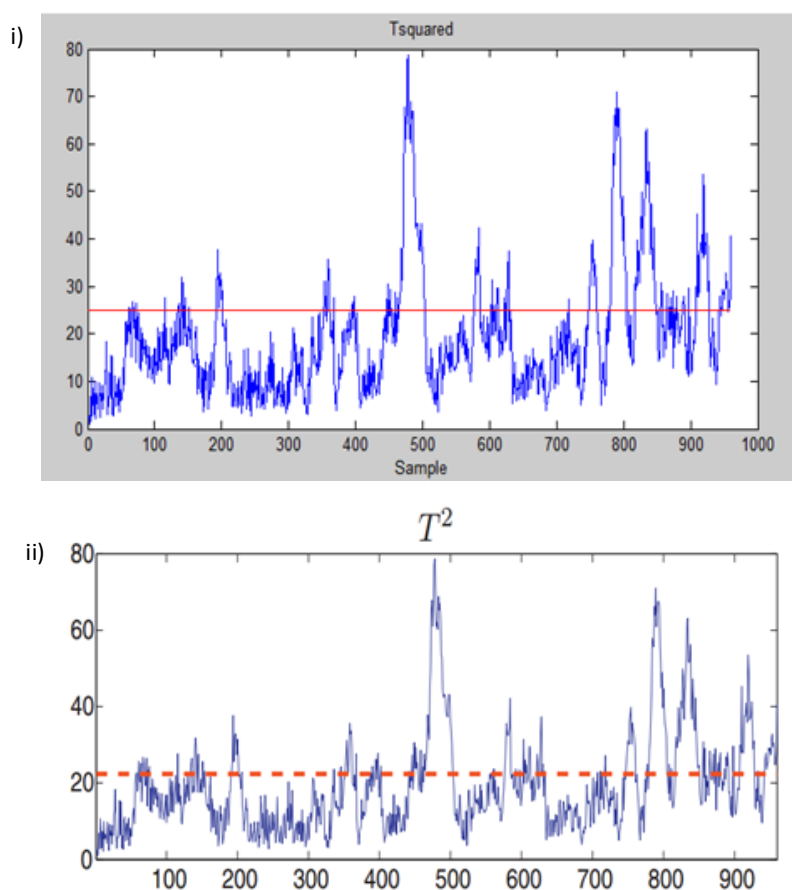The comparison of results for fault 16 is shown in Figure G.1.

Figure G.1: i) Fault 16 T^2-statistic result and ii) Fault 16 T^2-statistic taken from Yin *et al.* (2012).

The comparison of results for fault 16 is shown in Figure G.1.
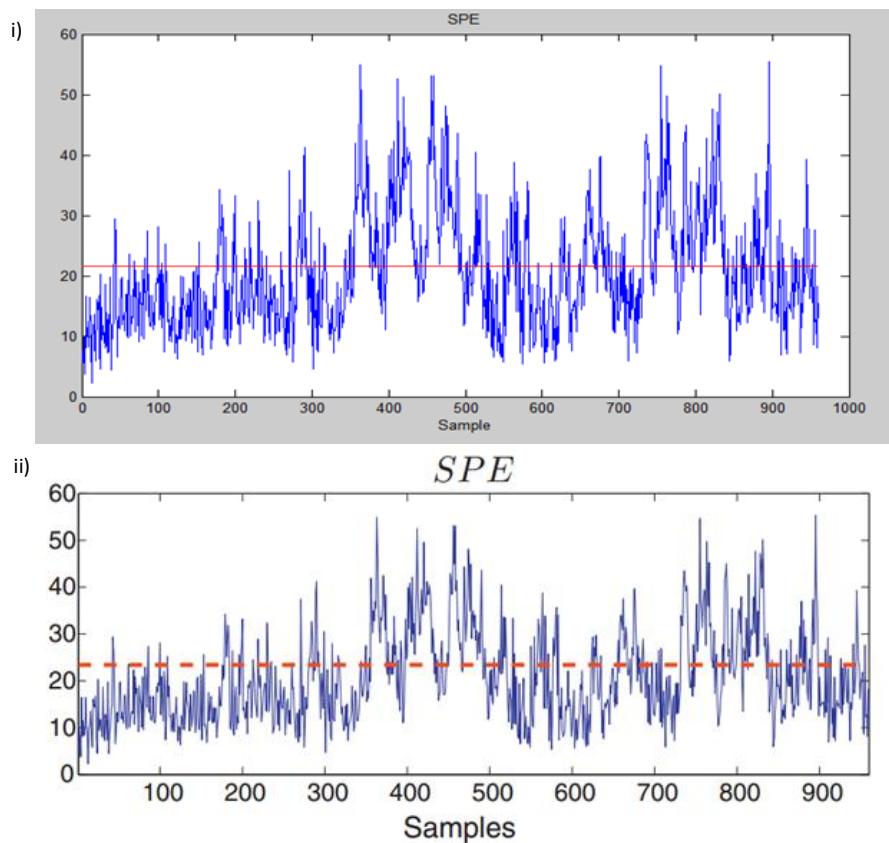
Figure G.2: i) Fault 17 SPE-statistic result and ii) Fault 17 SPE-statistic taken from Yin *et al.* (2012).

Other available results from Yin *et al.* (2012) were also compared. All results were similar and therefore verifying the PCA methodology developed in this work.

2. KPCA verification

Reproducing KPCA results is more challenging. Mainly due to the use of different kernel widths and kernel width selection procedures not always being stated clearly.

Results were compared to that of Aldrich and Auret (2012). The entire Tennessee Eastman process data set was used for training. 16 principal components were retained and the kernel width was selected from the 50th pairwise distance percentile.

The scree plot and fault 5 T^2-statistic result is shown in Figure G.3.
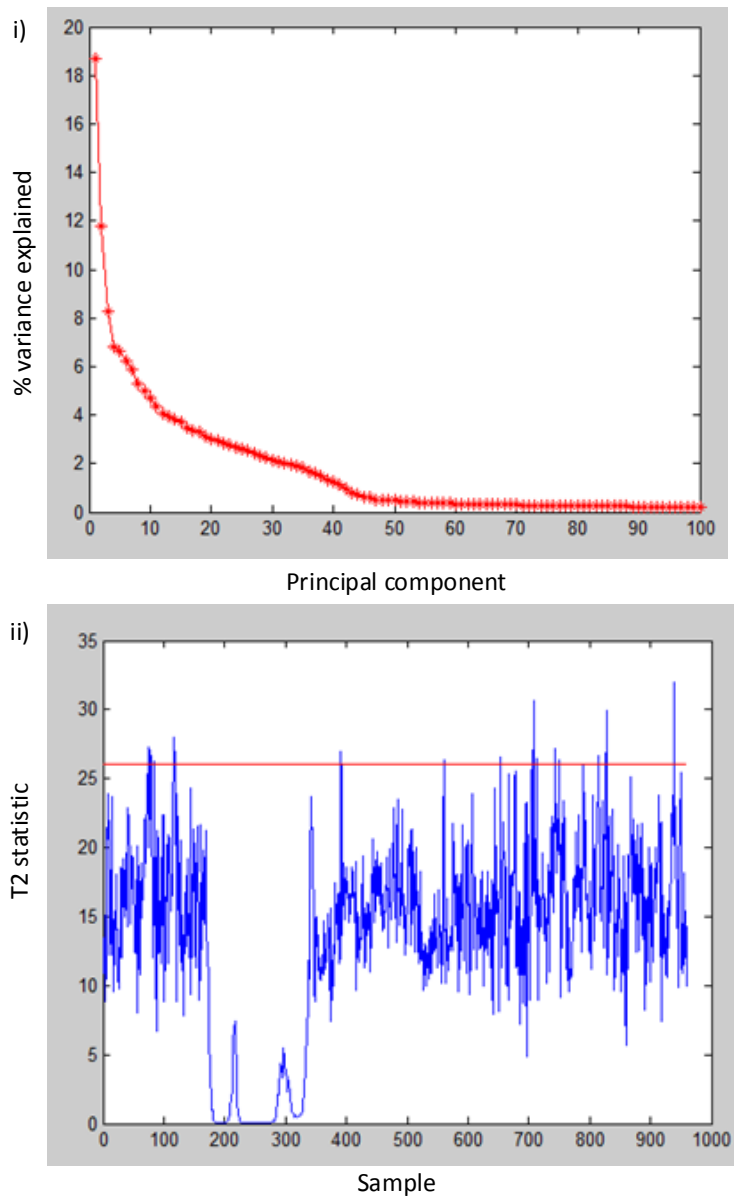
i)

ii)

Figure G.3: KPCA i) percentage variance explained and ii) Fault 5 T²-statistic result.

The results in Figure G.3 were comparable to the results obtained by Aldrich and Auret (2012). The results are similar and other fault results were also subsequently compared. The comparison verified the KPCA model developed in this work.